University of Alberta

Synthesis and Screening of Heterogeneous Multimetallic Nanoparticle Catalysts for Mono-, Poly- and Heteroaromatic Hydrogenation Activity under Mild Conditions

by

Nicole A. Beckers

A thesis submitted to the Faculty of Graduate Studies and Research
in partial fulfillment of the requirements for the degree of

Doctor of Philosophy

Department of Chemistry

Spring 2011
Edmonton, Alberta

Examining Committee

Jillian M. Buriak, Chemistry

Steven H. Bergens, Chemistry

Murray Gray, Chemical and Materials Engineering

Jonathan G. C. Veinot, Chemistry

Julianne Gibbs-Davis, Chemistry

Charles T. Campbell, University of Washington

Abstract

Nanoparticle catalysts have shown to be advantageous over traditional catalysts for many reasons and active for a wide variety of reactions. This thesis describes an approach for the synthesis and screening of heterogeneous multimetallic nanoparticle catalysts for aromatic hydrogenation activity in a quick and time efficient manner, as well as detailed testing and characterization of identified active catalysts.

Over 90 mono- and bimetallic nanoparticle catalysts supported on alumina were screened for toluene hydrogenation activity under ambient conditions. Through this approach, four catalysts were determined to be active: $RhPt/Al_2O_3$, $RuPt/Al_2O_3$, $IrPt/Al_2O_3$, and $IrRh/Al_2O_3$. These catalysts were further tested in bulk, and $RhPt/Al_2O_3$ was confirmed to be the catalyst with the highest observed rate of all the bimetallic combinations screened. Further studies were then performed where the metal loading, temperature, pressure and substrate to metal ratios were varied to determine the effects of these variables on the activity of the $RhPt/Al_2O_3$ catalyst, and a CS_2 poisoning study was performed on this catalyst to determine the number of active sites. TEM, XPS and BET were used to characterize the active catalysts.

Based on the success of the developed approach, a series of trimetallic nanoparticle catalysts were then synthesized and tested for the hydrogenation of toluene under ambient conditions and one trimetallic catalyst was selected for further studies. Next, a series of multimetallic nanoparticle catalysts supported on a variety of metal oxides were synthesized and screened for catalytic activity. Using the High Throughput Facility at the Centre for Catalysis Research and Innovation at the University of Ottawa, 72 different catalysts were screened for catalytic activity for the hydrogenation of

toluene, naphthalene, pyridine, indole, quinoline, thiophene and benzothiophene under mild conditions. Bulk kinetic studies, including temperature and pressure studies, were performed using select catalysts for the hydrogenation of naphthalene and quinoline and a quinoline loading study was also conducted. Standard materials characterization techniques were used to acquire information about the size and oxidation state of the nanoparticle catalysts.

To conclude this work, further research directions including expansions of this thesis work and further directions for the field of nanoparticle catalysis were suggested.

Acknowledgements

I am incredibly grateful to the following people who were part of my academic life at the University of Alberta. Without their assistance and support, this research and thesis would never have been completed.

Paramount, I would like to convey my deepest gratitude to my supervisor, Dr. Jillian Buriak. Her support and guidance throughout my time in her research group were invaluable.

I would like to thank my supervisory committee members, Dr. Steven Bergens, Dr. Murray Gray, Dr. Jon Veinot, and Dr. Julianne Gibbs-Davis for their valuable comments on my research. Special thanks must go to Dr. Charles T. Campbell from the University of Washington.

I was fortunate to work with so many talented colleagues and collaborators during my PhD. I would like to acknowledge the support and friendship from the past and present members of the Buriak group: Dr. Masato Aizawa, Dr. Usama Al-Atar, Dr. Steven Chai, Dr. Brian Daly, Dr. Anastasia Elias, Dr. Kenneth Harris, Dr. Lawrence Huck, Dr. Yunhui Li, Dr. Hidenori Mizuno, Dr. Yinghong Qiao, Dr. David Rider, Dr. Dong Wang, Dr. Vincent Wright, Dr. Lina Xu, Jennifer Bruce, Torsten Doerschel, Sean McClure, Jeffery Murphy, Sayed Nagy, Anne Slaney, Brian Worfolk, Nathanael Wu, Xiao Xing. I would especially like to thank Xiaojiang Zhang, a fellow graduate student in the Buriak group who performed the materials characterization and Steven Hyunh who worked as an USRA summer student on my research project for the summer of 2010.

Dr. Mike Xia of the NINT Chemical Analysis Lab is thanked for performing the GC-MS analysis and obtaining the BET measurements. The staff of the Department of

Chemistry Glass Shop are thanked for making the sample holders. Jian Chan and Peng Li from the NINT Electron Microscopy Lab are thanked for obtaining the TEM images. Shihong Xu from the Alberta Centre for Surface Engineering and Science (ACSES) is thanked for obtaining the XPS data. Roxanne Clement at the Catalysis Centre for Research and Innovation at the University of Ottawa is thanked for her help and guidance.

I would also like to thank all of my friends at the University of Alberta who made my life here enjoyable. Finally, I would like to thank my parents and my husband who have been incredibly supportive and encouraging.

Table of Contents

List of Tables

List of Figures

List of Abbreviations

BE	Binding energy
BET	Brunauer Emmett Teller
CNT	Carbon nanotubes
EDX	Energy dispersive x-ray spectroscopy
ETEM	Environmental transmission electron microscopy
EXAFS	Extended x-ray absorption fine structure
GC	Gas chromatography
GC-MS	Gas chromatography mass spectroscopy
HOSS	Heated orbital shaker system
MWNTs	Multiwalled carbon nanotubes
Obs. rate	Observed rate
STM	Scanning tunneling microscopy
TEM	Transmission electron microscopy
TOF	Turnover frequency
TON	Turnover number
XANES	X-ray absorption near edge structure
XPS	X-ray photoelectron spectroscopy
XRD	X-ray diffraction

Chapter 2 was reproduced in part with permission from:

Dehm, (Beckers) N. A.; Zhang, X.; Buriak, J. M. "Screening of Bimetallic Heterogeneous Nanoparticle Catalysts for Arene Hydrogenation Activity under Ambient Conditions."

Inorg. Chem. **2010,** 49, (6), 2706-2714.

Chapter 1

General Introduction

This thesis proposes an approach for the combinatorial synthesis and screening of mono-, bi- and trimetallic heterogeneous nanoparticle catalysts for the hydrogenation of aromatic substrates under mild conditions. We will present the strategy, catalyst synthesis and testing followed by the detailed kinetic and materials characterization of these heterogeneous nanoparticle catalysts as an approach to discover new families of nanoparticle catalysts in a quick and time efficient manner.

As an overview of the entire project, this first chapter describes the background behind this thesis work. We will then show some of the current methods for synthesizing both soluble and supported nanoparticle catalysts, including their drawbacks, and examples from the literature that use these nanoparticle catalysts for aromatic hydrogenation. Then we will focus on the use of metal oxides as catalyst supports, and will discuss the chemistry behind the synthesis of metal oxides. Next, combinatorial materials chemistry will be introduced as an approach to synthesizing and screening large numbers of new materials in a quick and time efficient manner. Lastly, we will describe how our synthesis and screening approach can lead to the discovery of new families of heterogeneous nanoparticle catalysts that are active for aromatic hydrogenation under mild conditions.

1.1 Background

Nanoparticle catalysts are advantageous over traditional catalysts for many reasons including high surface areas and energies, unique electronic effects and potentially lower cost: high surface to volume ratios mean less metal is 'wasted' in the particle interior, and higher selectivity produces fewer undesirable side products.[1,2] The composition, size and shape of nanoparticle catalysts can be easily tuned synthetically by varying the metal precursor, and the quantity and nature of the chosen ligand. Typically, spherical nanoparticles are thermodynamically favoured during synthesis, so certain reaction parameters must be altered to obtain nanoparticles of varying shapes.

Nanoparticle catalysts are a unique class of catalysts due to their size, they can possess properties of both the molecular and the bulk metal, though these properties can be size dependent. Nanoparticle catalysts can also possess properties that are not evident in the bulk metal. One of the best examples of a nanoparticle catalyst demonstrating properties not displayed by the bulk metal is gold. Bulk gold is quite resistant to oxidation and other chemical transformations, but once small gold nanoparticles are prepared, they are catalytically active for a variety of reactions including oxidations[3] and hydrogenations.[4]

However, not just any size of nanoparticle demonstrates catalytic properties. It has been demonstrated that only nanoparticles within a narrow size range (~2-4 nm) are catalytically active. This was well exemplified by Valden who used Au/TiO_2 nanoparticles of varying sizes for the oxidation of carbon monoxide.[5] They found only nanoparticles within a narrow size range were catalytically active (Fig. 1.1), and this

demonstrates one of the challenges when synthesizing nanoparticle catalysts. The catalytic activity of nanoparticles is size dependent because as the nanoparticle size decreases, the surface heterogeneity increases due to a change in the surface atom statistics and this in turn increases the surface roughness of the nanoparticle.[6] Smaller nanoparticles are composed of a higher fraction of coordinatively unsaturated surface atoms similar to a stepped single crystal. This increases the surface roughness while the surfaces of larger nanoparticles are terminated by low-index, high coordination surfaces with lower surface roughnesses.[6] The active sites of the nanoparticle catalysts are the coordinatively unsaturated metal atoms present on steps and edges on the surface of a nanoparticle. Furthermore, the activation energy of a reaction also decreases with a decrease in particle size.[6]

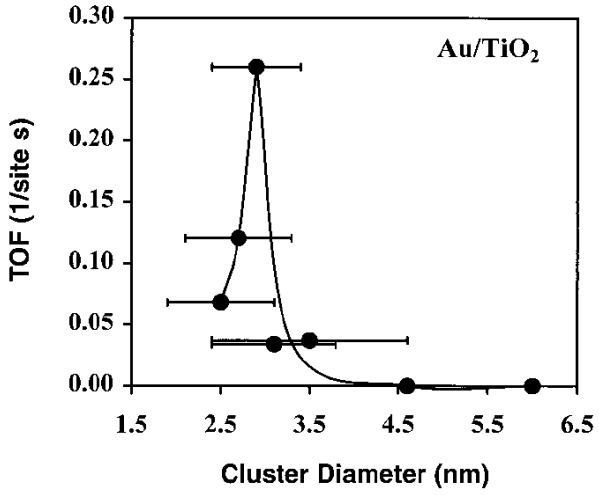

Figure 1.1. CO oxidation turnover frequencies (TOF)s at 300 K as a function of the size of the Au clusters supported on a high surface area TiO_2 support.[5,a]

---

[a] From Valden, M.; Lai, X.; Goodman, D. W., "Onset of catalytic activity of gold clusters on titania with the appearance of nonmetallic properties." *Science* **1998**, *281*, 1647-1650. Reprinted with permission from AAAS.

The small size of catalytically active nanoparticles makes them very interesting as catalysts. Often active nanoparticle catalysts are made from the expensive noble metals (e.g., Rh, Pt, or Pd), so it is desirable to waste as little of these expensive metals on the interior of a nanoparticle as possible. With the very small size of catalytically active nanoparticles, a large percentage of the metal atoms will be surface atoms, which have the potential to be catalytically active, with a minimal amount of the metal being "wasted" as interior metals atoms. For example, for a M^0 nanocluster that is composed of about ~300 atoms, 50% of those atoms are on the surface of the nanocluster.[7] Therefore, as the size of the nanoparticles decreases, you can get closer and closer to an "all surface" nanoparticle.

It is widely accepted that active sites of the nanoparticle catalysts are the coordinatively unsaturated metal atoms present on steps and edges on the surface of a nanoparticle. A larger number of steps and edges tend to be present on non-spherical nanoparticles, so one would anticipate that different nanoparticle shapes would demonstrate different catalytic activities. The El-Sayed group has investigated this effect by using Pt nanoparticles of different shapes for an electron-transfer reaction. They examined changes in activation energy and the percent shape change as a function of time using tetrahedral, cubic and spherical nanoparticles.[8] They found that while the nanoparticles with the largest number of edges and corners (tetrahedral nanoparticles) were the most active, they possessed a higher surface energy than the spherical nanoparticles, so they started to become spherical during the course of a catalytic reaction through rapid dissolution and surface reconstruction. Somorjai and co-workers performed a similar study, though instead of studying the activity and activation energy as a function

of nanoparticle shape, they investigated how selectivity varies with nanoparticle shape.[9] The hydrogenation of benzene with cubic and cuboctahedral nanoparticles was studied, and they found that while both cyclohexane and cyclohexene were produced as hydrogenation products using cuboctahedral nanoparticles, only cyclohexane was produced when cubic nanoparticles were used. From these two studies, it can be seen that both the selectivity of a catalytic reaction and the activity of a nanoparticle catalyst can be influenced by using nanoparticles of different shapes.

1.2 Approaches to Synthesizing Nanoparticle Catalysts

There are two different classes of nanoparticle catalysts that are used for catalytic reactions: soluble nanoparticle catalysts and supported nanoparticle catalysts. In this section, the two different classes of nanoparticle catalysts will be discussed along with their strengths and weaknesses. Different synthetic approaches to preparing soluble and supported catalysts will be addressed, with pertinent examples from the literature as they pertain to nanoparticle catalysts used for aromatic hydrogenation.

Soluble Nanoparticle Catalysts

Homogeneous catalysts are those in which the catalyst is in the same phase as the substrate in which it is acting upon, often a solution-solution reaction. Consequently, this requires that the nanoparticles are soluble in solution. To synthesize these nanoparticles, a stabilizer or ligand is required to prevent the aggregation and precipitation of the metal

nanoparticles out of solution. The aggregation occurs because at short interparticle distances, the van der Waals forces will cause two metallic nanoparticles to be attracted to one another.[10] If there are no repulsive forces present that are opposed to the van der Waals forces, then nanoparticles will aggregate and precipitate out of solution.

There are several routes that can be used to prevent the nanoparticles from aggregating, and involve using either charge stabilization,[7,11,12] steric stabilization[13] or a combination of the two. However, the ligands that prevent the aggregation of the nanoparticles may also block some of the catalytically active sites on the surface of the nanoparticles.[14] The challenge then arises in selecting a ligand that will successfully prevent the nanoparticles from aggregating under the reaction conditions without blocking all of the catalytically active sites. In addition to blocking some of the catalytic active surface sites, the ligand can change the surface chemistry of the nanoparticles which will have an influence on the catalytic activity.[15] To minimize the effect the ligand has on the catalytic activity of nanoparticles, a minimal amount of ligand must be used. If too small of a quantity of ligand is used, the nanoparticles may demonstrate a higher catalytic activity, but they will not be stable in solution for a prolonged period of time. If too large of a quantity of ligand is used, the nanoparticles may be quite stable under harsher conditions, but they will not demonstrate an appreciable catalytic activity. It then becomes a compromise between obtaining a high catalytic activity and using stable nanoparticle catalysts.

The synthesis of soluble metallic nanoparticle catalysts is fairly straightforward. Typically a metal salt is used as the nanoparticle precursor, and is dissolved in an appropriate solvent. This is followed by addition of the ligand and a reducing agent such

as an *in situ* hydrogen source like sodium borohydride.[11,13] Soluble nanoparticle catalysts have also been prepared through ligand reduction and displacement from organometallic precursors, through electrochemical reduction of metal salts, by thermal or photochemical decomposition or by metal vapor synthesis.[10,13]

As previously mentioned, there are several routes used to prevent nanoparticle aggregation. One of the routes to preventing nanoparticle aggregation and precipitation uses electrostatic repulsion to keep the nanoparticles physically separated. Electrostatic ligands such as halides, carboxylates and polyoxoanions[10] are frequently used and stabilization occurs because of coordination of the anionic ligands to the coordinatively unsaturated metal surface atoms on the metal nanoparticles.[13] These ionic stabilizers create an electrical double later around the nanoparticles, creating coulombic repulsion, and if the electrical potential is high enough then the electrostatic repulsion will prevent aggregation (Fig. 1.2).[10,13] However, if these charges are perturbed, this may result in precipitation of the nanoparticles out of solution.

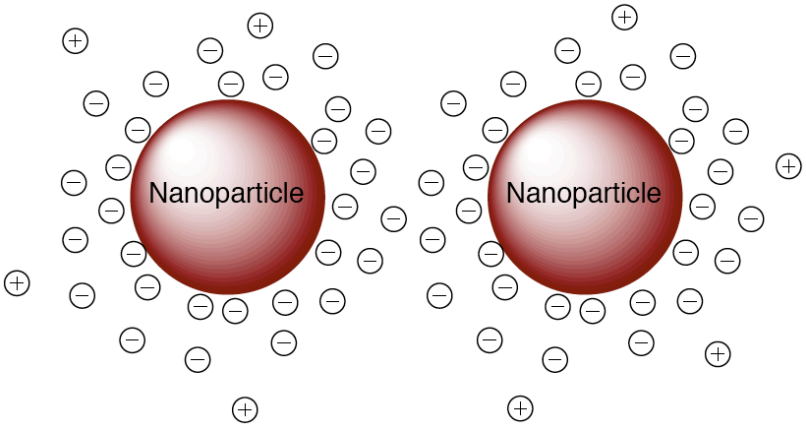

Figure 1.2. Schematic representation of electrostatic stabilization.

The other common method used to prevent nanoparticle aggregation relies on using the steric bulk of the ligand to prevent the nanoparticles from coming into physical contact with one another (Fig. 1.3). Ligands such as polymers (e.g. polyvinylpyrrolidione), dendrimers, and large alkylammonium cations are frequently used with good success.[13] One drawback to using these bulky ligands is they may prevent the catalytic substrate from accessing the surface of the nanoparticle. However, these ligands can be used in both aqueous and organic media, while charged ligands are frequently limited to aqueous solvents.

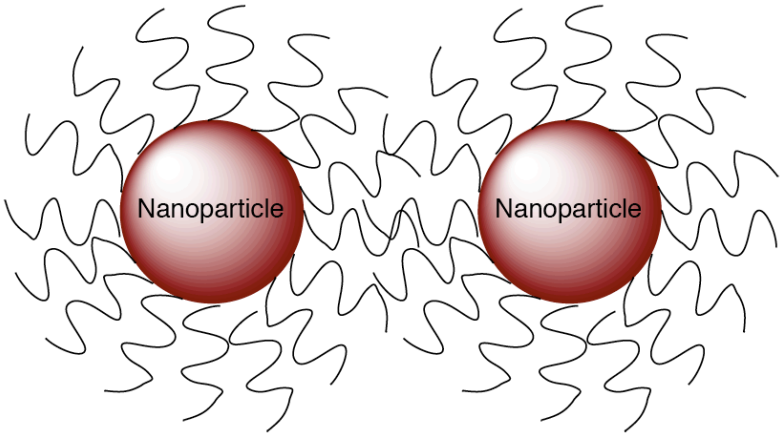

Figure 1.3. Schematic representation of steric stabilization.

Soluble catalysts do have several advantages over supported catalysts, but they also have some serious limitations. By using different quantities of ligands, one can effectively control the shape and size of the nanoparticles.[16] Futhermore, soluble nanoparticle catalysts can by synthesized under very mild conditions, and also tend to be more active under mild conditions.[13] They also tend to be more selective for certain

catalytic reactions, and are more easily characterized and studied than supported catalysts.[13] However, as previously mentioned, the ligand can block some of the active sites on the surface of the nanoparticle catalyst, consequently decreasing the catalytic activity. It can also be quite challenging to separate the soluble catalyst from the substrate and products.[17] Finally, these soluble catalysts tend to be less stable at elevated temperatures and pressure, which are frequently required for certain catalytic reactions, such as arene hydrogenations,[13] and industrial applications.

Heterogeneous Nanoparticle Catalysts

In the case of heterogeneous catalysis, the catalyst is in a different phase than the substrate. This situation could consist of a solid catalyst with the substrate being in a liquid or gaseous phase, or a biphasic system in which the catalyst is in one liquid phase, and the substrate is in a different liquid phase. While biphasic systems will be discussed briefly, the majority of the discussion will focus on supported nanoparticle catalysts.

While both unsupported and supported nanoparticle catalysts have demonstrated activity for arene hydrogenation, supported catalysts are more robust and also allow for easier separation of the catalyst from the reaction mixture enabling the catalyst to be more easily recycled.[18] In addition, there are important synergistic effects between the nanoparticle catalyst and the underlying support. For example, the acidity of the support, electron transfer to and from the support, and epitaxial stress at the nanoparticle-support boundary can all have a significant influence on the activity of the catalyst.[1,19,20] Heterogeneous nanoparticle catalysts have been supported on a variety of materials

including carbon nanotubes,[14,21-26] zeolites,[27,28] carbonaceous materials,[15,29-31] and metal oxides,[19,30,32-57] the latter being a very common family of supports currently used for bitumen processing catalysts. Metal oxides such as Al_2O_3, TiO_2 and SiO_2 are inexpensive, widely available commercially, and allow for control of parameters such as substrate acidity and porosity, among others, permitting tuning of catalyst activity.[19,20]

Heterogeneous catalysts do have many advantages over homogeneous catalysts. Because the heterogeneous catalysts are deposited on a solid material, it is quite easy to separate the solid catalyst from the reaction mixture, allowing the catalyst to be easily recycled. Furthermore, no ligands are required to keep the nanoparticles from aggregating because the nanoparticles are adhered to the support, so there is potential for an increased catalytic activity. Heterogeneous catalysts also tend to be more robust than homogeneous catalysts. One of the most logical approaches to preparing heterogeneous nanoparticle catalysts involves the absorption of the metal nanoparticles onto a solid support. However, during the course of the catalytic reaction, leaching of the nanoparticles into the reaction solution followed by aggregating of the nanoparticles may occur.[17]

There are several methods used to prepare heterogeneous nanoparticle catalysts, and they often depend on the type of catalyst support chosen. Carbon nanotubes are attractive as catalyst supports because of their electronic properties, physical and chemical stabilities and large surface area structures.[14] One method used to prepare catalytic nanoparticles on multiwalled carbon nanotubes (MWNTs) involves using a sonicating bath to disperse the carbon nanotubes, followed by addition of a metal salt solution, and a boron-containing reducing agent.[14,25] Another approach involves loading the carbon nanotubes and the metal chloride precursor which was dissolved in water into a stainless

steel autoclave.[26] The autoclave was purged with nitrogen, then sealed and heated at 400-450ºC for 2 hours, and then slowly cooled down to room temperature. Pd and Rh nanoparticles have also been supported on carbon nanotubes using a microemulsion-templated synthesis procedure.[23] A different approach involves mixing MWNTs with tridecylamine capped Rh nanoparticles followed by microwave treatment.[21] Similar to the wet impregnation method used to prepare nanoparticles on metal oxides, this method has also been used to prepare PtPd nanoparticles on MWNTs.[24]

The logic behind using zeolites as nanoparticle catalysts is by confining the nanoparticles to the pore and void spaces inside these mesoporous and microporous solids, aggregation of the nanoparticles can be successfully prevented. To prepare heterogeneous nanoparticle catalysts using zeolites as the catalyst support, ion exchange has been used to exchange the extra framework sodium cations with the transition metal cations. This is followed by reduction of the transition metal cations that were left in the cavities of the zeolite.[27,28] Often sodium borohydride is used as the reducing agent because the sodium cations can then reoccupy the empty cation sites left by the transition metal ions after reduction.[27,28] A simple impregnation method identical to the impregnation method used to prepare metal nanoparticles on metal oxides supports has also been used. Briefly, a solution containing the metal chloride precursor was added to a slurry of the zeolite followed by drying under mild conditions and a high temperature reduction.[41,58]

Carbonaceous materials have also been used as a catalyst support for aromatic hydrogenation. In addition to being a catalyst support, carbon blacks, and active carbon have exhibited some activity for the hydrogenation and hydrocracking of model coal

compounds under coal liquefaction conditions.[31] Nanoparticles on activated carbon have been prepared using the conventional impregnation method in which the activated carbon support is soaked in solution of the metal precursor followed by reduction of the metal precursor.[29-31] Rhodium nanoparticles supported on charcoal have also been prepared by refluxing preformed colloidal nanoparticles with activated charcoal in methanol.[15]

When metal oxides are used as catalyst supports, the traditional route known as the impregnation or incipient wetness method involves using a preformed support (i.e., Al_2O_3, TiO_2 or SiO_2) and then soaking the support in a solution of the desired metal salt.[19,30,34,37,39,41,47,49,53] Then the metal salt is reduced to give the zero oxidation state metal nanoparticles. While this method is simple, and the preformed supports are quite inexpensive, the metal nanoparticles that are formed are only on the surface of the support, and are not necessarily adhered very strongly to it. This can lead to leaching of the metal nanoparticles from the surface of the support followed by aggregation and precipitation of the nanoparticles out of the solution. In addition, there is no control over the size, shape or monodispersity of the nanoparticles being formed. On a slight variation of this procedure, a tetrairidium cluster was slurried together with alumina, followed by evacuation of the solvent and decarbonylation to give Ir_4 clusters supported on alumina.[44]

In a similar method to the impregnation route, both a preformed support and prepared nanoparticles can be used to generate a heterogeneous nanoparticle catalyst.[35] As opposed to soaking the support in a solution of the metal salt, the support is soaked in a solution containing the ligand stabilized metal nanoparticles. While this approach allows one to control the size and shape of the nanoparticles by previously preparing them using a ligand as a stabilizer, it does have the drawback of having the ligand present once

the nanoparticles are adhered to the support surface. To remove the ligand, heat is often used but this may leave carbon residues behind on the surface of the catalyst, and successfully removing all of the ligand to leave "clean" nanoparticles is very challenging.[14] This method has been used to deposit Pt nanoparticles stabilized by polyamidoamine dendrimers onto a high surface area silica support.[40] The dendrimer was then removed by thermal activation. By using a dendrimer as a ligand and preforming the nanoparticles before depositing them on the support, a high degree of control over the size of the nanoparticles was obtained. However, a Pt/SiO_2 catalyst was also prepared by insipient wetness impregnation of the same Pt precursor onto the same support, and when the catalytic activity for the hydrogenation of toluene was compared using the different catalysts, there was no appreciable difference in the catalytic activity. Similarly, this method has been used to deposit dendrimer encapsulated Pt-Cu nanoparticles onto commercial alumina supports[57] and dendrimer encapsulated Pt nanoparticles onto titania supports.[46]

As previously mentioned, biphasic reactions in which the catalyst is in one liquid phase and the substrate is in a different phase are also considered a heterogeneous reaction. While this type of heterogeneous catalysis is less common, several examples do exist frequently using ionic liquids as the solvent for the phase containing the nanoparticle catalysts. For example, Rh nanoparticles were synthesized using polyvinylpyrrolidone as a ligand in several different hydroxyl-functioned imidazolium ionic liquids for the hydrogenation of a variety of substrates.[59] The one advantage of this method is it is quite facile to separate the products from the ionic liquids, and often decantation will suffice. However, to use ionic liquids as the solvent frequently requires the ionic liquid is

synthesized and purified before use, introducing more synthetic steps to the preparation of the soluble nanoparticle catalysts. Similarly, Rh nanoparticles in ionic liquids were successfully used for the biphasic hydrogenation of benzene,[60,61,62] and toluene.[61,63] Biphasic reactions are not limited to using ionic liquids as one of the liquid media. For example, aqueous Rh nanoparticles stabilized by hydroxyalkylammonium salts were used for the biphasic hydrogenation of arenes,[12,64] and PVP capped aqueous Rh nanoparticles were used for the hydrogenation of a variety of different aromatic substrates.[65]

1.3 Metal Oxides as Catalyst Supports

As previously discussed, metal oxides have been widely used as catalyst supports. One of the most common methods used to synthesize metal oxides is the sol-gel route, which is a versatile solution based process.[66] This method has several advantages including high purity, homogeneous elemental distribution, controlled porosity, easily controlled composition and it allows for the formation of high surface materials at low temperatures.[67,68] The sol-gel method involves formation of a sol following by cross-linking to form an oxide gel and there are two steps involved:[66]

Hydrolysis: $M\text{-}OR + H_2O \rightarrow M\text{-}OH + ROH$

Condensation: $M\text{-}OR + M\text{-}OH \rightarrow [M\text{-}O\text{-}M]_n + ROH$

Si, Al, Ti and B alkoxides are commonly used in the sol-gel process, though $Si(OR)_4$ compounds, such as tetraexthoxysilane (TEOS), are the most commonly encountered.[66] However, due to the similar electronegativities of Si and O, the hydrolysis rate of Si

alkoxides is much slower than the other metal alkoxides. The general order of reactivity for common alkoxides is:[66]

$$Si(OR)_4 << Sn(OR)_4 \sim Al(OR)_3 < Zr(OR)_4 < Ti(OR)_4$$

In other words, the more electropositive metals are more susceptible to nucleophilic attack by water, and therefore the hydrolysis of most metal alkoxides is quite quick.[66] There are several ways to control the hydrolysis rate, including varying the ratio of water to metal alkoxide, changing the OR groups, or changing the metal coordination number.[66]

As previously mentioned, the hydrolysis of Si alkoxides is quite slow and can require several days for the reaction to go to completion. To increase this rate, either an acid or base can be added to act as a catalyst, though the catalyst will affect the properties of the final product. There are two different reaction mechanisms that occur, depending upon whether an acid or a base is chosen as the catalyst and both are shown below. In an acid catalyzed reaction (Fig. 1.4), the proton attacks the anionic oxygen that is directly connected to the metal ions which leads to the formation of linear chains.[66,69] These linear chains continue to form until the whole reaction volume is filled with linear oxide chains and then gel formation starts at inner chain positions.[69] As opposed to this, when a base is used as a catalyst, the hydroxide ion attacks directly at the metal ion, so condensation occurs at the central positions of the polyoxide chain and not at the terminal ends (Fig. 1.5).[66,69] This leads to the formation of small particles, and gel formation does not occur until the reaction volume is filled with small particles that begin to aggregate.[69] Generally, using an acid as a catalyst causes the network to form linear or randomly branched polymers as opposed to when a base is used in which highly branched clusters

form, as can be seen from Fig. 1.6.[66] Because using an acid catalyzed synthesis gives rise to linear and randomly branched polymers, this route should yield an amorphous, higher-surface area material than the base catalyzed route.

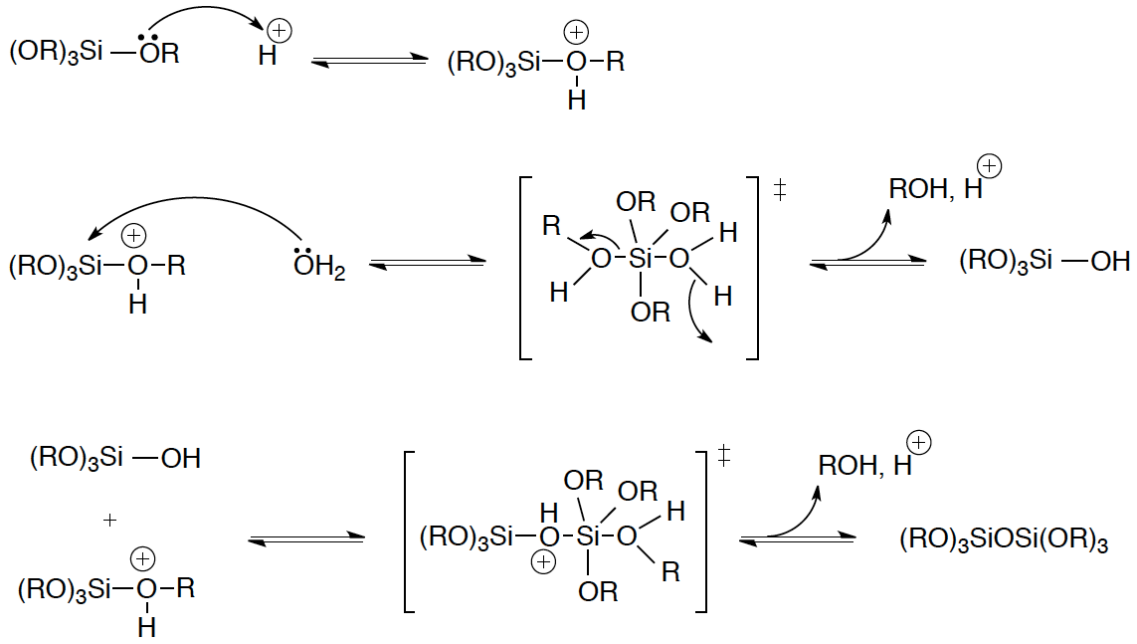

Figure 1.4. Reaction mechanism for the acid catalyzed hydrolysis and condensation of a silicon alkoxide precursor.[66,b]

[b] With kind permission from Springer Science+Business Media: Materials Chemistry, Chapter 2: Solid State Chemistry, 2008, page 66, Bradley D. Fahlman, Fig. 2.43.

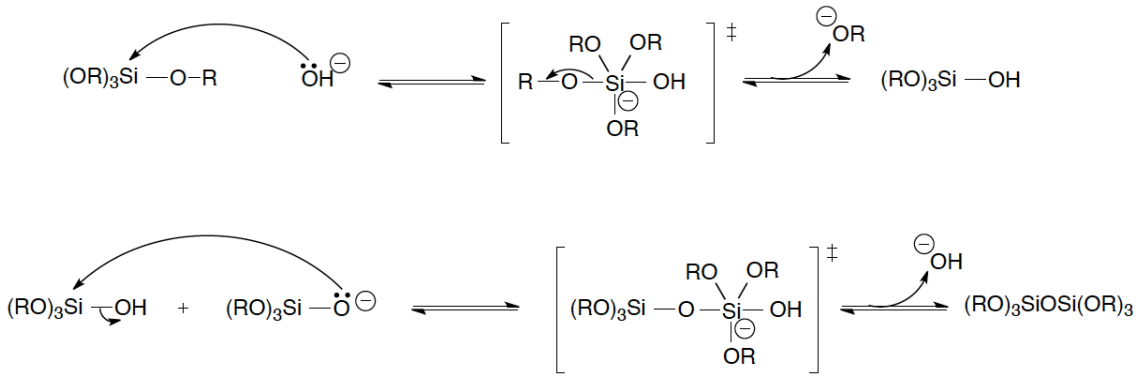

Figure 1.5. Reaction mechanism for the base catalyzed hydrolysis and condensation of a silicon alkoxide precursor.[66,c]

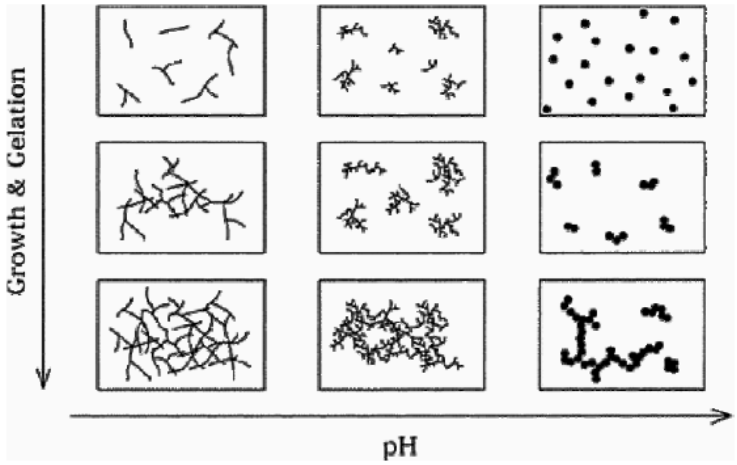

Figure 1.6. Comparison of the morphology observed by varying the pH of the sol-gel process.[66,d]

[c] With kind permission from Springer Science+Business Media: Materials Chemistry, Chapter 2: Solid State Chemistry, 2008, page 67, Bradley D. Fahlman, Fig. 2.44.

As the reaction progresses, the sol will set into a gel. These reactions are typically performed in an alcoholic solvent, so the gel will often contain solvent molecules within its structure, and the product at this point in the synthesis is often called an alcogel.[66] However, at this point in the reaction, the -O-Si-O- framework still tends to contain some unreacted alkoxide groups, so the gel must be allowed to further age to allow for complete hydrolysis and condensation so that the network is strong enough to prevent cracking during drying.[66] If the solvent that remains in an alcogel is removed through slow evaporation, the resulting material is quite porous and is known as a xerogel.[66] During drying of the xerogel, it may experience significant shrinking and cracking even under mild drying conditions, so it is crucial to remove all of the water before the xerogel is further dried to preserve the pore structure.[66] Attempts have been made to accelerate the hydrolysis and condensation steps of the sol-gel process by increasing the gelation temperature or removing solvent under vacuum or a stream of dry gas. However, if the gelation process was accelerated, the pore-size distribution was much broader, and the surface areas were much lower. Therefore, in order to obtain a high surface area material with a narrow pore size distribution, the gelation and aging processes must be allowed to occur under as mild of conditions as possible along with a slow temperature increase during calcination.[69]

---

[d] With kind permission from Springer Science+Business Media: Materials Chemistry, Chapter 2: Solid State Chemistry, 2008, page 67, Bradley D. Fahlman, Fig. 2.45.

Usually, these gels are not used until they are dehydrated through thermal removal of surface –OH groups, followed by a high-temperature annealing to convert the amorphous gel into a crystalline material.[66] For our purposes, the first heating step is performed to remove any remaining solvent, and the high-temperature annealing step is not executed. We wish to have a high surface area, porous material, and that necessitate the material remains in its amorphous state and does not become crystalline.

1.4 Combinatorial Materials Chemistry

A combinatorial approach towards drug discovery has long been applied to the pharmaceutical sciences, and involves rapidly screening a large number of potential compounds for a desired property. The advantage of this route is it is much more efficient than testing each new material in a linear fashion, and allows for much faster discovery times, but it does come with challenges. There are three main goals of the combinatorial materials approach.[70] The first goal is the development of new synthesis methods so that libraries of materials can be quickly and easily prepared. Reproducible rapid synthesis is a very important aspect of high-throughput screening. The second goal is to develop new methods characterizing the compounds prepared in the library, and the third and most challenging goal is detection of desired properties in the library. There have been a number of reviews discussing these challenges and limitations.[70-77]

One of the first examples of this combinatorial approach being applied to materials science was the use of a series of physical masks in conjunction with a RF magnetron sputtering gun with various target materials and thermal processing to prepare

libraries of copper oxide thin films[78] and magnetoresistant materials.[79] Photolithography, specifically photolithographic lift-off methods, followed by annealing have been used to generate photoluminescent libraries with a high density of sites.[80] Photolithography offers the advantages of high spatial resolution and alignment accuracy, however it is more costly than some of the other combinatorial synthesis methods. Libraries of phosphors have also been synthesized using a combination of electron beam evaporation, masking and subsequent oxidative thermal processing.[81,82]

To measure magnetic properties, specifically superconductivity, a parallel in-line four-point probe configuration has been used to measure the resistance at each new material as a function of temperature.[78] A similar detection system was used and involved using a four-probe contact method to measure the resistivity of each sample as a function of magnetic field to determine any magnetoresistant properties.[79] Photoluminescent properties have been determined by taking a photograph of the library under ultraviolet irradiation and using a scanning spectrophotometer to identify materials in the library possessing luminescent properties.[80] Similarly, libraries of potential phosphors have been imaged using a CCD camera while exciting luminescence.[81,82]

In addition to using a combinatorial approach for the discovery of new superconducting films, magnetoresistant materials and phosphors, this approach has also been used to synthesize and discover new catalysts. A sol-gel methodology has been used to synthesize amorphous microporous mixed oxides where small amounts of the sols were deposited into the small wells on the surface of a slate followed by controlled drying and calcination of the catalyst library.[83] Three catalytic reactions were examined, 1-hexyne hydrogenation at 100ºC, and isooctane and toluene oxidation at 350ºC. IR thermography

was used to identify any active catalysts by looking for temperature changes where differences of 0.1K were clearly resolved (Fig. 1.7). IR thermography has also been used to screen for catalytic hydrogen oxidation activity on a library of metals supported on alumina pellets.[84]

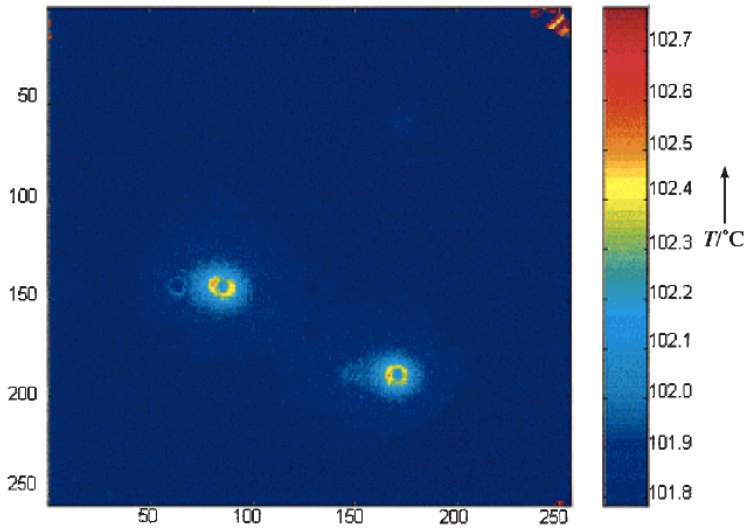

Figure 1.7. Emmissivity corrected IR-thermographic image of the catalyst library during 1-hexyne hydrogenation in the gas phase at 100º C.[83,e]

While the majority of researchers typically only report the activity of a catalyst, spatially resolved mass spectrometry has been used to study the selective oxidation of propene with air using a variety of amorphous microporous mixed oxide type catalysts.[85]

---

[e] Holzwarth, A.; Schmidt, H. W.; Maier, W. E., "Detection of catalytic activity in combinatorial libraries of heterogeneous catalysts by IR thermography." *Angew. Chem., Int. Ed.* 1998, *37*, 2644-2647. Copyright Wiley-VCH Verlag GmbH & Co. KGaA. Reproduced with permission.

A matrix of 33 different catalysts was studied and the oxidation reaction was carried out by decreasing the temperature from 550ºC to 250ºC in 15 min. From the spatially resolved mass spectrometry, very different selectivities were observed for different components of the catalyst libraries. More recently, an ink jet printing approach has been used to print patterns of oxide precursors onto a fluorine-doped tin oxide conductive glass substrate (Fig. 1.8).[86] These patterns were then pyrolyzed and were screened for activity for the photoelectrolysis of water by scanning a laser over the materials while they were submerged in an electrolyte solution and looking for a photocurrent response.

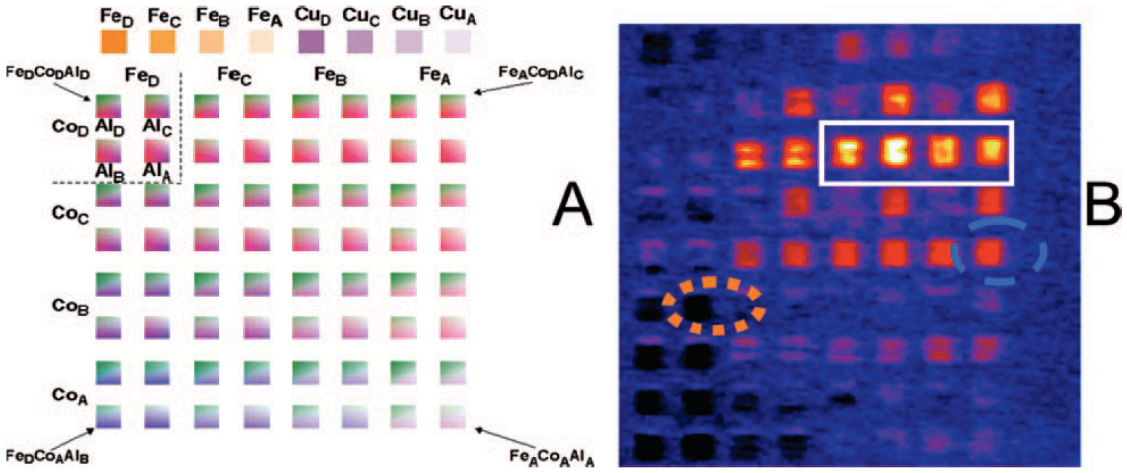

Figure 1.8. a) Printing template used for quantifying the optimal stoichiometry in the Co-Al-Fe system where known amounts of the components are printed into the individual 3 mm x 3 mm squares. b) False color photocurrent map with no applied bias at 532 nm in a 0.1 M NaOH solution.[86,f]

---

[f] Reprinted with permission from Woodhouse, M.; Parkinson, B. A., "Combinatorial discovery and optimization of a complex oxide with water photoelectrolysis activity." *Chem. Mater.* 2008, *20*, 2495-2502. Copyright 2008 American Chemical Society.

1.5 Development of Catalytic Screening Approach

From these works described *vide supra*, it was suggested that by using a combinatorial approach a large number of new heterogeneous nanoparticle catalysts could be efficiently synthesized and screened for catalytic activity. When synthesizing and testing new catalysts for a particular reaction, there are a large number of variables that can be controlled and modified. For example, when synthesizing a heterogeneous nanoparticle catalyst supported on a metal oxide, the type of metal oxide, the metal, type of metal precursor, and metal loading can all be altered. With regard to the actual catalytic reaction, the temperature, pressure, solvent, quantity of substrate, and stir speed can be varied. Due to the large number of variables to be controlled, it would be incredibly time consuming to screen each new catalyst in a linear fashion. This is where the advantage of using a combinatorial approach is evident. By using a combinatorial approach to synthesize and screen our catalysts, we would be able to determine very quickly which catalysts are active for a given reaction. It is important to remember that by using a combinatorial approach in this manner, we are able to determine what is catalytically active and what is not, but we do not know anything about the structure of the catalysts.

1.6 Organization of the Thesis

Based on the concept described above, this thesis presents a novel approach for the synthesis and screening of heterogeneous nanoparticle catalysts for arene

hydrogenation activity under mild conditions. Arene hydrogenation was chosen because it is an industrially challenging reaction, especially under mild conditions. Metal oxides were selected as the catalyst supports because they are currently used as industrial catalytic supports, are commercially available, and are inexpensive.

In Chapter 2, the design of an apparatus that would allow for the synthesis and screening of heterogeneous bimetallic nanoparticle catalysts supported on metal oxides for aromatic hydrogenation under mild conditions is described. Once a suitable apparatus was designed, a series of bimetallic nanoparticle catalysts supported on alumina were synthesized and screened for the hydrogenation of toluene under ambient conditions via gas chromatography. Upon the identification of an active catalyst, further kinetics and materials characterization studies were performed.

In Chapter 3, the screening approach was expanded to include trimetallic catalysts. From there, we expanded our screening procedure to include mixed metal oxides as the catalyst supports and poly- and heteroaromatic substrates. Utilizing the facilities at the Centre for Catalysis Research and Innovation at the University of Ottawa, 72 mono-, bi- and trimetallic nanoparticle catalysts were screened for catalytic activity for 7 different catalytic substrates under mild conditions. Select catalysts and substrates were then chosen for further temperature, pressure and loading studies.

Finally, Chapter 4 describes the summary of Chapters 2-3 followed by the potential research directions of this thesis work.

1.7 References:

(1) Narayanan, R.; El-Sayed, M. A. *J. Phys. Chem. B* **2005**, *109*, 12663-12676.

(2) Yoo, J. W.; Hathcock, D. J.; El-Sayed, M. A. *J. Catal.* **2003**, *214*, 1-7.

(3) Hou, W. B.; Dehm, N. A.; Scott, R. W. J. *J. Catal.* **2008**, *253*, 22-27.

(4) Dash, P.; Dehm, N. A.; Scott, R. W. J. *J. Mol. Catal. A: Chem.* **2008**, *286*, 114-119.

(5) Valden, M.; Lai, X.; Goodman, D. W. *Science* **1998**, *281*, 1647-1650.

(6) Panigrahi, S.; Basu, S.; Praharaj, S.; Pande, S.; Jana, S.; Pal, A.; Ghosh, S. K.; Pal, T. *J. Phys. Chem. C* **2007**, *111*, 4596-4605.

(7) Aiken, J. D.; Finke, R. G. *J. Am. Chem. Soc.* **1999**, *121*, 8803-8810.

(8) Narayanan, R.; El-Sayed, M. A. *J. Am. Chem. Soc.* **2004**, *126*, 7194-7195.

(9) Bratlie, K. M.; Lee, H.; Komvopoulos, K.; Yang, P.; Somorjai, G. A. *Nano Lett.* **2007**, *7*, 3097-3101.

(10) Roucoux, A. *Top. Organomet. Chem.* **2005**, *16*, 261-279.

(11) Schulz, J.; Levigne, S.; Roucoux, A.; Patin, H. *Adv. Synth. Catal.* **2002**, *344*, 266-269.

(12) Schulz, J.; Roucoux, A.; Patin, H. *Chem. Eur. J.* **2000**, *6*, 618-624.

(13) Widegren, J. A.; Finke, R. G. *J. Mol. Catal. A: Chem.* **2003**, *191*, 187-207.

(14) Pan, H. B.; Wai, C. M. *J. Phys. Chem. C* **2010**, *114*, 11364-11369.

(15) Park, K. H.; Jang, K.; Kim, H. J.; Son, S. U. *Angew. Chem., Int. Ed.* **2007**, *46*, 1152-1155.

(16) Ahmadi, T. S.; Wang, Z. L.; Green, T. C.; Henglein, A.; El-Sayed, M. A. *Science* **1996**, *272*, 1924-1926.

(17) Harada, T.; Ikeda, S.; Ng, Y. H.; Sakata, T.; Mori, H.; Torimoto, T.; Matsumura, M. *Adv. Func. Mater.* **2008**, *18*, 2190-2196.

(18) Widegren, J. A.; Finke, R. G. *Inorg. Chem.* **2002**, *41*, 1558-1572.

(19) Pawelec, B.; Castano, P.; Arandes, J. M.; Bilbao, J.; Thomas, S.; Pena, M. A.; Fierro, J. L. G. *Appl. Catal., A* **2007**, *317*, 20-33.

(20) Bertolini, J.-C.; Rousset, J.-L. *Nanomaterials and Nanochemistry*; Springer, 2008.

(21) Kakade, B. A.; Sahoo, S.; Halligudi, S. B.; Pillai, V. K. *J. Phys. Chem. C* **2008**, *112*, 13317-13319.

(22) Yoon, B.; Pan, H. B.; Wai, C. M. *J. Phys. Chem. C* **2009**, *113*, 1520-1525.

(23) Yoon, B.; Wai, C. M. *J. Am. Chem. Soc.* **2005**, *127*, 17174-17175.

(24) Pawelec, B.; La Parola, V.; Navarro, R. M.; Murcia-Mascaros, S.; Fierro, J. L. G. *Carbon* **2006**, *44*, 84-98.

(25) Pan, H. B.; Wai, C. M. *J. Phys. Chem. C* **2009**, *113*, 19782-19788.

(26) Sun, Z. Y.; Liu, Z. M.; Han, B. X.; Wang, Y.; Du, J. M.; Xie, Z. L.; Han, G. J. *Adv. Mater.* **2005**, *17*, 928-932.

(27) Zahmakiran, M.; Tonbul, Y.; Ozkar, S. *J. Am. Chem. Soc.* **2010**, *132*, 6541-6549.

(28) Zahmakiran, M.; Ozkar, S. *Langmuir* **2008**, *24*, 7065-7067.

(29) Hiyoshi, N.; Rode, C. V.; Sato, O.; Masuda, Y.; Yamaguchi, A.; Shirai, M. *Chem. Lett.* **2008**, *37*, 734-735.

(30) Su, F.; Lv, L.; Lee, F. Y.; Liu, T.; Cooper, A. I.; Zhao, X. S. *J. Am. Chem. Soc.* **2007**, *129*, 14213-14223.

(31) Zhang, Z. G.; Okada, K.; Yamamoto, M.; Yoshida, T. *Catalysis Today* **1998**, *45*, 361-366.

(32) Park, I. S.; Kwon, M. S.; Kang, K. Y.; Lee, J. S.; Park, J. *Adv. Synth. Catal.* **2007**, *349*, 2039-2047.

(33) Lin, S. D.; Vannice, M. A. *J. Catal.* **1993**, *143*, 554-562.

(34) Cunha, D. S.; Cruz, G. M. *Appl. Catal., A* **2002**, *236*, 55-66.

(35) Mevellec, V.; Nowicki, A.; Roucoux, A.; Dujardin, C.; Granger, P.; Payen, E.; Philippot, K. *New J. Chem.* **2006**, *30*, 1214-1219.

(36) Marconi, G.; Pertici, P.; Evangelisti, C.; Caporusso, A. M.; Vitulli, G.; Capannelli, G.; Hoang, M.; Turney, T. W. *J. Organomet. Chem.* **2004**, *689*, 639-646.

(37) Spinace, E. V.; Vaz, J. M. *Catal. Commun.* **2003**, *4*, 91-96.

(38) Yuan, T.; Fournier, A. R.; Proudlock, R.; Marshall, W. D. *Environ. Sci. Technol.* **2007**, *41*, 1983-1988.

(39) Dominguez-Quintero, O.; Martinez, S.; Henriquez, Y.; D'Ornelas, L.; Krentzien, H.; Osuna, J. *J. Mol. Catal. A: Chem.* **2003**, *197*, 185-191.

(40) Lang, H. F.; May, R. A.; Iversen, B. L.; Chandler, B. D. *J. Am. Chem. Soc.* **2003**, *125*, 14832-14836.

(41) Pawelec, B.; Campos-Martin, J. M.; Cano-Serrano, E.; Navarro, R. M.; Thomas, S.; Fierro, J. L. G. *Environ. Sci. Technol.* **2005**, *39*, 3374-3381.

(42) Gao, H.; Angelici, R. J. *J. Am. Chem. Soc.* **1997**, *119*, 6937-6938.

(43) Marecot, P.; Mahoungou, J. R.; Barbier, J. *Appl. Catal., A* **1993**, *101*, 143-149.

(44) Zhao, A.; Gates, B. C. *J. Catal.* **1997**, *168*, 60-69.

(45) Ioannides, T.; Verykios, X. E. *J. Catal.* **1993**, *143*, 175-186.

(46) Crump, C. J.; Gilbertson, J. D.; Chandler, B. D. *Topics in Catalysis* **2008**, *49*, 233-240.

(47) Lin, S. D.; Vannice, M. A. *J. Catal.* **1993**, *143*, 539-553.

(48) Takagi, H.; Isoda, T.; Kusakabe, K.; Morooka, S. *Energy & Fuels* **1999**, *13*, 1191-1196.

(49) Santana, R. C.; Jongpatiwut, S.; Alvarez, W. E.; Resasco, D. E. *Ind. Eng. Chem. Res.* **2005**, *44*, 7928-7934.

(50) Owusu-Boakye, A.; Dalai, A. K.; Ferdous, D.; Adjaye, J. *Energy & Fuels* **2005**, *19*, 1763-1774.

(51) Hu, L.; Xia, G.; Qu, L.; Li, M.; Li, C.; Xin, Q.; Li, D. *J. Catal.* **2001**, *202*, 220-228.

(52) Venezia, A. M.; La Parola, V.; Pawelec, B.; Fierro, J. L. G. *Appl. Catal., A* **2004**, *264*, 43-51.

(53) Wan, G.; Duan, A.; Zhao, Z.; Jiang, G.; Zhang, D.; Li, R.; Dou, T.; Chung, K. H. *Energy & Fuels* **2009**, *23*, 81-85.

(54) Gelman, F.; Avnir, D.; Schumann, H.; Blum, J. *J. Mol. Catal. A: Chem.* **2001**, *171*, 191-194.

(55) Thomas, J. M.; Johnson, B. F. G.; Raja, R.; Sankar, G.; Midgley, P. A. *Acc. Chem. Res.* **2003**, *36*, 20-30.

(56) Fujikawa, T.; Idei, K.; Ebihara, T.; Mizuguchi, H.; Usui, K. *Appl. Catal., A* **2000**, *192*, 253-261.

(57) Hoover, N. N.; Auten, B. J.; Chandler, B. D. *J. Phys. Chem. B* **2006**, *110*, 8606-8612.

(58) Sidhpuria, K. B.; Parikh, P. A.; Bahadur, P.; Jasra, R. V. *Ind. Eng. Chem. Res.* **2008**, *47*, 4034-4042.

(59) Yang, X.; Yan, N.; Fei, Z.; Crespo-Quesada, R. M.; Laurenczy, G.; Kiwi-Minsker, L.; Kou, Y.; Li, Y.; Dyson, P. J. *Inorg. Chem.* **2008**, *47*, 7444-7446.

(60) Mu, X. D.; Meng, J. Q.; Li, Z. C.; Kou, Y. *J. Am. Chem. Soc.* **2005**, *127*, 9694-9695.

(61) Leger, B.; Denicourt-Nowicki, A.; Olivier-Bourbigou, H.; Roucoux, A. *Inorg. Chem.* **2008**, *47*, 9090-9096.

(62) Zhao, C.; Wang, H. Z.; Yan, N.; Xiao, C. X.; Mu, X. D.; Dyson, P. J.; Kou, Y. *J. Catal.* **2007**, *250*, 33-40.

(63) Prechtl, M. H. G.; Scariot, M.; Scholten, J. D.; Machado, G.; Teixeira, S. R.; Dupont, J. *Inorg. Chem.* **2008**, *47*, 8995-9001.

(64) Schulz, J.; Roucoux, A.; Patin, H. *Chem. Commun.* **1999**, 535-536.

(65) Pellegatta, J. L.; Blandy, C.; Colliere, V.; Choukroun, R.; Chaudret, B.; Cheng, P.; Philippot, K. *J. Mol. Catal. A: Chem.* **2002**, *178*, 55-61.

(66) Fahlman, B. D. *Materials Chemistry*; Springer, 2007.

(67) Lopez, T.; Bosch, P.; Moran, M.; Gomez, R. *J. Phys. Chem.* **1993**, *97*, 1671-1677.

(68) Klein, J.; Lettmann, C.; Maier, W. F. *J. Non-Cryst. Solids* **2001**, *282*, 203-220.

(69) Frenzer, G.; Maier, W. F. *Ann. Rev. Mater. Res.* **2006**, *36*, 281-331.

(70) Maier, W. F. *Angew. Chem., Int. Ed.* **1999**, *38*, 1216-1218.

(71) Bein, T. *Angew. Chem., Int. Ed.* **1999**, *38*, 323-326.

(72) Scheidtmann, J.; Weib, P. A.; Maier, W. F. *Appl. Catal., A* **2001**, *222*, 79-89.

(73) Maier, W. F.; Stowe, K.; Sieg, S. *Angew. Chem., Int. Ed.* **2007**, *46*, 6016-6067.

(74) Crabtree, R. H. *Chem. Commun.* **1999**, 1611-1616.

(75) Kirsten, G.; Maier, W. F. *Applied Surface Science* **2004**, *223*, 87-101.

(76) Shimizu, K. D.; Snapper, M. L.; Hoveyda, A. H. *Chem. Eur. J.* **1998**, *4*, 1885-1889.

(77) Liu, D. R.; Schultz, P. G. *Angew. Chem., Int. Ed.* **1999**, *38*, 36-54.

(78) Xiang, X. D.; Sun, X.; Briceno, G.; Lou, Y.; Wang, K. A.; Chang, H.; Wallace-Freedman, W. G.; Chen, S. W.; Schultz, P. G. *Science* **1995**, *268*, 1738-1740.

(79) Briceno, G.; Chang, H.; Sun, X.; Schultz, P. G.; Xiang, X. D. *Science* **1995**, *270*, 273-275.

(80) Wang, J.; Yoo, Y.; Gao, C.; Takeuchi, I.; Sun, X.; Chang, H.; Xiang, X.-D.; Schultz, P. G. *Science* **1998**, *279*, 1712-1715.

(81) Danielson, E.; Golden, J. H.; McFarland, E. W.; Reaves, C. M.; Weinberg, W. H.; Wu, X. D. *Nature* **1997**, *389*, 944-948.

(82) Danielson, E.; Devenney, M.; Giaquinta, D. M.; Golden, J. H.; Haushalter, R. C.; McFarland, E. W.; Poojary, D. M.; Reaves, C. M.; Weinberg, W. H.; Wu, X. D. *Science* **1998**, *279*, 837-840.

(83) Holzwarth, A.; Schmidt, H. W.; Maier, W. E. *Angew. Chem., Int. Ed.* **1998**, *37*, 2644-2647.

(84) Moates, F. C.; Somani, M.; Annamalai, J.; Richardson, J. T.; Luss, D.; Willson, R. C. *Ind. Eng. Chem. Res.* **1996**, *35*, 4801-4803.

(85) Orschel, M.; Klein, J.; Schmidt, H. W.; Maier, W. F. *Angew. Chem., Int. Ed.* **1999**, *38*, 2791-2794.

(86) Woodhouse, M.; Parkinson, B. A. *Chem. Mater.* **2008**, *20*, 2495-2502.

Chapter 2

Bimetallic Catalysts for Toluene Hydrogenation

2.1 Introduction

In northern Alberta, vast areas of land contain oil sands deposits, of which bitumen is one of the main components. There are over 173 billion barrels of recoverable reserves represented by the verified deposits in Alberta, which cover approximately 140,000 square kilometers of land.[1] Bitumen is composed of asphaltenes, complex arenes, cycloparaffins and other hetero-atom containing compounds of high molecular weights, all of which must be removed before most direct uses.[2] Specifically, hydrogenation of the large polyaromatic hydrocarbons found in bitumen is one of the steps involved in upgrading bitumen into synthetic crude oil, and thus this challenging catalytic reaction is of great importance to the petrochemical industry.[2-5] This reaction is, however, difficult due to the stability of the aromatic rings, and thus harsh conditions are required in excess of 340ºC and 1000 psi to achieve successful hydrogenation.[5] In addition, under typical hydrotreating conditions, the hydrogenation reaction becomes reversible, so it is not possible to obtain complete hydrogenation of the large polyaromatic hydrocarbons due to equilibrium limitations.[6] Further complicating matters, metal catalysts are vulnerable to poisoning due to the sulfur and nitrogen contaminants found in bitumen.[7] All these factors increase crude oil costs and thus it is of interest to find new families of catalysts that can function with less energy input, are

sulfur and nitrogen tolerant, and are selective with respect to the desired hydrogenation products.

Bimetallic Nanoparticle Catalysts

Nanoparticle catalysts have been used for a wide variety of reactions including both olefin[8,9] and arene[5-7,9-64] hydrogenations. The order of activity of the noble metal catalysts that are often used for the heterogeneous hydrogenation of arenes follows the order Rh > Ru > Pt > Ni > Pd.[28] The use of Rh and Ru nanoparticles for arene hydrogenation has been widely reported, while there are fewer examples of Pd, Pt and Ni being used.[56] Both mono-[6,10-50,63,65-74] and bimetallic[5,7,11,12,51-55,60] nanoparticle catalysts have been studied for arene hydrogenation, and bimetallic catalysts are of particular interest, due to the potential for enhanced activity and an increased tolerance to sulfur and nitrogen contaminants.[7] For example, Yoon demonstrated that a bimetallic RhPd/CNT catalyst had an unusually high catalytic activity for the hydrogenation of anthracene at 147 psi H_2 and 25ºC when compared to the monometallic Rh/CNT and Pd/CNT catalysts.[12] In 2009, Yoon also showed while Au/CNT and Pd/CNT catalysts had a negligible activity for the room temperature hydrogenation of benzene, the Pd-Au/CNT catalyst had a much higher activity.[11]

Several different bimetallic nanoparticle structures can be formed upon the introduction of a second metal, including core-shell, alloy and cluster-in-cluster structures (Fig. 2.1). While alloy, and to some extent cluster-in-cluster structures can form simply by incorporating a second metal, typically core-shell structures require a more directed synthesis. To prepare core-shell structures, typically a small nanoparticle or "seed" is

synthesized first, followed by controlled growth of the shell on top of the nanoparticle seed. When preparing bimetallic nanoparticles it is also critical to make sure that the two metals are in physical contact with each other, and that monometallic nanoparticles of the two different metals have not been formed.

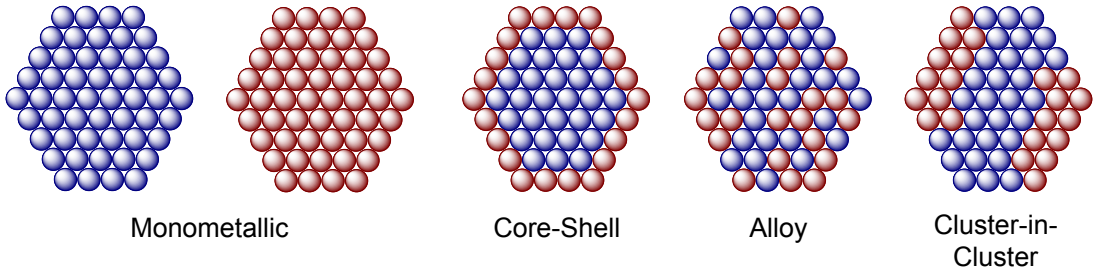

Figure 2.1. Various mono- and bimetallic nanoparticle structures.

Monoaromatic Hydrogenation

The field of arene hydrogenation is well established industrially with a variety of heterogeneous catalysts being used (e.g., Raney nickel, metal sulfides, and CoMo, MoW and NiMo supported on alumina),[2,5,13,75] but relatively harsh conditions are required to achieve required catalyst activities. As a result, there has been interest in developing catalysts that are active under milder conditions. For example, Rh nanoparticles stabilized by copolymers demonstrated a TOF (turnover frequency) of 250 h^{-1} and a TTO (total turnover) of 20 000 mol/mol Rh for benzene hydrogenation at 580 psi H_2 and 75ºC.[30,31] Magnetically recoverable Rh nanoparticles were very active for benzene hydrogenation with a TOF of 825 h^{-1} at 88 psi H_2 and 75ºC.[32] Pillai reported a TOF of 6600 h^{-1} for benzene hydrogenation and 4950 h^{-1} for toluene hydrogenation at 290 psi H_2 and 40ºC using Rh nanoparticles on multi-walled carbon nanotubes.[10] Ambient conditions (15 psi H_2, 22ºC) however, are obviously the most challenging for arene

hydrogenation and there are very few examples in the literature.[17,18,26-28,72] Roucoux showed that unsupported Rh nanoparticles were active for benzene and toluene hydrogenation under ambient conditions (15 psi H_2, 20ºC) with TOFs of 57 h^{-1} and 53 h^{-1}, respectively (TOF reported as mol H_2 per mol of Rh).[26] Park used Rh nanoparticles on charcoal to hydrogenate benzene and toluene under ambient conditions with TOFs of 600 h^{-1} for each substrate (TOF reported as mol of H_2 consumed per mol of total metal per hour).[72]

Shown below (Fig. 2.2) is a proposed mechanism for aromatic hydrogenation using a heterogeneous catalyst similar to that proposed by Horiuti-Polanyi.[76] The reaction begins with hydrogen activation through the dissociative adsorption of hydrogen onto the metal surface and adsorption of the aromatic substrate also onto the metal surface. Next, reversible insertion of one of the hydrogen atoms occurs followed by irreversible insertion of the second hydrogen atom. Because no partially hydrogenated intermediates were detected during the course of the catalytic reaction, it is unlikely that the aromatic substrate desorbs from the surface of the support at this point in the process. Then the hydrogen activation and insertion steps continue to occur. To terminate the catalytic cycle, it is likely that reductive elimination occurs giving the fully hydrogenated product and the regenerated catalyst. Support for the pairwise addition of hydrogen atoms comes from the use of parahydrogen-induced polarization (PHIP) for study of alkene hydrogenation on heterogeneous catalysts.[77]

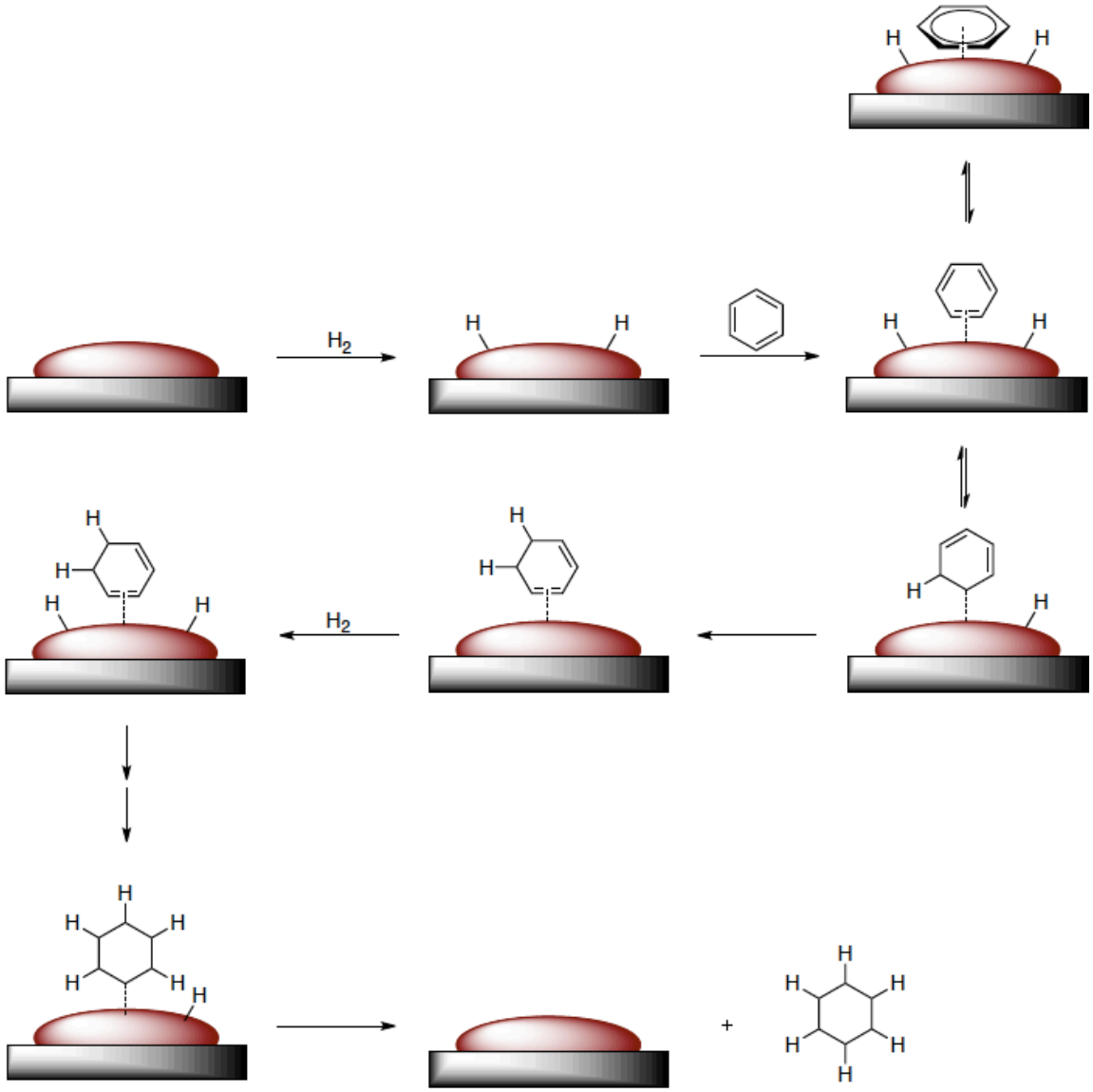

Figure 2.2. Proposed mechanism for aromatic hydrogenation using a heterogeneous nanoparticle catalyst.

Not only can spilled over hydrogen be used in hydrogenation reactions, it can also create active sites on some metal oxide surfaces.[68] For polyaromatic hydrocarbons, the hydrogenation process is also believed to proceed stepwise with partially hydrogenated

intermediates not being detected.[20] In addition, aromatic hydrogenation is exothermic, so selectivities can be increased by performing the reaction at a lower temperature.[20]

At present, a limited number of bimetallic combinations are known to be active as nanoparticle arene hydrogenation catalysts.[5,7,11,12,51-55,60] It would, therefore be interesting to screen a large number of bimetallic combinations, in parallel, to identify new bimetallic catalysts active for arene hydrogenation under mild conditions (15 psi H_2, 22ºC). Taking into account the many possible variables, including the ratio of the two metals, metal loading, support types, substrates, etc., it would be incredibly time consuming to test each individual catalyst one by one in an empirical fashion. Recently, combinatorial or high-throughput screening has proven to be an efficient means of synthesizing and screening large numbers of potential materials for a desired property, leading to much shorter discovery times.[78-91] Based on the prior success and potential of the combinatorial approach for catalyst synthesis and testing, a library of potential catalysts could be prepared and tested for arene hydrogenation activity under ambient conditions, allowing for efficient identification of active catalysts.

In this chapter, a variety of mono- and bimetallic nanoparticle catalysts supported on alumina were synthesized and assessed using a simple parallel screening approach, under ambient conditions, for toluene hydrogenation activity. In total, 91 catalysts were screened using thirteen representative transition metals from the first, second and third rows of the periodic table. One particularly active catalyst was identified and further characterized in bulk and studied (kinetics and materials characterizations) and is described here.

2.2 Results and Discussion

Catalyst Synthesis and Screening.

Supported nanoparticle catalysts have been made by a variety of methods, with one of the more common methods being the impregnation or incipient wetness approach.[17,19,92] This method is frequently employed in industrial applications and involves impregnation of a prefabricated metal oxide support by an aqueous solutions of metal salts.[93-95] This is then followed by drying of the catalyst and reduction of the metal salts under a flow of hydrogen at elevated temperatures (e.g. 500°C). Using this methodology, pioneering work was performed where several supported bimetallic heterogeneous catalysts (Ru-Cu and Ru-Os) were synthesized and were investigated for the hydrogenolysis of ethane to methane,[93,95] and the dehydrogenation of cyclohexane to benzene[93] where the effects on the catalytic activity as a function of the composition of the catalysts were examined. This is one of the first examples in the literature where the activity of a heterogeneous catalyst was investigated as a function of the composition of the catalyst.

Another approach involves a multi-step synthesis utilizing preformed stabilized nanoparticles that are then absorbed to the support.[92] In contrast, the *in situ* one-pot method used by Maier and others involves synthesizing the nanoparticles and the support simultaneously; the metal precursors and the water-sensitive metal alkoxide are mixed together and processed in one batch (Fig. 2.3).[83,96,97] These steps were followed by hydrolysis and condensation of the metal alkoxide to give the metal oxide in which the metal precursor is encapsulated. The metal precursor is not reduced to nanoparticles until the hydrogen anneal step is performed, leading to reduced metal nanoparticles on a metal

oxide support. The advantage of this approach is it is a one-pot method, no stabilizer is required for the nanoparticles to form, and it can be performed in laboratory ambient conditions, further simplifying the procedure.

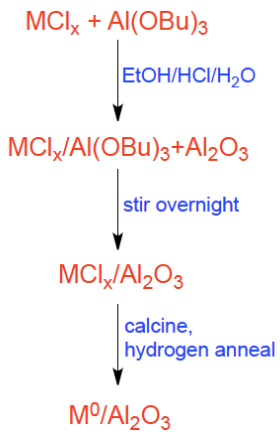

Figure 2.3. Scheme depicting the steps for catalyst synthesis.

For the combinatorial synthesis and screening of these heterogeneous catalysts, there were several crucial requirements in the design of the sample holders for us to synthesize and screen the nanocatalysts in a one pot *in situ* approach. First of all, one of the aims behind utilizing a combinatorial approach for the synthesis and screening of the nanocatalysts is they be synthesized in small amounts. Therefore, a sample holder whose volume would be sufficient for both synthesis and screening of nanoparticle catalysts was required. To determine the preferred volume of the sample holder, both the volume of solvent required for the synthesis, that of the solvent and substrate for the screening had to be considered. In addition, we had decided to monitor the catalytic reactions via gas chromatography, which required a minimum reaction volume so that a suitable amount of reaction solution could be analyzed to obtain well-resolved peaks in the gas chromatograph. Furthermore, both the sol-gel synthesis and screening required constant

stirring. Due to the scaled down quantities, very small glass coated stir bars were required. The stir bars had to be glass coated because the alumina catalyst support is very coarse and if Teflon coated stir bars were used, the Teflon would be worn away. To achieve adequate stirring, the sample holder had to fit on the surface of a stir plate, and therefore was limited to dimensions of the stir plate. In addition, to synthesize the catalysts using a one-pot *in situ* approach, a calcination and hydrogen anneal step were required and were performed in a tube furnace. Due to the dimensions of the quartz tube in the tube furnace, the size of the sample holder (specifically the height and width) were consequently also limited. The temperature at which the calcination and hydrogen anneal steps were performed also necessitates the stir bars and the sample holder be able to undergo these steps without subsequent deformation or melting, thereby demanding that they be made out of glass. Taken into account, all of the aforementioned requirements gave rise to the sample holder shown in Fig. 2.4.

Figure 2.4. Initial screening apparatus. Each sample holder has a volume of approximately 1 ml.

Metal chloride salts were used as the nanoparticle precursors, and over 90 mono- and bimetallic nanoparticle catalysts were synthesized and tested for arene hydrogenation activity based on the reaction shown at the top of Fig. 2.5. Since the goal of this work

was the development of air stable, easily handled and synthesized catalysts, all steps involved exposure to an open atmosphere. Our initial screening apparatus utilized a multi-well glass sample holder, as shown in Fig. 2.4, but cross-contamination by the volatile toluene precursor and methylcyclohexane product led to spurious results; a system that isolates each vessel was required in which each vessel has its own separate gas supply (Figures 2.6 and 2.7). The set up was very similar to that used previously except the sample holders were not connected together, allowing them to be isolated in vial capped with a septum. To allow for easy identification of the active catalysts and simple interpretation of the results, a visualization approach of the data was used, with the results shown in Fig. 2.5. The reactions were commenced and arrested after 4 hours to identify active catalyst combinations.

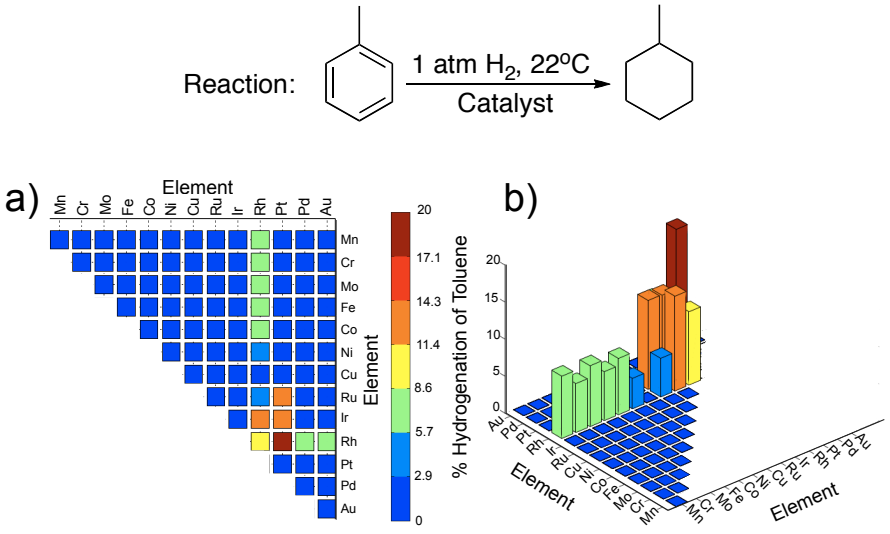

Figure 2.5. 3D bar graphs a) (top down view) and b) (side view) of screening results. The x- and y- axes represent the different transition metals used, with the z- axis showing the percent hydrogenation after four hours.

Figure 2.6. Modified sample holder and testing set-up. Each individual sample holder has a volume of approximately 2 ml. The sample holder was placed in a 20 ml glass vial and was capped with a 14/20 septum.

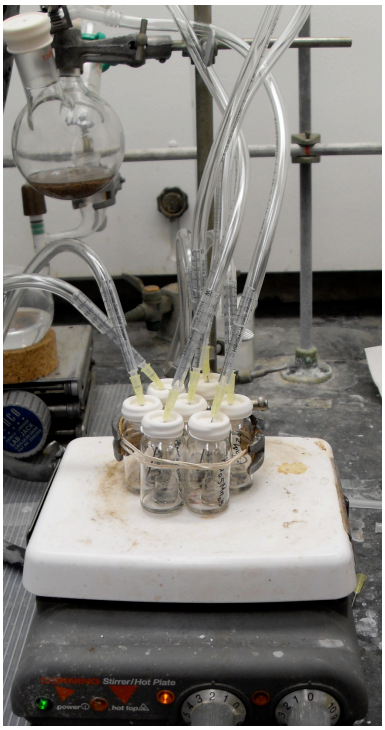

Figure 2.7. Catalyst screening set up. The seven vials were secured with rubber bands and centered on the stir plate. Each vial has its own gas line to provide H_2, effectively isolating it from the other vials.

As can be seen from the side view of the bar graphs shown in Fig. 2.5b, there are several catalysts that are active, and a large number of inactive combinations under the screening conditions. From the top down view of the 3D bar graph (Fig. 2.5a), it can be easily identified that bimetallic catalysts containing Rh were the most consistent for activity, with the exception of the RhCu combination. The deactivation of a catalytically active metal upon incorporation of Cu has been observed before with a PtCu bimetallic catalyst, and was attributed to an enrichment of catalytically inactive copper on the surface of the nanoparticles.[98] From the screening results, the most active catalysts were

identified to be $Rh_{0.5}Pt_{0.5}/Al_2O_3$, $Ir_{0.5}Pt_{0.5}/Al_2O_3$, $Ru_{0.5}Pt_{0.5}/Al_2O_3$, $Ir_{0.5}Rh_{0.5}/Al_2O_3$, and Rh_1/Al_2O_3 in order of highest activity to lowest activity, and the results obtained for $Rh_{0.5}Pt_{0.5}/Al_2O_3$ were performed in triplicate. It is of note that the monometallic Ru_1/Al_2O_3, Pt_1/Al_2O_3 and Ir_1/Al_2O_3 catalysts were inactive for the hydrogenation of toluene under these conditions, but upon alloying with Rh or Pt, the bimetallic catalysts exhibited a higher activity than either of their parent metals. For all of the screened catalysts, only methylcyclohexane was observed as a hydrogenation product, with no partially hydrogenated or ring opening products detected by gas chromatography.

From the screening results, the four most active bimetallic catalysts ($Rh_{0.5}Pt_{0.5}/Al_2O_3$, $Ir_{0.5}Pt_{0.5}/Al_2O_3$, $Ru_{0.5}Pt_{0.5}/Al_2O_3$, and $Ir_{0.5}Rh_{0.5}/Al_2O_3$) were then screened again using varying ratios of the two metals in 10% increments while holding the metal loading constant at 1 mol %. These results are shown in Fig. 2.8. In the case of RhIr (Fig. 2.8a), the more active catalysts were those that are richer in Rh, whereas with RhPt (Fig. 2.8b) the more active catalysts were those that were richer in Pt. In contrast to these trends, with IrPt and RuPt (Fig. 2.8c and 2.8d), the most active catalysts were those that have approximately equal amounts of the two metals.

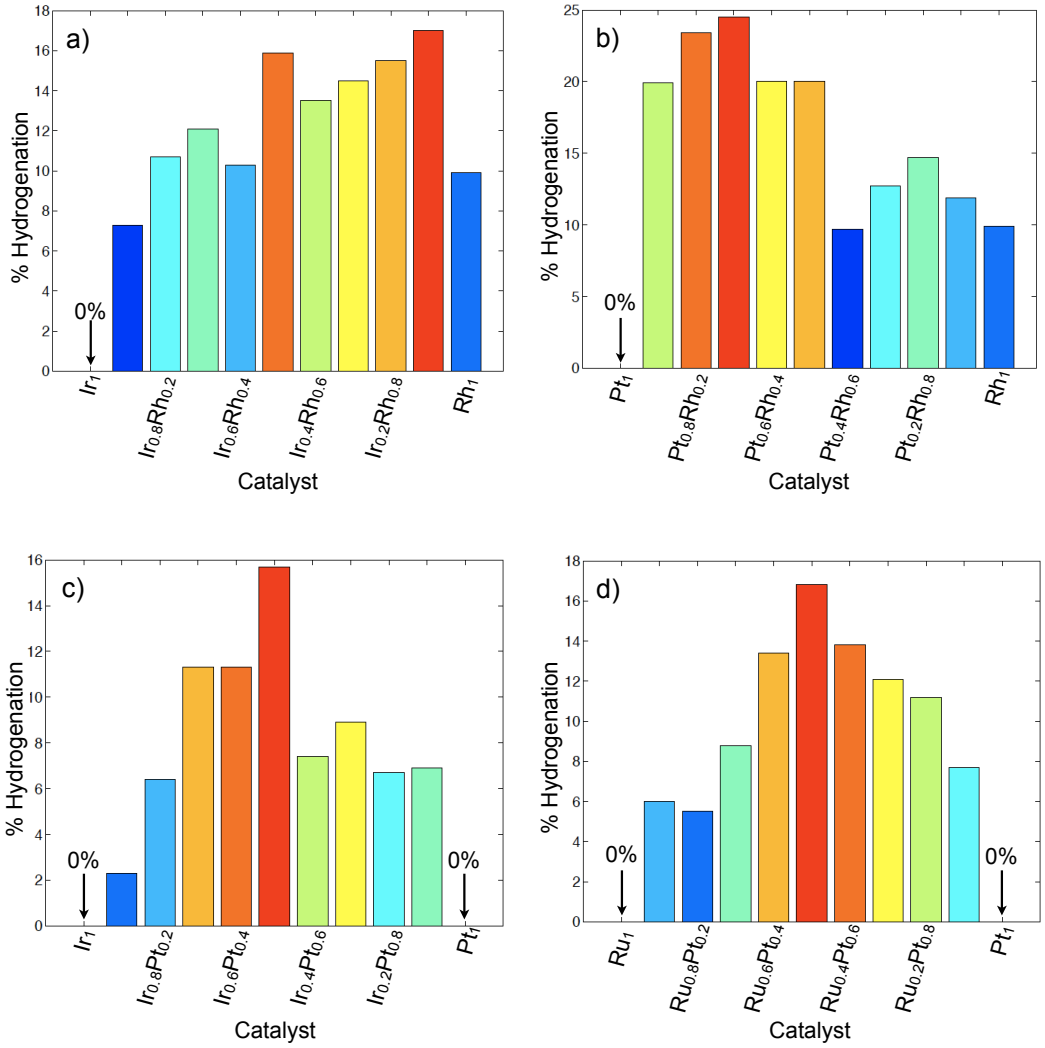

Figure 2.8. Bar graphs with varying ratios of metals, metal loading held constant at 1 mol%. a) $IrRh/Al_2O_3$, b) $RhPt/Al_2O_3$, c) $IrPt/Al_2O_3$, d) $RuPt/Al_2O_3$. The percent hydrogenation was measured after 4 hours.

The five most active catalysts ($Rh_{0.5}Pt_{0.5}/Al_2O_3$, $Ir_{0.5}Pt_{0.5}/Al_2O_3$, $Ru_{0.5}Pt_{0.5}/Al_2O_3$, $Ir_{0.5}Rh_{0.5}/Al_2O_3$, and Rh_1/Al_2O_3) were synthesized and tested in bulk (using ~0.4 g of catalyst per reaction) to confirm their activity with the results shown in Table 2.1. Toluene hydrogenation reactions were performed at atmospheric pressure and

temperature in laboratory batch reactors. The progress of the reactions was monitored through gas chromatography in which no partially hydrogenated intermediates were detected, only the fully hydrogenated product of methylcyclohexane, which was also confirmed for a representative reaction by GC-MS. The observed rate (obs. rate) relative to the methylcyclohexane hydrogenation product was calculated during the first two hours of hydrogenation results, where

$$\text{obs. rate} = \frac{\text{mol methylcyclohexane / mol metal in catalyst}}{\text{time (h)}}$$

As can be seen from Table 2.1, entries 1-5, $Rh_{0.5}Pt_{0.5}/Al_2O_3$was confirmed to be the most active catalyst with an observed rate of 24.9 $\pm$ 2.8 h^{-1} based on experiments performed in triplicate. The next most active catalysts were determined to be $Ir_{0.5}Pt_{0.5}/Al_2O_3$ and $Ru_{0.5}Pt_{0.5}/Al_2O_3$ followed by $Ir_{0.5}Rh_{0.5}/Al_2O_3$. The trends in bulk activity correspond well with the trends observed for the screening results (Fig. 2.9), validating the screening results. While none of these bimetallic catalysts have been previously reported as arene hydrogenation catalysts with the exception of RuPt (Midgley reported Ru_5Pt_1 and $Ru_{10}Pt_2$ to be successful benzene hydrogenation catalysts at 80ºC and 290 psi H_2 pressure[53]), it is of note that RuPt nanoparticles have been previously used as a catalyst for preferential CO oxidation in the presence of hydrogen feeds,[99,100] RhPt nanoparticles have been used as CO oxidation catalysts[101,102] and the RhPt combination has been used as an electrocatalyst for the dehydrogenative oxidation of cyclohexane to benzene.[103]

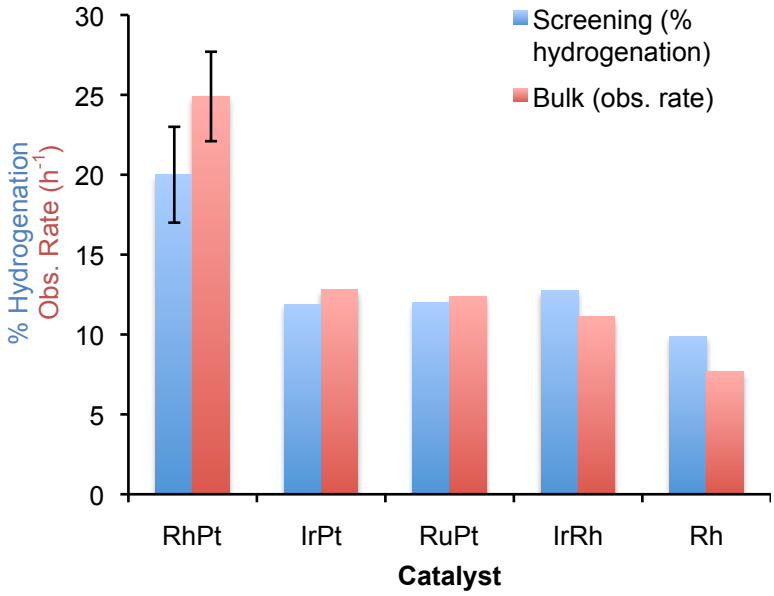

Figure 2.9. Comparison of trends observed in screening results with those obtained in bulk. Shown in blue are the screening results, with the y-axis representing the % hydrogenation after 4 hours. Shown in red are the bulk results, with the y-axis representing the observed rate (obs. rate). RhPt: 20 $\pm$ 3% (screening, performed in triplicate), 24.9 $\pm$ 2.8 h^{-1} (bulk, performed in triplicate). IrPt: 11.85% (screening), 12.8 h^{-1} (bulk). RuPt: 12% (screening), 12.4 h^{-1} (bulk). IrRh: 12.75% (screening), 11.1 h^{-1} (bulk). Rh: 9.9% (screening), 7.7 h^{-1} (bulk).

Batch Toluene Hydrogenation Results.

Since the RhPt bimetallic combination led to the highest observed rate, this catalyst system was studied in further detail. Toluene hydrogenation reactions were performed on the alumina supported RhPt bimetallic catalyst in bulk in a laboratory batch reactor. Observed rates were measured during the first two hours of the hydrogenation reaction and normalized against the number of moles of metal in the catalyst. A number

of parameters were varied, including metal loading, temperature, amount of substrate and hydrogen pressure, to determine the effect these variables would have on the observed rates of the RhPt catalyst. A CS_2 poisoning study was also performed on the RhPt catalyst to determine the number of catalytically active sites in the catalyst.[104] The hydrogenation of toluene was performed using ethanol as solvent (Table 2.1, entry 6), and a decrease in the observed rate of the catalyst was observed; therefore isopropanol was used as the solvent for the remainder of this study. The metal loading of the RhPt catalyst was varied between 0.5% and 5% while holding the ratios of Rh and Pt constant (Table 2.1, entries 7-9). It was found that the observed rate increased slightly as the loading was decreased to 0.5% but with metal loadings of 2% and 5%, the observed rate greatly decreased.

Table 2.1. Batch Toluene Hydrogenation Results.[a]

Entry	Catalyst[b]	Obs. rate [h^{-1}]	% Conv. (2 h)	% Conv. (7 h)
1	Rh_1	7.7	17.8	58
2	$Ir_{0.5}Rh_{0.5}$	11.1	22.8	36
3	$Ir_{0.5}Pt_{0.5}$	12.8	27.2	47
4	$Ru_{0.5}Pt_{0.5}$	12.4	23.1	52
5	$Rh_{0.5}Pt_{0.5}$[c]	24.9	51.3	90
6	$Rh_{0.5}Pt_{0.5}$[d]	14.6	26.2	54
7	$Rh_{0.25}Pt_{0.25}$	27.1	45.4	85.3
8	Rh_1Pt_1	6.2	14.4	46.0
9	$Rh_{2.5}Pt_{2.5}$	5.0	12.2	42.9

[a]**Reaction conditions:** 3.8 x 10^{-5} mol metal, 10.0 ml isopropanol substrate/cat. = 100:1 = 3.8 x 10^{-3} mol toluene, 22ºC, 15 psi H_2

[b]All catalysts were supported on Al_2O_3, with the subscripts indicating the mol% of the metals.

[c]Observed rate based on results obtained in triplicate, and is given as the average of the three results.

[d]Ethanol used as the solvent instead of isopropanol.

The temperature of the hydrogenation reaction was increased to determine the range of temperatures in which the catalyst was active. Initially, the temperature of the hydrogenation reaction was varied in 20-degree increments from 0ºC to 80ºC, and the results are shown in Fig. 2.10a. The observed rate of the reaction increased somewhat linearly with respect to temperature, with the maximum rate occurring at 60ºC. At the highest temperature studied (80ºC), there was a substantial decrease in activity, suggesting that deactivation of the catalyst was occurring. To allow for comparison among other known arene hydrogenation catalysts, the hydrogenation of toluene was examined, in triplicate, between 0ºC and 40ºC to calculate the activation energy. The

initial rates were measured during the first 30 minutes of the toluene hydrogenation reaction. The results were plotted in an Arrhenius plot (Fig. 2.10b), and the activation energy was calculated to be 30.4 kJ/mol. This activation energy is moderate when compared to those previously reported for arene hydrogenation. Dupont, for instance, reported an activation energy of 42.0 kJ/mol for the hydrogenation of toluene with Ru nanoparticles[50] and Somorjai reported activation energies of 34.7 kJ/mol and 45.6 kJ/mol for benzene hydrogenation with cuboctahedral and cubic Pt nanoparticles, respectively.[29] Because we obtained a lower activation energy than those commonly encountered in the literature, it suggests that a lower amount of energy is required to initiate the hydrogenation reaction which is why our bimetallic $Rh_{0.5}Pt_{0.5}/Al_2O_3$ catalyst is active under ambient conditions while so many catalysts are not.

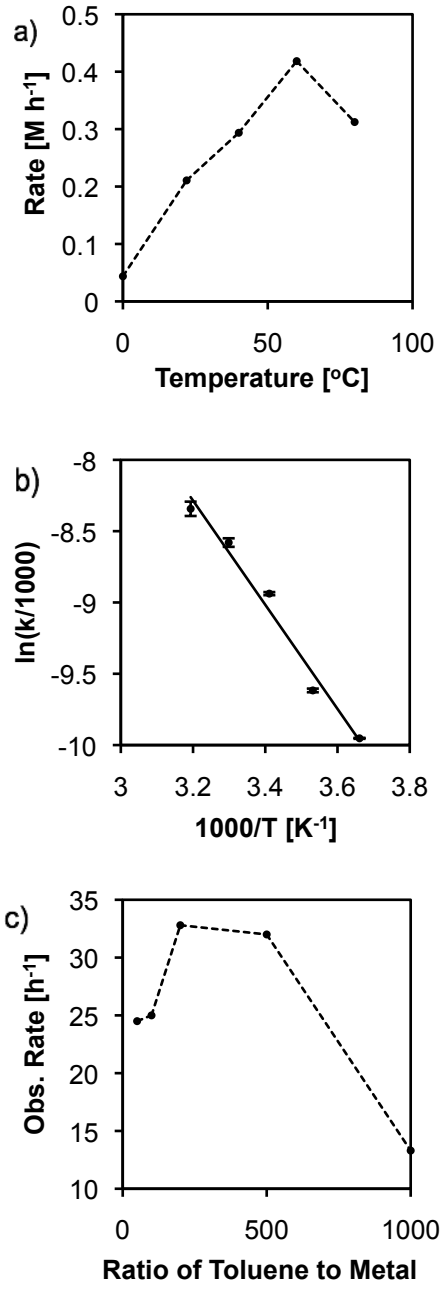

Figure 2.10. a) Rate as a function of temperature for toluene hydrogenation. b) Arrhenius plot, with the slope of the trend line equaling -3.65. c) Observed rate as a function of the ratio of toluene to metal. Lines within the plots are drawn merely as a visual aide.

The molar ratio of toluene to metal in the catalyst was varied at ratios of 50, 200, 500 and 1000, with the results shown in Fig 2.10c. The highest observed rates were obtained for the ratios of 200 and 500. When the ratio was further increased to 1000, there was a substantial decrease in activity, suggestive of substrate inhibition. Preliminary pressure studies were also done, and showed a relatively linear increase in reaction rate versus hydrogen pressure (Fig. 2.11).

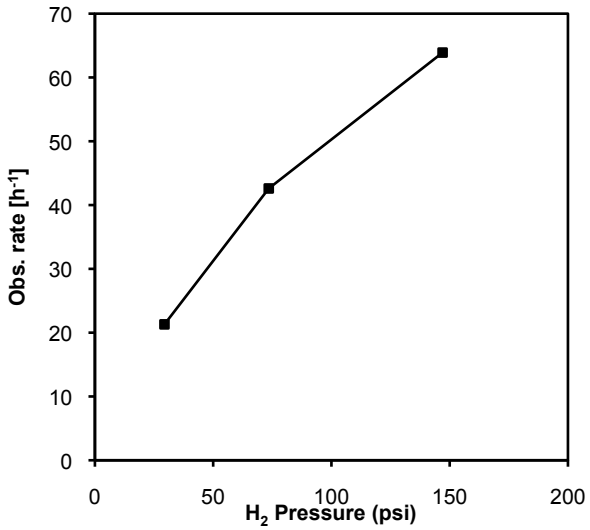

Figure 2.11. Observed rate as a function of H_2 pressure for the hydrogenation of toluene using $Rh_{0.5}Pt_{0.5}/Al_2O_3$. The line is drawn as a visual aide.

To determine the number of catalytically active sites present, and to allow for more accurate comparison of the activities of different catalysts, a series of CS_2 poisoning experiments were performed on the $Rh_{0.5}Pt_{0.5}/Al_2O_3$ and commercial 0.5% Rh/Al_2O_3 catalysts in triplicate.[104] Known amounts of CS_2 were added to the toluene hydrogenation reaction, and the activity of the catalysts was measured by determining the amount of

hydrogen consumed as a function of time. The rates of the unpoisoned $Rh_{0.5}Pt_{0.5}/Al_2O_3$ and 0.5% Rh/Al_2O_3 catalysts were measured at an initial pressure of 73 psig H_2 and 295 K, and the results are shown in Table 2.2. Using these rates, the TOFs were calculated based on the molar amount of metal used, which was the same for the two different catalysts. As already shown in Table 2.2, the $Rh_{0.5}Pt_{0.5}/Al_2O_3$ catalyst is more active, with a TOF of 43.8 h^{-1}, than the 0.5% Rh/Al_2O_3 catalyst which has a TOF of 27.2 h^{-1}. Upon performing the poisoning studies, the amount of CS_2 required to completely deactivate each catalyst was calculated to be 0.081 mol CS_2 / mol total metal for the $Rh_{0.5}Pt_{0.5}/Al_2O_3$ catalyst and 0.046 mol CS_2 / mol total metal for the 0.5% Rh/Al_2O_3 catalyst (Fig. 2.12). The higher value for the $Rh_{0.5}Pt_{0.5}/Al_2O_3$ catalyst suggests that there are more catalytically active sites present in this bimetallic catalyst than in the commercial catalyst. Hornstein *et al* assumed a 1/5 poison to metal-atom stoichiometry ratio to calculate corrected TOF values for each catalyst.[104] Based on this assumption, the corrected TOFs for the $Rh_{0.5}Pt_{0.5}/Al_2O_3$ and the 0.5% Rh/Al_2O_3 catalysts are 108 h^{-1} and 118 h^{-1}, respectively. Although these values for the corrected TOFs are similar, the need for a higher quantity of catalyst poison (CS_2) for the bimetallic catalysts suggests that there are more active (but less reactive) sites than in the commercial 0.5% Rh/Al_2O_3 catalyst.

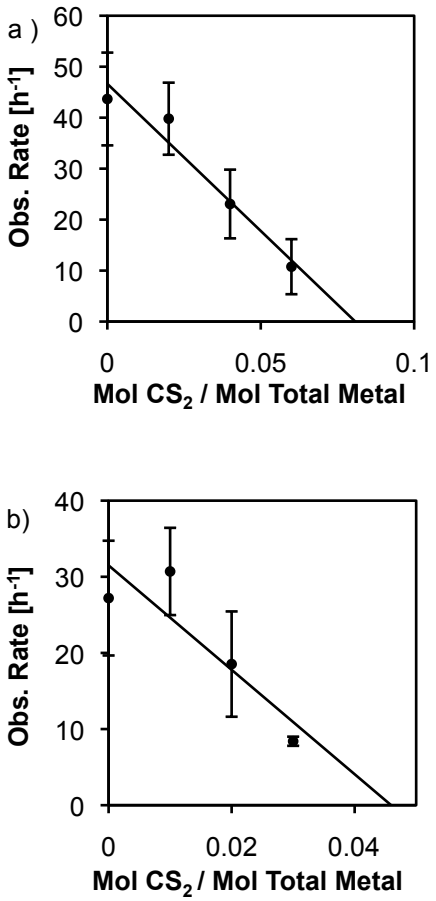

Figure 2.12. Plot of observed rate vs moles of CS_2 / moles of total metal for the hydrogenation of toluene by a) $Rh_{0.5}Pt_{0.5}/Al_2O_3$ and b) 0.5% Rh/Al_2O_3. Observed rates were measured by following the H_2 pressure as a function of time for 1 h in triplicate. The $x_{intercept}$ for $Rh_{0.5}Pt_{0.5}/Al_2O_3$ is 0.081 mol of CS_2 / mol of total metal and for 0.5% Rh/Al_2O_3 is 0.046 mol of CS_2 / mol of total metal.

Table 2.2. Summary of the CS_2 Poisoning Results and Catalytic Activities of the Prepared $Rh_{0.5}Pt_{0.5}/Al_2O_3$ and Commercial 0.5% Rh/Al_2O_3 Catalysts.[a]

	$Rh_{0.5}Pt_{0.5}/Al_2O_3$	0.5% Rh/Al_2O_3
rate[b]	0.76 ± 0.16 psi/h	0.47 ± 0.13 psi/h
TOF	43.8 h^{-1}	27.2 h^{-1}
mol CS_2 / mol total metal[c]	0.081	0.046
TOF (corrected)[d]	108 h^{-1}	118 h^{-1}
Rel. TOF	1	1.09

[a]Catalytic activities measured at 73 psig initial H_2 pressure, 295 K

[b]Values based on 3.8 x 10^{-5} mol of total metal.

[c]Ratio of mol CS_2 / mol total metal required to deactivate catalyst. Determined from results shown in Fig. 2.12.

[d]TOF is corrected for active Rh and Pt atoms determined by CS_2 poisoning and using a 1/5 poison/metal stoichiometry ratio, as previously described by Hornstein *et al*.[104]

Materials Characterization

Since the synthesis is based upon a one-pot *in situ* production of both the support and the nanoparticles simultaneously, little is known about the morphology or structure of the resulting catalyst. From the TEM image of $Rh_{0.5}Pt_{0.5}/Al_2O_3$ catalyst (Fig. 2.13a) the size of the nanoparticles was measured to be 3.1 ± 1.0 nm. When TEM images were obtained upon the completion of the hydrogenation reaction using the $Rh_{0.5}Pt_{0.5}/Al_2O_3$ catalyst, the size of the nanoparticles was measured to be 3.3 ± 1.1 nm, indicating no significant change in size or morphology of the nanoparticles during the course of the reaction (Fig. 2.14). The size of the nanoparticles in the $Ir_{0.5}Pt_{0.5}/Al_2O_3$ catalyst was measured to be 2.9 ± 0.9 nm (Fig. 2.13b), 3.8 ± 1.2 nm for the $Ir_{05}Rh_{0.5}/Al_2O_3$ catalyst

(Fig. 2.13c), 4.2 ± 1.5 nm for the $Ru_{0.5}Pt_{0.5}/Al_2O_3$ catalyst (Fig. 2.13d), and 5.2 ± 1.6 nm for the commercial 0.5% Rh/Al_2O_3 catalyst (Fig. 2.13e). From the nanoparticle sizes obtained from the TEM images, the surface areas of each catalyst may be calculated and the TOF determined taking into account the total surface area of the catalyst used for a given reaction. For each catalytic reaction performed in bulk, 3.8×10^{-5} mol of metal was used, and this amount of metal was used to calculate the total surface area. One assumption was also made when determining the surface area of the catalyst: only 66% of the total surface area was available due to the portion of each metal nanoparticle encapsulated by the metal oxide support. So for the $Rh_{0.5}Pt_{0.5}/Al_2O_3$ catalyst, a total surface area of 0.433 m^2 was calculated, and for the commercial 0.5% Rh/Al_2O_3 catalyst a surface area of 0.240 m^2 was determined. While these values are within an order of magnitude, they do give very similar corrected TOF values. Using the data and TOF values given in Table 2.2, for the $Rh_{0.5}Pt_{0.5}/Al_2O_3$ catalyst, a TOF (corrected for total surface area) was determined to be 3.84×10^{-3} mol of methylcyclohexane formed per hour per m^2 of catalyst and 4.31×10^{-3} for the commercial 0.5% Rh/Al_2O_3 catalyst. These values give relative TOFs of 1 for the $Rh_{0.5}Pt_{0.5}/Al_2O_3$ catalyst and 1.12 for the commercial 0.5% Rh/Al_2O_3 catalyst, which are very similar to the relative TOFs calculated from the number of active sites determined from the CS_2 poisoning experiments (Table 2.2).

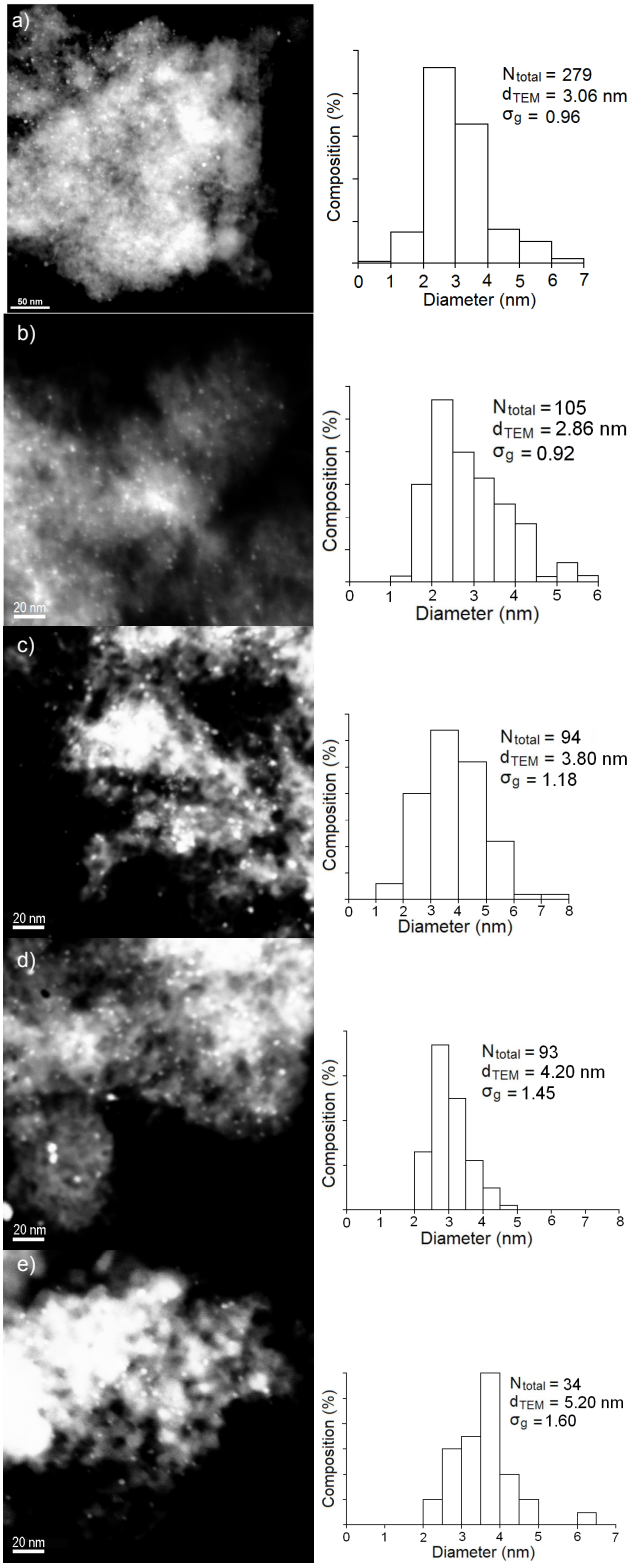
a)
50 nm
Composition (%)
Diameter (nm)
N_{total} = 279
d_{TEM} = 3.06 nm
σ_g = 0.96
b)
20 nm
Composition (%)
Diameter (nm)
N_{total} = 105
d_{TEM} = 2.86 nm
σ_g = 0.92
c)
20 nm
Composition (%)
Diameter (nm)
N_{total} = 94
d_{TEM} = 3.80 nm
σ_g = 1.18
d)
20 nm
Composition (%)
Diameter (nm)
N_{total} = 93
d_{TEM} = 4.20 nm
σ_g = 1.45
e)
20 nm
Composition (%)
Diameter (nm)
N_{total} = 34
d_{TEM} = 5.20 nm
σ_g = 1.60

Figure 2.13. Dark field TEM images and particle size histograms of nanoparticle catalysts: a) $Rh_{0.5}Pt_{0.5}/Al_2O_3$, b) $Ir_{0.5}Pt_{0.5}/Al_2O_3$, c) $Ir_{0.5}Rh_{0.5}/Al_2O_3$, d) $Ru_{0.5}Pt_{0.5}/Al_2O_3$, e) 0.5% Rh/Al_2O_3.

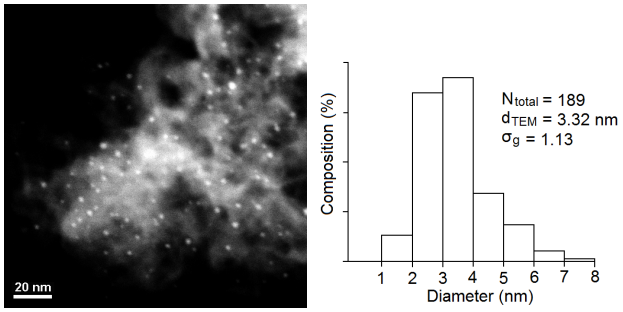

Figure 2.14. Dark field TEM image and particle size histogram of $Rh_{0.5}Pt_{0.5}/Al_2O_3$ catalyst after the toluene hydrogenation reaction. The size of the nanoparticles was measured to be 3.3 ± 1.1 nm.

XPS analysis of the $Rh_{0.5}Pt_{0.5}Al_2O_3$ catalyst was performed to determine the oxidation states of the two metals present in the catalyst. An electron gun was used to prevent charging for all of the samples during XPS analysis. The survey scan shown in Fig. 2.15 shows the XPS spectra before (spectra shown in black) and after (spectra shown in red) the toluene hydrogenation reaction. The two spectra are very similar and the Rh 3d, Al 2s, Al 2p, and Pt 4f peaks can be clearly identified in both, though the Al 2p and Pt 4f peaks overlap. All of the binding energies that were observed were referenced against those in the NIST XPS database to determine the oxidation states of the relevant metal peaks.

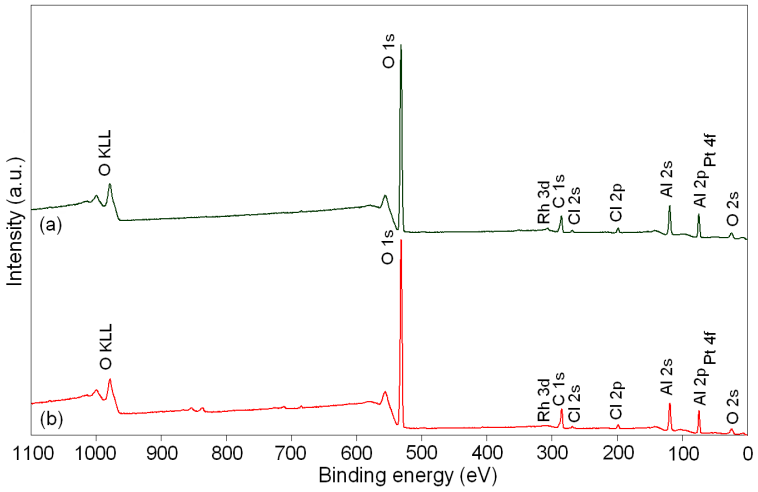

Figure 2.15. X-ray photoelectron spectra survey scans for $Rh_{0.5}Pt_{0.5}/Al_2O_3$. The spectra indicated in black (a) corresponds to the catalyst before the toluene hydrogenation reaction, and the spectra in red (b) corresponds to the catalyst after the toluene hydrogenation reaction.

From the high-resolution spectra of Rh in $Rh_{0.5}Pt_{0.5}/Al_2O_3$ (Fig. 2.16) the binding energy (BE) of Rh was measured to be 306.7 eV before the reaction and 307.1 eV after the reaction indicating that there was no change in the oxidation state of the metal during the catalytic reaction. From the high-resolution spectra of Pt in $Rh_{0.5}Pt_{0.5}/Al_2O_3$ (Fig. 2.17), a curve-fitting program (CasaXPS) was used to obtain information about the Pt 4f peak since it overlaps with the Al 2p peak. The BE of Pt was determined to be 71.4 eV before the hydrogenation and 71.2 eV after the hydrogenation. By considering the BE of the Rh and Pt peaks before and after the hydrogenation reactions, it can be seen that there was no substantial deviation in the BE, suggesting the oxidation state of the metal does not change substantially during the course of the reaction.

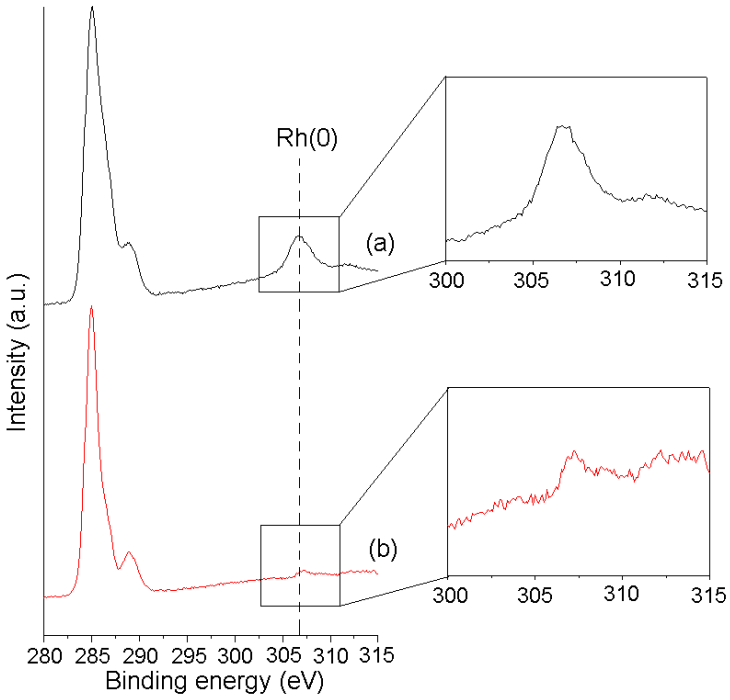

Figure 2.16. High-resolution XPS of the Rh 3d peak in $Rh_{0.5}Pt_{0.5}/Al_2O_3$. The spectra indicated in black (a) is before the toluene hydrogenation reaction and the spectra indicated in red (b) is after the toluene hydrogenation reaction. The binding energy for Rh 3d before and after reaction are 306.7 eV and 307.1 eV, respectively.

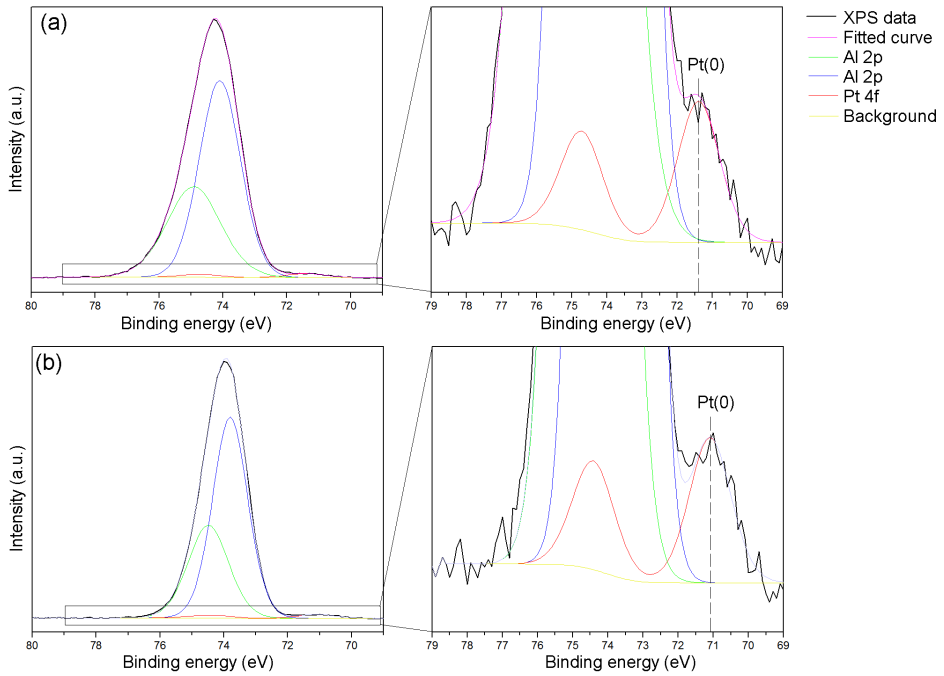

Figure 2.17. High-resolution XPS of Pt in $Rh_{0.5}Pt_{0.5}/Al_2O_3$. The spectra indicated in (a) are before the toluene hydrogenation reaction and the spectra indicated in (b) are after the toluene hydrogenation reaction. The BE for Pt before and after reaction are 71.4 eV and 71.2 eV, respectively.

XPS spectra were also obtained for the 0.5% Rh/Al_2O_3, $Ru_{0.5}Pt_{0.5}/Al_2O_3$, $Ir_{0.5}Pt_{0.5}/Al_2O_3$ and $Ir_{0.5}Rh_{0.5}/Al_2O_3$ catalysts (Fig. 2.18). For the commercial catalyst, 0.5% Rh/Al_2O_3, the high resolution XPS spectra showed a BE of 308.8 eV for Rh (Fig. 2.19), suggesting that the Rh was oxidized to Rh(III). However, XPS binding energies are also known to shift with nanoparticle sizes due to less final-state relaxation of the core hole via screening by conduction electrons in small particles compared to bulk metal.[105] For $Ru_{0.5}Pt_{0.5}/Al_2O_3$ (Fig. 2.20 and 2.21), the BE for Ru was 280.1 eV and 71.2 eV for Pt, indicating that both metals are in the zero oxidation state. From the high-

resolution spectra for $Ir_{0.5}Pt_{0.5}/Al_2O_3$ (Figs. 2.22 and 2.23) the BE for Ir was 60.7 eV and 71.4 eV for Pt, indicating that both metals were in the zero oxidation states. For $Ir_{0.5}Rh_{0.5}/Al_2O_3$ (Figs. 2.24 and 2.25), the BE for Ir and Rh were 60.4 eV and 306.7 eV, respectively, corresponding to the zero oxidation states for both metals.

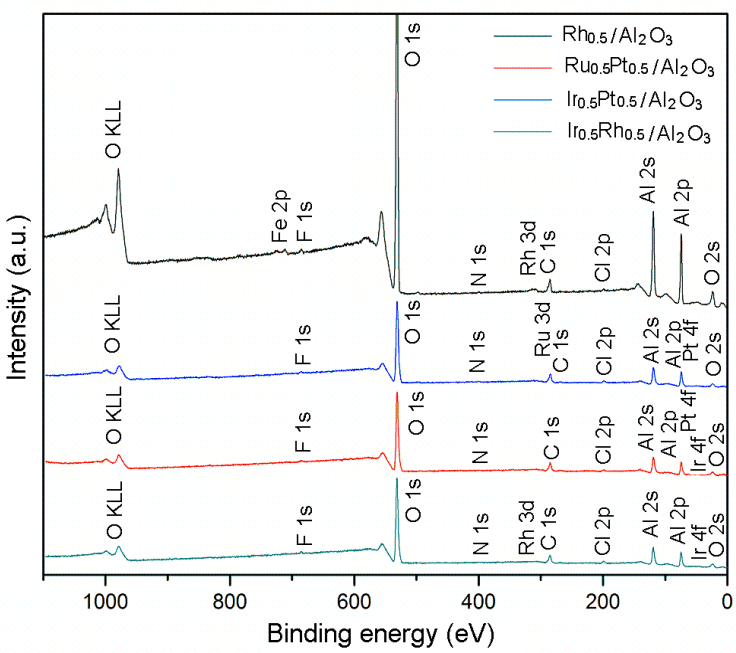

Figure 2.18. X-ray photoelectron spectra survey scans for the 0.5% Rh/Al_2O_3, $Ru_{0.5}Pt_{0.5}/Al_2O_3$, $Ir_{0.5}Pt_{0.5}/Al_2O_3$ and $Ir_{0.5}Rh_{0.5}/Al_2O_3$ catalysts.

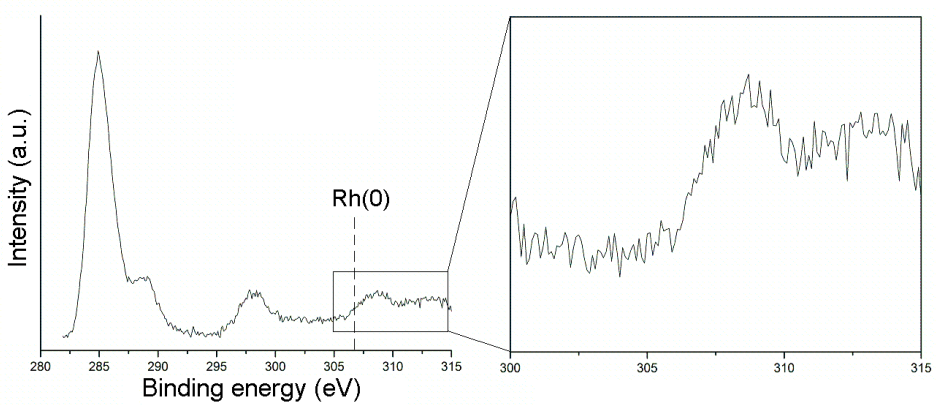

Figure 2.19. High-resolution XPS spectra of Rh in 0.5% Rh/Al_2O_3. The Rh 3d peak is at 308.8 eV, suggesting that it has been oxidized to Rh(III).

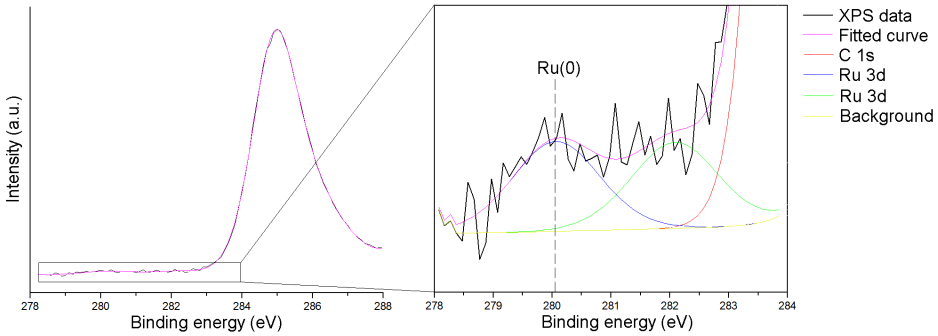

Figure 2.20. High-resolution XPS spectra of Ru in $Ru_{0.5}Pt_{0.5}/Al_2O_3$. The Ru $3d_{5/2}$ peak is at 280.1 eV and is partly obscured by the much stronger C 1s feature. The shift of the apparent Ru $3d_{5/2}$ feature indicates that the metal is in the zero oxidation state.

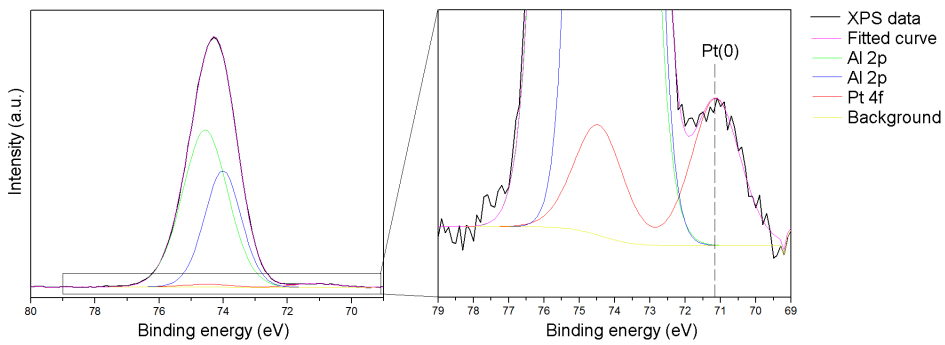

Figure 2.21. High-resolution XPS spectra of Pt in $Ru_{0.5}Pt_{0.5}/Al_2O_3$. The Pt 4f peak at 71.2 eV indicates that it is Pt(0).

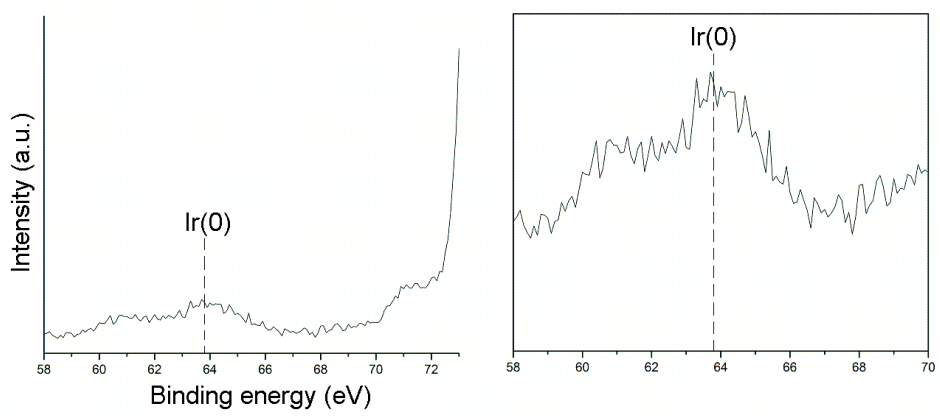

Figure 2.22. High-resolution XPS spectra of Ir in $Ir_{0.5}Pt_{0.5}/Al_2O_3$. The apparent Ir $4f_{7/2}$ peak is at 60.7 eV, which corresponds to Ir(0).

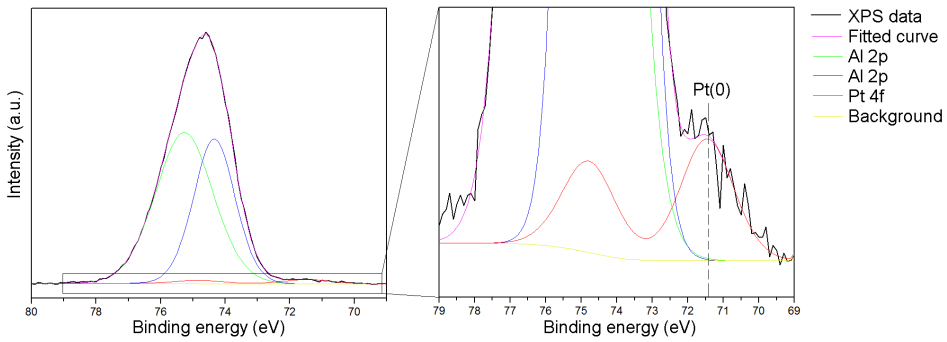

Figure 2.23. High-resolution XPS spectra of Pt in $Ir_{0.5}Pt_{0.5}/Al_2O_3$. The apparent Pt $4f_{7/2}$ peak is at 71.4 eV, corresponding to Pt(0).

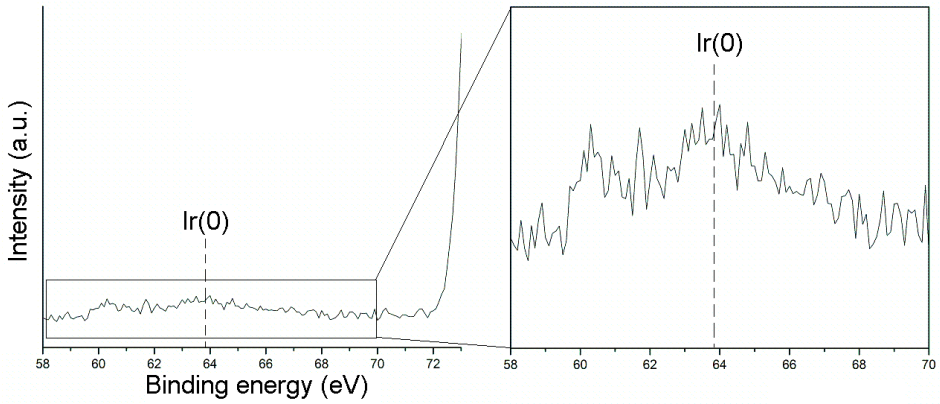

Figure 2.24. High-resolution XPS spectra of Ir in $Ir_{0.5}Rh_{0.5}/Al_2O_3$. The apparent Ir $4f_{7/2}$ peak is at 60.4 eV, which corresponds to Ir(0).

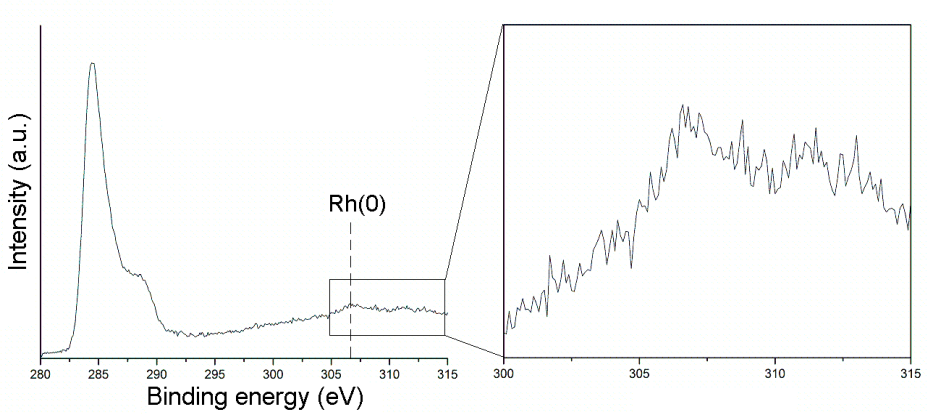

Figure 2.25. High-resolution XPS spectra of Rh in $Ir_{0.5}Rh_{0.5}/Al_2O_3$. The apparent Rh 3d peak is at 306.7 eV, corresponding to Rh(0).

Since acid-catalyzed sol-gel syntheses are known to give high-surface area metal oxides,[106] BET measurements were performed to measure the surface area of the blank support and the catalyst. The surface area of the blank support was measured to be 434 m^2/g, which is in the range of surface areas reported in the literature for alumina.[107,108] The surface area of the $Rh_{0.5}Pt_{0.5}/Al_2O_3$ catalyst was measured to be 557 m^2/g (Fig. 2.26).

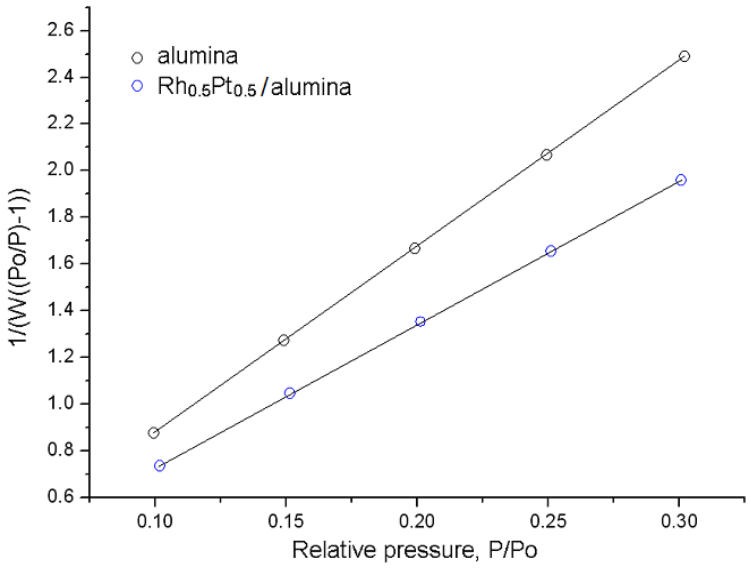

Figure 2.26. Five-point BET surface area plot. The blank (non-metallized) Al_2O_3 has a BET surface area of 434 m^2/g while the $Rh_{0.5}Pt_{0.5}/Al_2O_3$ has a BET surface area of 557 m^2/g.

2.3 Conclusions

Through a straightforward screening approach, four active bimetallic catalysts (RhPt, RuPt, IrPt, and IrRh) were identified. Through confirmation of the results in bulk, $Rh_{0.5}Pt_{0.5}/Al_2O_3$ was found to be the most active catalyst, which was then tested under a variety of parameters, and the activation energy was measured to be 30.4 kJ/mol. Through the use of standard materials characterization techniques, all of the bimetallic catalysts were determined to consist of small, zero oxidation state nanoparticles that were well dispersed throughout the alumina supports. Future work on this project will involve screening tri-metallic combinations for catalytic activity, and screening for activity on

mixed metal oxide supports and in the presence of sulfur and nitrogen containing compounds.

2.4 Experimental Section

Materials

$CuCl_2•2H_2O$ (99.999%-Cu), $CrCl_3•6H_2O$, $HAuCl_4•XH_2O$ (99.9985%-Au), $RuCl_3•XH_2O$ (99.9%-Ru), $IrCl_3•XH_2O$ (99.9%-Ir), $MnCl_2•4H_2O$ (99.999%-Mn), $PdCl_2$ (99.9%-Pd), $CoCl_2•6H_2O$ (99.999%-Co), $Na_2PtCl_4•XH_2O$, $NiCl_2•6H_2O$ (99.999+%-Ni), $FeCl_2•4H_2O$ (99%), $MoCl_5$ (anhydrous, 99.6%), $RhCl_3•xH_2O$ (38-41% Rh), and 0.5% Rh/Al_2O_3 (pellets) were purchased from Strem Chemicals and were used without further purification. Aluminum-sec-butoxide (95%), decahydronaphthaplene, cis + trans (97%), and methylcyclohexane (99+%) were purchased from Alfa Aesar. Ethanol (100%, anhydrous) was purchased from Commercial Alcohol. Millipore water was used throughout. Hydrochloric acid (concentrated), and silica gel were purchased from EMD. Dichloromethane (ACS), isopropanol, toluene were purchased from Fischer Scientific. Carbon disulfide was purchased from Sigma-Aldrich and was used without further purification. Isopropanol was dried over molecular sieves and stored under argon before use. Toluene was purified through a solvent purification system and was stored under argon until used. Hydrogen, argon, and 5% hydrogen / 95% argon were supplied by Praxair.

Instrumentation

A Varian CP-3800 Gas Chromatograph with a CP-4800 autosampler with a fused silica capillary column and a FID detector was used to analyze the samples of the reaction mixture. A Corning Model PC-420 Laboratory stirrer/hot plate was used throughout, except for the temperature studies, in which an IKA Works Ceramag Midi stirrer/hot plate with an IKA ETS-D4 temperature sensor was used for temperatures above ambient. An Agilent 6890 gas chromatography with a 5973 mass detector was used for the GC-MS experiments. A Parr pressure vessel, model 4774-T-SS-3000 and a model 4838 controller with a pressure display module were used for the pressure and CS_2 poisoning studies. For the TEM analysis, a JEOL JEM-2200FS TEM was used in STEM mode. For XPS a Kratos Analytical, Axis-Ultra instrument was used for the sample analysis. XPS were performed under UHV conditions ($<10^{-8}$ Torr). Surface areas were measured by nitrogen adsorption at 77.3 K using an Autosorb-1 high performance surface area and pore size analyzer (Quantachrome Instruments).

Catalyst screening synthesis of 1 mol% metal loading

The procedure for the catalyst synthesis was based on modified procedures established by Maier.[83,109] 0.133 M solutions of the required metal salts in ethanol were prepared, as was a 1.788 M solution of aluminum-sec-butoxide in dichloromethane and a solution consisting of 1.0 ml ethanol, 13 μl concentrated hydrochloric acid and 71 μl of water. The sample holders were centered on the stir plate, and glass coated stir bars (5 mm x 6 mm) were added to each well. The desired amount of each metal salt solution was added quickly (in under one second) to each well to give the desired metal loading

and ratio of the two metals (e.g. 10 μl of each metal salt solution would give a 50:50 ratio of the two metals with a total metal loading of 1 mol %). Then 300 μl of ethanol followed by 298 μl of 1.788 M aluminum-sec-butoxide were quickly (under one second) added to each well via pipette. After stirring for approximately five minutes, 218 μl of the ethanol/hydrochloric acid/water solution was quickly (under one second) added. Each sample holder was covered with parafilm; the parafilm was punctured several times above each well and the solution was allowed to age and dry overnight in laboratory ambient conditions. After processing, each sample holder was placed in a vial, which was capped with a septum (Fig 2.6).

Batch catalyst synthesis of 1 mol% metal loading

The catalyst screening synthesis was scaled up, and the catalyst was prepared in a 100 ml polypropylene beaker with a Teflon coated stir bar. After processing, the powder was transferred to a vial for immediate use or stored under argon.

Processing

All catalysts were calcined in air in a tube furnace using the following program: heat to 65ºC (rate 1ºC/min), hold at 65ºC for 30 minutes, heat to 250ºC (rate 1ºC /min), hold at 250ºC for 3 hours, cool to 25ºC (rate 1ºC /min). Then the catalyst was hydrogen annealed under a 5% H_2 / 95% Ar atmosphere as follows: heat to 300ºC (rate 5ºC/min), hold at 300ºC for 3 hours, cool down to 25ºC rapidly by opening the furnace.

Screening

A solution of 7.7 ml isopropanol, 0.456 ml decahydronaphthalene (internal standard) and 0.308 ml toluene was prepared. A necessary number of lines on the Schlenk line were split with Y joints and additional tubes were attached. A syringe barrel was inserted into the end of each tube and a needle was attached to each syringe. As described earlier (Catalyst screening synthesis of 1 mol% metal loading) each sample holder containing the prepared catalyst is located in an individual vial. The septum on each vial was pierced with a needle that was attached to the Schlenk line (Fig. 2.7). The vials underwent three of the following cycles: the vials were placed under vacuum and then back filled with Ar. This was repeated with Ar and then with H_2. 1 ml of isopropanol was added to the bottom of each vial (but not to the sample holder), to minimize evaporation losses from the sample holder. Next, 0.77 ml of the previously prepared solution was added to each sample holder. The vials were stirred for 4 hours under 15 psi H_2 pressure and at 22ºC. After 4 hours, each sample holder was removed from the vial. As much of the reaction mixture as possible was removed from the sample holder with a Pasteur pipette. The reaction mixture was filtered through a different Pasteur pipette packed with a small amount silica gel directly into a GC vial. The substrate and products were diluted with 1.0 ml dichloromethane. The screening hydrogenation results obtained for $Rh_{0.5}Pt_{0.5}/Al_2O_3$ were performed in triplicate.

General batch hydrogenation

The appropriate amount of catalyst to give 3.8×10^{-5} mol of metal was added to a 25 mL 3 neck round-bottomed flask. A glass coated stir bar was added and the flask was

capped with two septa and a gas adapter. The flask was placed under vacuum and then back filled with Ar; this was repeated two more times with Ar. Next, 10.0 mL of isopropanol was added. The flask was placed under vacuum and then back filled with H_2 for a total of three times. 0.59 mL (3.8×10^{-3} mol) of decahydronaphthalene and 0.40 mL (3.8×10^{-3} mol) toluene were added by syringe and the reaction was stirred under ambient conditions (15 psi H_2, 22ºC). The reaction was monitored every 15 minutes for the first 2 hours, and then every hour for an additional 5 hours via gas chromatography (GC). To prepare samples for GC analysis, 0.4 ml samples of the reaction mixture were removed from the flask with a syringe. The contents of the syringe were filtered through a silica gel filter as previously described. The bulk hydrogenation results obtained for $Rh_{0.5}Pt_{0.5}/Al_2O_3$ were performed in triplicate.

Batch toluene studies

The hydrogenation was performed as specified in the procedure for general batch hydrogenation, with varying amounts of toluene depending on the desired ratio of catalyst to substrate.

Batch temperature studies

The hydrogenation was performed as specified in the procedure for general batch hydrogenation, except that if heating the reaction mixture above room temperature, a reflux condenser was attached to the middle neck of the round bottom flask and a gas adapter was connected to the top of the reflux condenser. The other two necks on the round bottom flask were sealed with septa. For cooling below room temperature, an ice

bath was used to achieve a temperature of 0ºC, and a bath consisting of dioxane and CO_2(s) was used for a 10ºC bath.

Batch pressure studies

The quantities of catalyst, solvent and substrate were scaled up by a factor of two for the batch pressure studies, and decahydronaphthalene was not added. The catalyst was added to the stainless steel bottom of the pressure reactor, and then isopropanol and toluene were sequentially added. The pressure reactor was assembled, and hydrogen was gently flowed through the reactor for 30 s. Then the reactor was sealed, pressurized to the desired pressure, and the course of the reaction was monitored via a Parr pressure controller interfaced with a computer. After the reaction was complete, the reactor was disassembled and a sample of the reaction mixture was analyzed by gas chromatography as previously described.

CS_2 Poisoning Studies

The following CS_2 poisoning studies were done based on a modified procedure by Hornstein *et al*. and were performed in triplicate.[104] 0.3893 g of the $Rh_{0.5}Pt_{0.5}/Al_2O_3$ catalyst or 0.782 g of the 0.5% Rh/Al_2O_3 catalyst was weighed into a clean 20 ml beaker. A glass coated stir bar was added to the beaker followed by 5.0 ml of isopropanol. A 0.038 M solution of CS_2 in isopropanol was prepared fresh each day and the required amount of the solution was added to the beaker. Ratios of 0, 0.02, 0.04, 0.06 and 0.08 mol CS_2 / mol total metal were used for the $Rh_{0.5}Pt_{0.5}/Al_2O_3$ catalyst and ratios of 0, 0.01, 0.02, 0.03 and 0.04 mol CS_2 / mol total metal were used for the commercial 0.5%

Rh/Al_2O_3 catalyst. Then an additional 5.0 ml of isopropanol was added to the beaker followed by 0.40 ml of toluene. Decahydronaphthalene was not added. The beaker was placed into the bottom of the Parr reactor with the hydrogen inlet placed directly in the reaction solution and then the reactor was assembled. The Parr reactor was sealed and the solution was stirred for 30 s at a stir speed of 7. Then the stirrer was turned off and hydrogen gas was gently flowed through the reactor for 30 s. The reactor was then sealed and pressurized to 73 psig. The course of the reaction was monitored via a Parr pressure controller interfaced with a computer for 1 h. After 1 h, the reactor was depressurized and dissembled.

Sample preparation for XPS, TEM and BET

XPS: The dried sample was first finely grounded to reduce the particle size. The ground powders were then placed into a die and pressed into a pellet under high pressure. The pellet was then used for XPS analysis. An electron gun was used to prevent charging for all of the samples during XPS analysis. The CasaXPS software program was used to perform the curve fitting, and all binding energies were referenced against those in the NIST XPS database to determine oxidation states. TEM (before hydrogenation): Raw samples were carefully ground with a mortar and pestle for 20 minutes. The average particle size is less then 100 nm after ground. A small amount of the ground powder was then mounted on a carbon-coated grid for TEM analysis. TEM (after hydrogenation): After reaction, the solvent was removed/vaporized under vacuum overnight. The raw sample was then ground and sprayed on a carbon coated TEM grid. BET: Before analysis, samples were degassed at 250°C for 23 h under vacuum.

2.5 References

(1) Government of Alberta. *http://oilsands.alberta.ca/1.cfm* **2009**.

(2) Song, C.; Nihonmatsu, T.; Nomura, M. *Ind. Eng. Chem. Res.* **1991**, *30*, 1726-1734.

(3) Beltramone, A. R.; Resasco, D. E.; Alvarez, W. E.; Choudhary, T. V. *Ind. Eng. Chem. Res.* **2008**, *47*, 7161-7166.

(4) Strausz, O. P.; Mojelsky, T. W.; Payzant, J. D.; Olah, G. A.; Prakash, G. K. S. *Energy & Fuels* **1999**, *13*, 558-569.

(5) Owusu-Boakye, A.; Dalai, A. K.; Ferdous, D.; Adjaye, J. *Energy & Fuels* **2005**, *19*, 1763-1774.

(6) Sidhpuria, K. B.; Parikh, P. A.; Bahadur, P.; Jasra, R. V. *Ind. Eng. Chem. Res.* **2008**, *47*, 4034-4042.

(7) Hu, L.; Xia, G.; Qu, L.; Li, M.; Li, C.; Xin, Q.; Li, D. *J. Catal.* **2001**, *202*, 220-228.

(8) Aiken, J. D.; Finke, R. G. *Chem. Mater.* **1999**, *11*, 1035-1047.

(9) Yang, X.; Yan, N.; Fei, Z.; Crespo-Quesada, R. M.; Laurenczy, G.; Kiwi-Minsker, L.; Kou, Y.; Li, Y.; Dyson, P. J. *Inorg. Chem.* **2008**, *47*, 7444-7446.

(10) Kakade, B. A.; Sahoo, S.; Halligudi, S. B.; Pillai, V. K. *J. Phys. Chem. C* **2008**, *112*, 13317-13319.

(11) Yoon, B.; Pan, H. B.; Wai, C. M. *J. Phys. Chem. C* **2009**, *113*, 1520-1525.

(12) Yoon, B.; Wai, C. M. *J. Am. Chem. Soc.* **2005**, *127*, 17174-17175.

(13) Park, I. S.; Kwon, M. S.; Kang, K. Y.; Lee, J. S.; Park, J. *Adv. Synth. Catal.* **2007**, *349*, 2039-2047.

(14) Su, F.; Lv, L.; Lee, F. Y.; Liu, T.; Cooper, A. I.; Zhao, X. S. *J. Am. Chem. Soc.* **2007**, *129*, 14213-14223.

(15) Lin, S. D.; Vannice, M. A. *J. Catal.* **1993**, *143*, 554-562.

(16) Cunha, D. S.; Cruz, G. M. *Appl. Catal., A* **2002**, *236*, 55-66.

(17) Mevellec, V.; Nowicki, A.; Roucoux, A.; Dujardin, C.; Granger, P.; Payen, E.; Philippot, K. *New J. Chem.* **2006**, *30*, 1214-1219.

(18) Marconi, G.; Pertici, P.; Evangelisti, C.; Caporusso, A. M.; Vitulli, G.; Capannelli, G.; Hoang, M.; Turney, T. W. *J. Organomet. Chem.* **2004**, *689*, 639-646.

(19) Spinace, E. V.; Vaz, J. M. *Catal. Commun.* **2003**, *4*, 91-96.

(20) Yuan, T.; Fournier, A. R.; Proudlock, R.; Marshall, W. D. *Environ. Sci. Technol.* **2007**, *41*, 1983-1988.

(21) Dominguez-Quintero, O.; Martinez, S.; Henriquez, Y.; D'Ornelas, L.; Krentzien, H.; Osuna, J. *J. Mol. Catal. A: Chem.* **2003**, *197*, 185-191.

(22) Lang, H. F.; May, R. A.; Iversen, B. L.; Chandler, B. D. *J. Am. Chem. Soc.* **2003**, *125*, 14832-14836.

(23) Pawelec, B.; Campos-Martin, J. M.; Cano-Serrano, E.; Navarro, R. M.; Thomas, S.; Fierro, J. L. G. *Environ. Sci. Technol.* **2005**, *39*, 3374-3381.

(24) Marecot, P.; Mahoungou, J. R.; Barbier, J. *Appl. Catal., A* **1993**, *101*, 143-149.

(25) Zhao, A.; Gates, B. C. *J. Catal.* **1997**, *168*, 60-69.

(26) Schulz, J.; Roucoux, A.; Patin, H. *Chem. Commun.* **1999**, 535-536.

(27) Schulz, J.; Roucoux, A.; Patin, H. *Chem. Eur. J.* **2000**, *6*, 618-624.

(28) Deshmukh, R. R.; Lee, J. W.; Shin, U. S.; Lee, J. Y.; Song, C. E. *Angew. Chem., Int. Ed.* **2008**, *47*, 8615-8617.

(29) Bratlie, K. M.; Lee, H.; Komvopoulos, K.; Yang, P.; Somorjai, G. A. *Nano Lett*. **2007**, *7*, 3097-3101.

(30) Mu, X. D.; Meng, J. Q.; Li, Z. C.; Kou, Y. *J. Am. Chem. Soc*. **2005**, *127*, 9694-9695.

(31) Zhao, C.; Wang, H. Z.; Yan, N.; Xiao, C. X.; Mu, X. D.; Dyson, P. J.; Kou, Y. *J. Catal*. **2007**, *250*, 33-40.

(32) Jacinto, M. J.; Kiyohara, P. K.; Masunaga, S. H.; Jardim, R. F.; Rossi, L. M. *Appl. Catal., A* **2008**, *338*, 52-57.

(33) Schulz, J.; Levigne, S.; Roucoux, A.; Patin, H. *Adv. Synth. Catal*. **2002**, *344*, 266-269.

(34) Harada, T.; Ikeda, S.; Ng, Y. H.; Sakata, T.; Mori, H.; Torimoto, T.; Matsumura, M. *Adv. Func. Mater*. **2008**, *18*, 2190-2196.

(35) Zahmakiran, M.; Ozkar, S. *Langmuir* **2008**, *24*, 7065-7067.

(36) Hagen, C. M.; Widegren, J. A.; Maitlis, P. M.; Finke, R. G. *J. Am. Chem. Soc*. **2005**, *127*, 4423-4432.

(37) Widegren, J. A.; Finke, R. G. *Inorg. Chem*. **2002**, *41*, 1558-1572.

(38) Weddle, K. S.; Aiken, J. D.; Finke, R. G. *J. Am. Chem. Soc*. **1998**, *120*, 5653-5666.

(39) Leger, B.; Denicourt-Nowicki, A.; Roucoux, A.; Olivier-Bourbigou, H. *Adv. Synth. Catal*. **2008**, *350*, 153-159.

(40) Pellegatta, J. L.; Blandy, C.; Colliere, V.; Choukroun, R.; Chaudret, B.; Cheng, P.; Philippot, K. *J. Mol. Catal. A: Chem*. **2002**, *178*, 55-61.

(41) Simon, L.; van Ommen, J. G.; Jentys, A.; Lercher, J. A. *J. Phys. Chem. B* **2000**, *104*, 11644-11649.

(42) Hiyoshi, N.; Rode, C. V.; Sato, O.; Masuda, Y.; Yamaguchi, A.; Shirai, M. *Chem. Lett.* **2008**, *37*, 734-735.

(43) Leger, B.; Denicourt-Nowicki, A.; Olivier-Bourbigou, H.; Roucoux, A. *Inorg. Chem.* **2008**, *47*, 9090-9096.

(44) Ohde, H.; Ohde, M.; Wai, C. M. *Chem. Commun.* **2004**, 930-931.

(45) Hiyoshi, N.; Inoue, T.; Rode, C.; Sato, O.; Shirai, M. *Catal. Lett.* **2006**, *106*, 133-138.

(46) Graydon, W. F.; Langan, M. D. *J. Catal.* **1981**, *69*, 180-192.

(47) Zhang, Z. G.; Okada, K.; Yamamoto, M.; Yoshida, T. *Catalysis Today* **1998**, *45*, 361-366.

(48) Lu, F.; Liu, J.; Xu, H. *Adv. Synth. Catal.* **2006**, *348*, 857-861.

(49) Hiyoshi, N.; Osada, M.; Rode, C. V.; Sato, O.; Shirai, M. *Appl. Catal., A* **2007**, *331*, 1-7.

(50) Prechtl, M. H. G.; Scariot, M.; Scholten, J. D.; Machado, G.; Teixeira, S. R.; Dupont, J. *Inorg. Chem.* **2008**, *47*, 8995-9001.

(51) Venezia, A. M.; La Parola, V.; Pawelec, B.; Fierro, J. L. G. *Appl. Catal., A* **2004**, *264*, 43-51.

(52) Wan, G.; Duan, A.; Zhao, Z.; Jiang, G.; Zhang, D.; Li, R.; Dou, T.; Chung, K. H. *Energy & Fuels* **2009**, *23*, 81-85.

(53) Thomas, J. M.; Johnson, B. F. G.; Raja, R.; Sankar, G.; Midgley, P. A. *Acc. Chem. Res.* **2003**, *36*, 20-30.

(54) Gelman, F.; Avnir, D.; Schumann, H.; Blum, J. *J. Mol. Catal. A: Chem.* **2001**, *171*, 191-194.

(55) Pawelec, B.; La Parola, V.; Navarro, R. M.; Murcia-Mascaros, S.; Fierro, J. L. G. *Carbon* **2006**, *44*, 84-98.

(56) Roucoux, A.; Schulz, J.; Patin, H. *Chem. Rev.* **2002**, *102*, 3757-3778.

(57) Barbaro, P.; Bianchini, C.; Dal Santo, V.; Meli, A.; Moneti, S.; Psaro, R.; Scaffidi, A.; Sordelli, L.; Vizza, F. *J. Am. Chem. Soc.* **2006**, *128*, 7065-7076.

(58) Hiyoshi, N.; Miura, R.; Rode, C. V.; Sato, O.; Shirai, M. *Chem. Lett.* **2005**, *34*, 424-425.

(59) Barbaro, P.; Bianchini, C.; Dal Santo, V.; Meli, A.; Moneti, S.; Pirovano, C.; Psaro, R.; Sordelli, L.; Vizza, F. *Organometallics* **2008**, *27*, 2809-2824.

(60) Fujikawa, T.; Idei, K.; Ebihara, T.; Mizuguchi, H.; Usui, K. *Appl. Catal., A* **2000**, *192*, 253-261.

(61) Roucoux, A. *Top. Organomet. Chem.* **2005**, *16*, 261-279.

(62) Liang, C.; Zhao, A.; Zhang, X.; Ma, Z.; Prins, R. *Chem. Commun.* **2009**, 2047-2049.

(63) Pan, H. B.; Wai, C. M. *J. Phys. Chem. C* **2009**, *113*, 19782-19788.

(64) Zahmakiran, M.; Tonbul, Y.; Ozkar, S. *J. Am. Chem. Soc.* **2010**, *132*, 6541-6549.

(65) Gao, H.; Angelici, R. J. *J. Am. Chem. Soc.* **1997**, *119*, 6937-6938.

(66) Ioannides, T.; Verykios, X. E. *J. Catal.* **1993**, *143*, 175-186.

(67) Crump, C. J.; Gilbertson, J. D.; Chandler, B. D. *Topics in Catalysis* **2008**, *49*, 233-240.

(68) Lin, S. D.; Vannice, M. A. *J. Catal.* **1993**, *143*, 539-553.

(69) Takagi, H.; Isoda, T.; Kusakabe, K.; Morooka, S. *Energy & Fuels* **1999**, *13*, 1191-1196.

(70) Santana, R. C.; Jongpatiwut, S.; Alvarez, W. E.; Resasco, D. E. *Ind. Eng. Chem. Res.* **2005**, *44*, 7928-7934.

(71) Pawelec, B.; Castano, P.; Arandes, J. M.; Bilbao, J.; Thomas, S.; Pena, M. A.; Fierro, J. L. G. *Appl. Catal., A* **2007**, *317*, 20-33.

(72) Park, K. H.; Jang, K.; Kim, H. J.; Son, S. U. *Angew. Chem., Int. Ed.* **2007**, *46*, 1152-1155.

(73) Yang, S. Y.; Stock, L. M. *Energy & Fuels* **1998**, *12*, 644-648.

(74) Widegren, J. A.; Finke, R. G. *J. Mol. Catal. A: Chem.* **2003**, *191*, 187-207.

(75) Cooper, B. H.; Donnis, B. B. L. *Appl. Catal., A* **1996**, *137*, 203-223.

(76) Horiuti, I.; Polanyi, M. *Trans. Faraday Soc.* **1934**, *30*, 1164-1172.

(77) Kovtunov, K. V.; Beck, I. E.; Bukhtiyarov, V. I.; Koptyug, I. V. *Angew. Chem., Int. Ed.* **2008**, *47*, 1492-1495.

(78) Wang, J.; Yoo, Y.; Gao, C.; Takeuchi, I.; Sun, X.; Chang, H.; Xiang, X.-D.; Schultz, P. G. *Science* **1998**, *279*, 1712-1715.

(79) Danielson, E.; Devenney, M.; Giaquinta, D. M.; Golden, J. H.; Haushalter, R. C.; McFarland, E. W.; Poojary, D. M.; Reaves, C. M.; Weinberg, W. H.; Wu, X. D. *Science* **1998**, *279*, 837-840.

(80) Woodhouse, M.; Parkinson, B. A. *Chem. Mater.* **2008**, *20*, 2495-2502.

(81) Tai, C. C.; Chang, T.; Roller, B.; Jessop, P. G. *Inorg. Chem.* **2003**, *42*, 7340-7341.

(82) Xiang, X. D.; Sun, X.; Briceno, G.; Lou, Y.; Wang, K. A.; Chang, H.; Wallace-Freedman, W. G.; Chen, S. W.; Schultz, P. G. *Science* **1995**, *268*, 1738-1740.

(83) Holzwarth, A.; Schmidt, H. W.; Maier, W. E. *Angew. Chem., Int. Ed.* **1998**, *37*, 2644-2647.

(84) Orschel, M.; Klein, J.; Schmidt, H. W.; Maier, W. F. *Angew. Chem., Int. Ed.* **1999**, *38*, 2791-2794.

(85) Klein, J.; Lehmann, C. W.; Schmidt, H. W.; Maier, W. F. *Angew. Chem., Int. Ed.* **1998**, *37*, 3369-3373.

(86) Kirsten, G.; Maier, W. F. *Applied Surface Science* **2004**, *223*, 87-101.

(87) Scheidtmann, J.; Weib, P. A.; Maier, W. F. *Appl. Catal., A* **2001**, *222*, 79-89.

(88) Maier, W. F. *Angew. Chem., Int. Ed.* **1999**, *38*, 1216-1218.

(89) Maier, W. F.; Stowe, K.; Sieg, S. *Angew. Chem., Int. Ed.* **2007**, *46*, 6016-6067.

(90) Danielson, E.; Golden, J. H.; McFarland, E. W.; Reaves, C. M.; Weinberg, W. H.; Wu, X. D. *Nature* **1997**, *389*, 944-948.

(91) Briceno, G.; Chang, H.; Sun, X.; Schultz, P. G.; Xiang, X. D. *Science* **1995**, *270*, 273-275.

(92) Yoo, J. W.; Hathcock, D. J.; El-Sayed, M. A. *J. Catal.* **2003**, *214*, 1-7.

(93) Sinfelt, J. H. *J. Catal.* **1973**, *29*, 308-315.

(94) Carter, J. L.; Cusumano, J. A.; Sinfelt, J. H. *J. Catal.* **1971**, *20*, 223-229.

(95) Sinfelt, J. H. *Science* **1977**, *195*, 641-646.

(96) Schubert, U.; Amberg-Schwab, S.; Breitscheidel, B. *Chem. Mater.* **1989**, *1*, 2.

(97) Castillo, S.; MoranPineda, M.; Gomez, R.; Lopez, T. *J. Catal.* **1997**, *172*, 263-266.

(98) Hoover, N. N.; Auten, B. J.; Chandler, B. D. *J. Phys. Chem. B* **2006**, *110*, 8606-8612.

(99) Alayoglu, S.; Nilekar, A. U.; Mavrikakis, M.; Eichhorn, B. *Nature Mater*. **2008**, *7*, 333-338.

(100) Alayoglu, S.; Eichhorn, B. *J. Am. Chem. Soc*. **2008**, *130*, 17479-17486.

(101) Abdelsayed, V.; Aljarash, A.; El-Shall, M. S.; Al Othman, Z. A.; Alghamdi, A. H. *Chem. Mater*. **2009**, *21*, 2825-2834.

(102) Park, J. Y.; Zhang, Y.; Grass, M.; Zhang, T.; Somorjai, G. A. *Nano Lett*. **2008**, *8*, 673-677.

(103) Kim, H. J.; Choi, S. M.; Nam, S. H.; Seo, M. H.; Kim, W. B. *Appl. Catal., A* **2009**, *352*, 145-151.

(104) Hornstein, B. J.; Aiken, J. D.; Finke, R. G. *Inorg. Chem*. **2002**, *41*, 1625-1638.

(105) Campbell, C. T. *Surface Science Reports* **1997**, *27*, 1-111.

(106) Fahlman, B. D. *Materials Chemistry*; Springer, 2007.

(107) Ennas, G.; Falqui, A.; Paschina, G.; Marongiu, G. *Chem. Mater*. **2005**, *17*, 6486-6491.

(108) Corrias, A.; Casula, M. F.; Falqui, A.; Paschina, G. *Chem. Mater*. **2004**, *16*, 3130-3138.

(109) Klein, J.; Lettmann, C.; Maier, W. F. *J. Non-Cryst. Solids* **2001**, *282*, 203-220.

Chapter 3

Synthesis and Screening of Multimetallic Catalysts for Mono-, Poly,- and Heteroaromatic Hydrogenation Activity

3.1 Introduction

Using the approach for the synthesis and screening of heterogeneous bimetallic nanoparticle catalysts described in Chapter 2, we expanded the composition of the metal nanoparticles to include a third transition metal. We also explored the effect of using mixed-metal oxides as the catalyst support and screened for catalytic activity for the hydrogenation of mono-, poly-, and heteroaromatic substrates under mild conditions.

While arene hydrogenation is a challenging catalytic reaction due to the stability of the aromatic rings, polyaromatic and heteroaromatic hydrogenation present another unique set of challenges. Harsh conditions are often required for the hydrogenation of polyaromatic hydrocarbons in order to obtain complete or deep hydrogenation of all of the aromatic rings. These harsh conditions, however, may deactivate the catalyst. In the case of heteroaromatic hydrogenation, the heteroaromatic substrate may behave as a catalyst poison. Sulfur poisoning has been thoroughly investigated but nitrogen poisoning is not as well explored. It is of consequence to be able to hydrogenate these

types of substrates because heteroaromatic hydrogenation is involved hydrodenitrogenation and hydrodesulfurization, two industrially challenging steps involved in oil sands upgrading. In addition, the hydrogenation of quinoline is of interest for the production of petrochemicals, fine chemicals and pharmaceuticals.[1]

Nanoparticle catalysts have shown to be advantageous as catalysts for many reasons including high surface areas and energies, unique electronic effects and potentially lower cost.[2,3] Furthermore, bimetallic catalysts possess the potential for enhanced activity and selectivity and an increased tolerance to nitrogen and sulfur containing compounds. For example, Yoon demonstrated that a bimetallic RhPd/CNT catalyst had an unusually high catalytic activity for the hydrogenation of anthracene at 147 psi H_2 and 25ºC when compared to the monometallic Rh/CNT and Pd/CNT catalysts.[4] Venezia showed that a Au-Pd/SiO_2-Al_2O catalyst had a high turnover frequency for the hydrogenation of toluene in the presence of sulfur.[5] In 2009, Yoon also showed while Au/CNT and Pd/CNT catalysts had negligible activities for the room temperature hydrogenation of benzene, the Pd-Au/CNT catalyst was much more active.[6] Based on these observations, there is the possibility that by using a bi- or multi-metallic catalyst for the hydrogenation of heteroaromatic substrates we could exploit their enhanced sulfur and nitrogen resistance.

Polyaromatic Hydrogenation

As previously mentioned, harsh conditions are often required to achieve the complete hydrogenation of polyaromatic hydrocarbons.[7] This becomes quite evident when studying the hydrogenation of larger aromatic hydrocarbons such as anthracene or phenanthrene. Because of this, the majority of the research thus far has focused on the hydrogenation of naphthalene, one of the simplest polyaromatic hydrocarbons, and anthracene, a tricyclic polyaromatic hydrocarbon.

For example, Park used Rh nanoparticles on aluminum oxyhydroxide nanofibers for the hydrogenation of naphthalene at room temperature with a hydrogen balloon, and after 3 hours, predominantly tetralin was observed, but upon allowing the reaction to continue for an additional 7 hours, only decalin was found (cis/trans = 88/12).[8] The hydrogenation of naphthalene has also been investigated using activated-carbon supported Rh, Ru, Pd and Pt catalysts using supercritical carbon dioxide as a solvent,[9-11] and in one of the studies they found the Rh catalyst was the most active but the Ru catalyst had the highest selectivity for *cis*-decahydronaphthalene.[12] Tetrahedral and spherical Rh nanoparticles on charcoal were used for the hydrogenation of naphthalene under ambient conditions and they observed 100% conversion to octahydronaphthalene with a TOF of 250 h^{-1} (Note, TOF was defined as mol of H_2 consumed per mol of total metal per hour).[13] The hydrogenation of naphthalene has also been investigated using a combination catalyst consisting of a homogenous catalyst tethered to a heterogeneous catalyst.[14] When Rh-CNR_3/Pd-SiO_2 combination catalyst was used, a TOF of 4.7 with a TON of 3700 were observed with $C_{10}H_{12}$ and $C_{10}H_{18}$ as the products, and when Rh-CNR_2/Pd-SiO_2 was used, the observed TOF was 6.3 with a TON of 1560 and $C_{10}H_{12}$ as

the only product.[14] A Pd/C catalyst was used for the hydrogenation of naphthalene in the presence of an ionic liquid additive at room temperature and 15 psi H_2 pressure.[15] They observed over 99% conversion of naphthalene with both tetrahydronaphthalene and decahydronaphthalene as the observed products. On a side note, the hydrogenation of tetrahydronaphthalene has also been studied using a Pt/Al_2O_3 catalysts using an integral fixed bed reactor at 500 psig at 553-573 K.[16] The hydrogenation of naphthalene in the presence of dibenzothiophene has been studied using Al_2O_3, SiO_2-Al_2O_3 and zeolite supported palladium catalysts and it was observed that the Pd/SiO_2-Al_2O_3 catalyst demonstrated a higher catalytic activity.[17] The main product that they observed for all of the catalysts was tetrahydronaphthalene. Cobalt silicide nanoparticles deposited on meosporous silica have been used for the hydrogenation of naphthalene in a fixed-bed reactor at 340ºC at 580 psi hydrogen pressure.[18] They used different CoSi loadings and observed high selectivites for the hydrogenation of naphthalene to tetrahydronaphthalene.

The hydrogenation of anthracene has been studied using Rh nanoparticles on aluminum oxyhydroxide nanofibers,[8] carbon-supported Ni catalysts,[19] tetrahedral and spherical Rh nanoparticles on charcoal,[13] $CoSi/SiO_2$ and Co/SiO_2 catalysts,[20] Rh nanoparticles on multiwalled carbon nanotubes,[21] commercial Pd/C catalysts,[15,22] Pd/Al_2O_3,[23,24] Rd, Rh and Pd/Rh nanoparticles on carbon nanotubes,[4] and sodium dodecyl sulfate and hexadecyltrimethylammonium bromide stabilized Au NPs.[25]

Heteroaromatic Hydrogenation

There are few examples in the literature of nanoparticle catalysts that have been shown to be active for the hydrogenation of N- and S-heteroaromatic compounds. Sánchez-Delgado and co-workers demonstrated the hydrogenation of quinoline by poly(4-vinylpyridine) immobilized Ru nanoparticles at 120ºC and 580 psi H_2.[26] Mévellec used Rh(0) nanoparticles to hydrogenate a variety of substrates including pyridine and quinoline at 15 psi H_2, 20ºC.[27] Grobas used a Pd/C catalyst to hydrogenate several substrates including quinoline in the presence of formic acid at 301 K and atmospheric pressure.[28] Piccolo used commercial Pd, Rh or Ru/Al_2O_3 catalysts for the hydrogenation of quinoline at 100ºC and 294 psi H_2.[1] Vaccari used a Rh-containing pillared layered clay catalysts for the hydrogenation of quinoline at 100-200ºC and 294 psi H_2.[29] Park used Rh nanoparticles on aluminum oxyhydroxide nanofibers for the neat hydrogenation of quinoline, and after 30 hours 1,2,3,4-tetrahydroquinoline was obtained in a 94% yield with a TOF of 16 h^{-1} and a TON of 500.[8] However, to the best of our knowledge, there are currently no examples of heterogeneous bimetallic nanoparticle catalysts that are active for the hydrogenation of N- or S-heteroaromatic substrates under mild conditions in the literature.

Mixed Metal Oxides

In addition to modifying the metals that compose the nanoparticle catalyst to increase their ability to resist becoming poisoned, the composition of the catalyst support can also be altered. Previously, three different metal oxides (Al_2O_3, SiO_2 and TiO_2) were

used as catalyst supports for the hydrogenation of toluene where it was discerned that nanoparticles supported on Al_2O_3 were the most active, closely followed by those supported on TiO_2. The nanoparticles that were supported on SiO_2 were only slightly active for the hydrogenation of toluene under ambient conditions. Due to this observation, we had previously limited ourselves to only utilizing Al_2O_3 as a catalytic support. Consequently, we were interested in exploring how the catalytic activity would be altered by using mixed-metal oxides as the catalyst supports because it has been previously reported that noble metal catalysts deposited on acidic supports are more catalytically active than those deposited on nonacidic supports.[17,30,31]

Noble metal catalysts, such as Rh and Pt, are often preferred for aromatic hydrogenation reactions because they can operate at lower reaction temperatures, allowing them to avoid some of thermodynamic constraints that are encountered when the typical sulfided metal oxide catalysts are used.[32] However, as previously discussed, these catalysts are more sensitive to poisoning by S- and N- containing heteroaromatic compounds. Sulfur and nitrogen tolerance may be enhanced by using acidic supports for these noble metal catalysts.[32] There are several proposed explanations as to why the catalysts become more tolerant when deposited on acidic supports. It has been suggested this may be due to either the polarization of the metal nanoparticles by nearby cations or to a metal-support interaction that induces a partial electron transfer between the metal and the oxide ions.[17,31-33] When this occurs, there is a higher electron density near the support interface while the atoms on the opposite side of the nanoparticles (i.e., those that participate in the catalytic reaction) are more electron deficient.[33] Overall, there is no net change in the electron density of the nanoparticle. These electron deficient metal sites

may lower the strength of the sulfur-metal bond, thereby increasing the metal's ability to remain unpoisoned.

As mentioned in Chapter 1, acidic reaction conditions were used to synthesize the metal oxide supports because using an acid as a catalyst causes the network to form linear or randomly branched polymers, which should yield an amorphous material with a higher surface area. There is another advantage to using an acid as a catalyst, specifically when it comes to synthesizing mixed metal oxides. By using acidic reactions conditions, precipitation and phase separation of one metal oxide during the sol-gel synthesis can be avoided because differences in the electronegativity of the metal ions only have a small effect on the electron density of the adjacent oxygen atoms, and therefore the attacking proton does not distinguish between the different types of metal ions.[34,35] Precipitation and phase separation are indicative of undesirable domain formation, which suggests that there is not a homogeneous distribution of the elemental oxides.[34] If domain formation is problematic, prehydrolysis of the less reactive species or modification of the more highly labile species *via* chelation have been used to compensate for the differences in the hydrolysis and condensation rates of the two different metal alkoxides.[36]

3.2 Results and Discussion

Synthesis and Screening of Trimetallic Nanoparticle Catalysts

The synthesis and screening of heterogeneous mono- and bimetallic nanoparticle catalysts for the hydrogenation of toluene under ambient conditions were previously discussed in Chapter 2. To screen for catalytic activity using trimetallic nanoparticle

catalysts, the four previously identified active bimetallic catalysts (RhPt, RuPt, IrRh, IrPt) were used as two of the three metals that would constitute the trimetallic catalysts. The third metal that was added was one of Cr, Mn, Fe, Co, Ni, Cu or Mo. These metals were selected because they are more economical than the metals that compose the active bimetallic catalysts, are typically not active as monometallic catalysts for the hydrogenation of arenes, and may increase the ability of these catalysts to resist poisoning by sulfur and nitrogen containing compounds. By using these metals in combination with the metals used in the active bimetallic catalysts (Rh, Ir, Ru and Pt), we hoped we would be able to identify a new catalyst that had an enhanced activity for the hydrogenation of arenes or an enhanced tolerance to common catalytic poisons due to the presence on the third metal.

All of the trimetallic catalysts that were synthesized were supported on Al_2O_3, and all three metals were used in equal amounts (1:1:1 ratio of each) with a total metal loading of 1 mol%. The catalysts were screened for toluene hydrogenation activity under ambient conditions, using isopropanol as a solvent and a 1:100 catalyst:substrate ratio. Shown on the leftmost side of each of the figures for the preliminary trimetallic hydrogenation screening results is the percent hydrogenation of the two parent metals at a 0.67% metal loading so that the percent hydrogenation due to those two metals at the loading used for the trimetallic catalysts could be known, and it could be determined if there was an enhancement in activity due to the addition of the third metal. On the rightmost side of each figure is the percent hydrogenation using the two metals at a 1:1 ratio and 1 mol% metal loading. Ranging in between these two bimetallic catalysts are the trimetallic catalysts using the same parent metals with a different third metal in each

case. Shown in Fig. 3.1 are the percent hydrogenation results using IrRh as the parent metals. What can be seen is that none of the trimetallic catalysts demonstrate an activity as high as the bimetallic 0.67% IrRh catalyst. However, the IrRhCr, IrRhMn and IrRhMo catalysts all exhibit a higher catalytic activity than the 1% IrRh catalyst. The other metals (Fe, Co, Ni and Cu) appear to be causing a decrease in the catalytic activity, and in the case of using Cu as the third metal, there was complete deactivation of the catalyst.

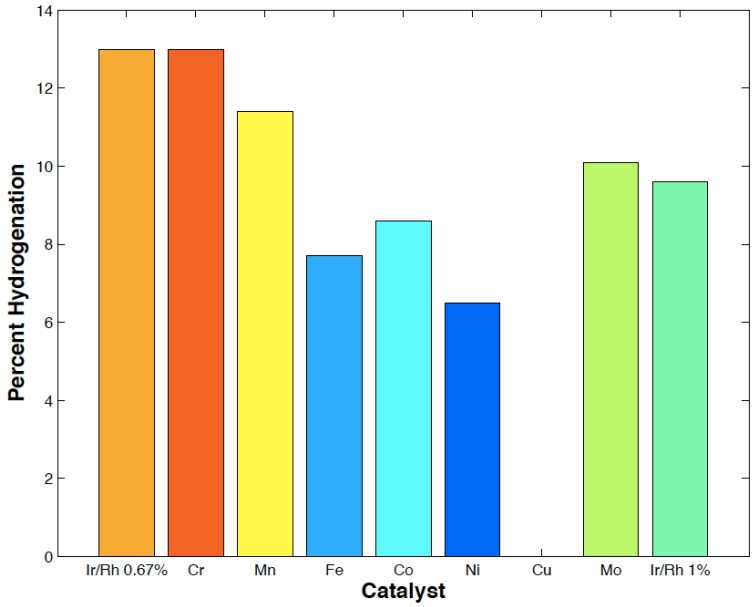

Figure 3.1. IrRhM/Al_2O_3 hydrogenation results where M = Cr, Mn, Fe, Co, Ni, Cu or Mo. The percent hydrogenation was measured after 4 hours and was determined by gas chromatography.

When using Ir and Pt as the parent metals (Fig. 3.2), it can be seen that in all cases the incorporation of a third metal caused a decrease in the catalytic activity. The decrease in catalytic activity was relatively minor when Cr and Mn were used as the third metal and this could be within experimental error, but incorporation of the other metals caused

a significant decrease in activity. These decreases in activity suggest that addition of Mn, Fe, Co, Ni or Cu causes poisoning of the catalyst, with addition of Cu completely deactivating the catalyst, as was previously observed with the IrRhCu catalyst.

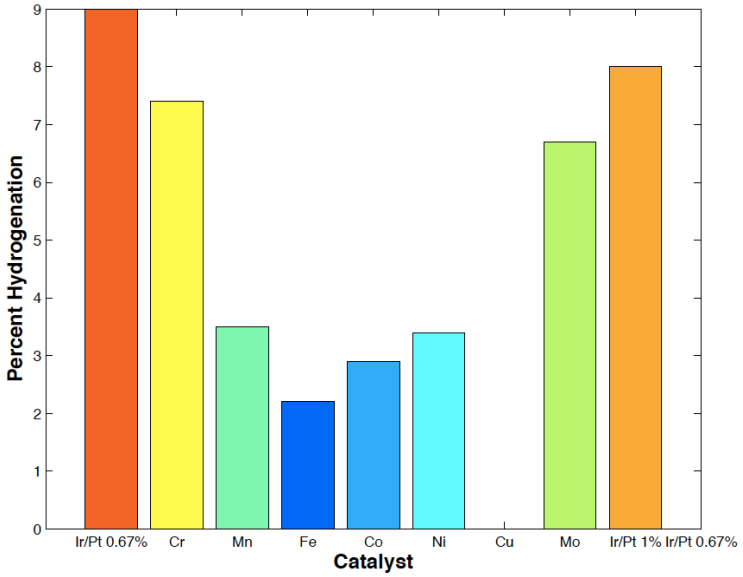

Figure 3.2. IrPtM/Al_2O_3 hydrogenation results where M = Cr, Mn, Fe, Co, Ni, Cu or Mo. The percent hydrogenation was measured after 4 hours and was determined by gas chromatography.

When Mn was added to the RhPt catalyst (Fig. 3.3) there was an increase in activity above either the percent hydrogenation values for the 1% or 0.67% bimetallic RhPt catalysts. When Cr, Fe or Co was added, the percent hydrogenation values were comparable to the bimetallic RhPt catalysts, suggesting these metals neither enhance nor poison the catalyst. However, when Ni or Mo was added, there was a decrease in activity, and when Cu was added, no catalytic activity was observed.

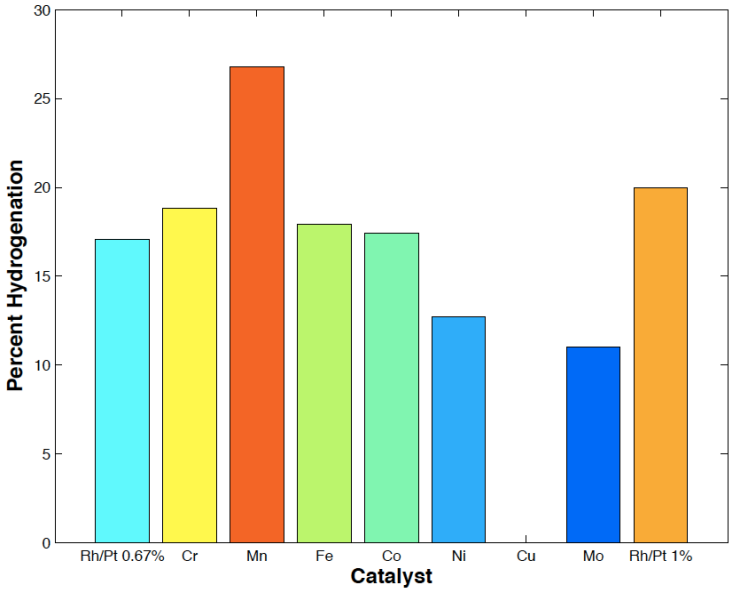

Figure 3.3. $RhPtM/Al_2O_3$ hydrogenation results where M = Cr, Mn, Fe, Co, Ni, Cu or Mo. The percent hydrogenation was measured after 4 hours and was determined by gas chromatography.

The last bimetallic combination in which a third metal was added to was RuPt (Fig. 3.4). When Mn and Mo were added, there was an increase in activity compared to the value for the 1% RuPt catalyst, but these two values were slightly lower than the values for the 0.67% RuPt catalyst. The addition of Cr, Fe Co and Ni gave percent hydrogenation values similar to the 1% RuPt catalyst, while there was a lower percent hydrogenation value observed when Cu was added. However, unlike with the other parent bimetallic catalysts, the RuPtCu catalyst did demonstrate some catalytic activity. This was the only trimetallic catalyst that contained Cu and demonstrated some degree of catalytic activity.

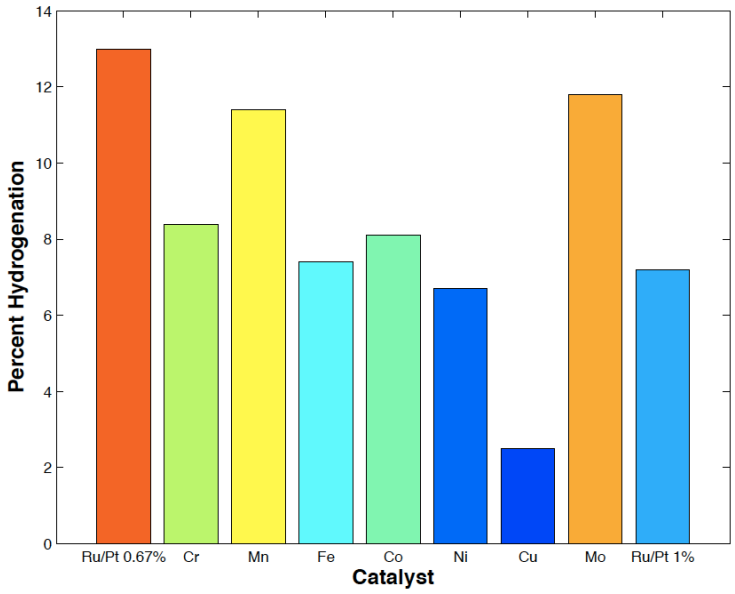

Figure 3.4. RuPtM/Al_2O_3 hydrogenation results where M = Cr, Mn, Fe, Co, Ni, Cu or Mo. The percent hydrogenation was measured after 4 hours and was determined by gas chromatography.

Once these preliminary screens had been performed to determine which metal combinations showed an enhancement in catalytic activity, the next step was to determine the quantity of the third metal that could be added to the two parent metals to achieve the maximum catalytic activity. To determine this, the active trimetallic combinations were screened using 0.1% increments of the third metal, with the two parent metals making up the remainder of the 1% total metal loading in equal amounts. When the amount of Cr in IrPtCr was varied in 0.1% increments between 0% Cr and 1% Cr, the percent hydrogenation increased slightly from $Ir_{0.5}Pt_{0.5}$ to $Ir_{0.45}Pt_{0.45}Cr_{0.1}$, but then the catalytic activity steadily decreased as the amount of Cr was progressively increased (Fig. 3.5a). When Mo was used as the tertiary metal, there was an increase in catalytic activity as the

amount of Mo was increased until the composition of $Ir_{0.35}Pt_{0.35}Mo_{0.3}$ was reached, and then the catalytic activity steadily decreased as the amount of Mo was further increased (Fig. 3.5b).

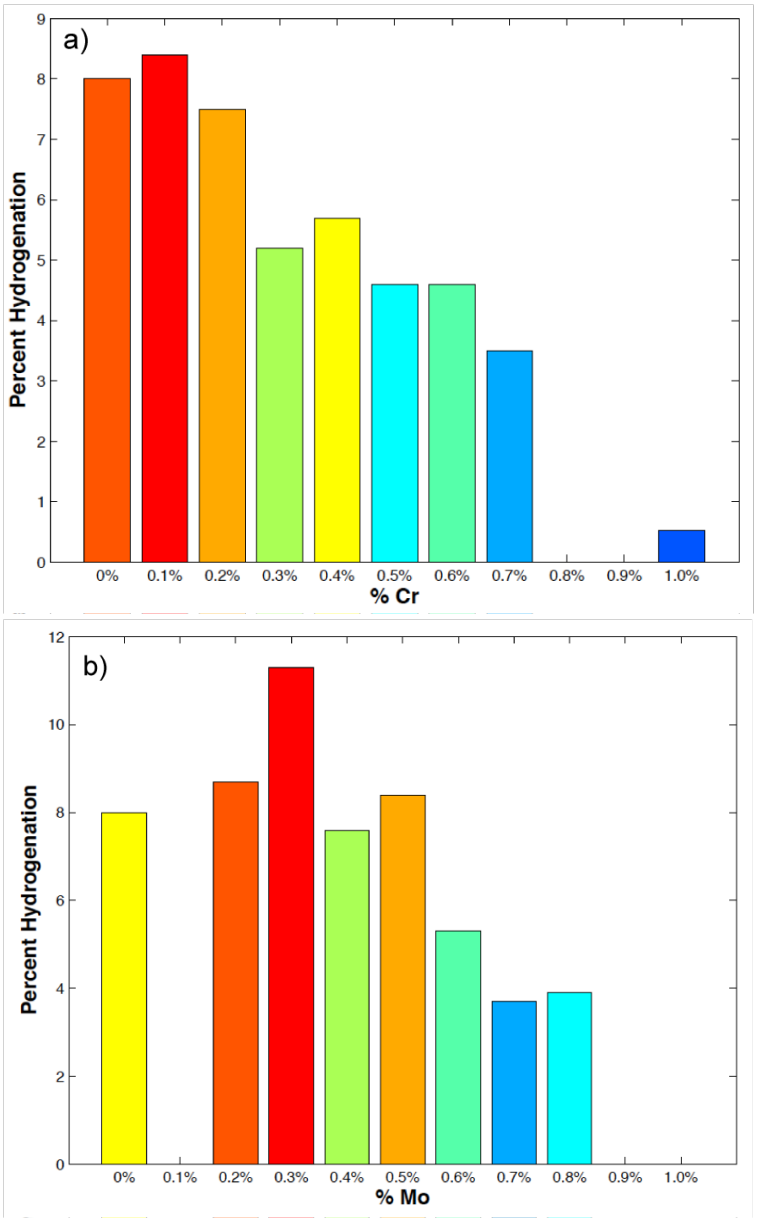

Figure 3.5. a) IrPtCr/Al_2O_3 and b) IrPtMo/Al_2O_3 hydrogenation results. The percent hydrogenation was measured after 4 hours and was determined by gas chromatography.

For the IrRh bimetallic combination, three metals were chosen for further studies: Cr, Mn and Mo (Fig. 3.6a). Beginning with IrRhCr combination, there was a slight increase in activity observed as the amount of Cr was increased from 0% to 0.1%, but as the amount of Cr was further increased, a steady decrease in the catalytic activity was detected. For both IrRhMn (Fig. 3.6b) and IrRhMo (Fig. 3.6c), the catalytic activity decreased as the proportion of the third metal increased.

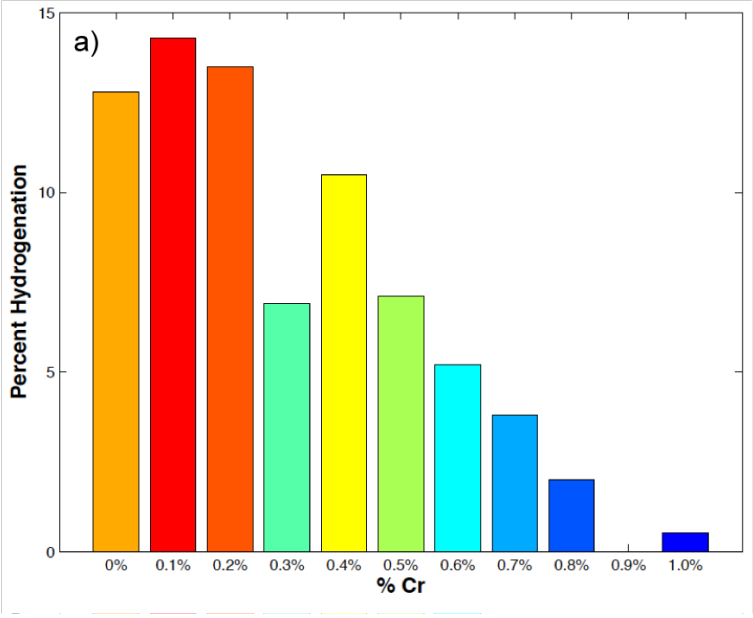

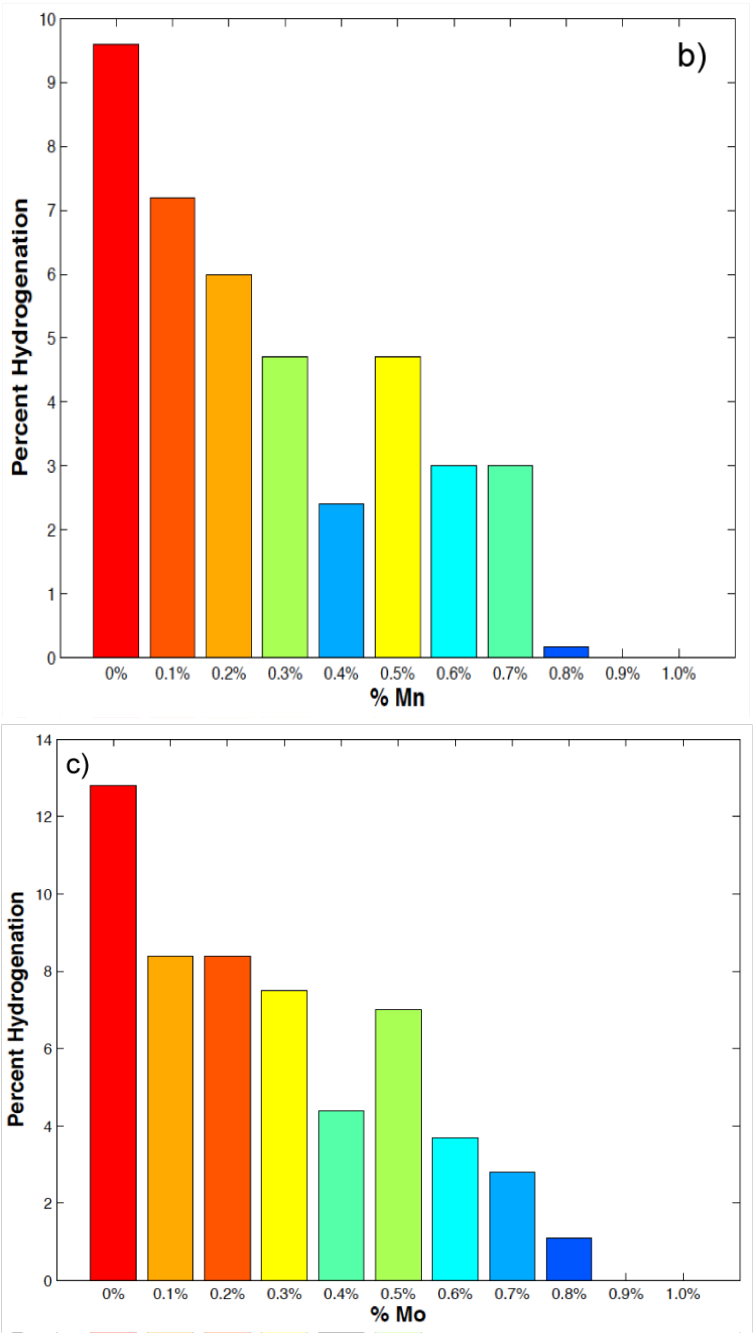

Figure 3.6. a) $IrRhCr/Al_2O_3$, b) $IrRhMn/Al_2O_3$, and c) $IrRhMo/Al_2O_3$ hydrogenation results. The percent hydrogenation was measured after 4 hours and was determined by gas chromatography.

For RhPt, the addition of either Cr or Mn demonstrated an increase in activity so these metals were chosen for further study. There was a small drop in activity when the amount of Cr was increased from 0% to 0.1% (Fig. 3.7 a), but then an increase in activity as the amount of Cr was further increased to 0.2%. From this point, the catalytic activity then constantly decreased as the amount of Cr was increased. When Mn was added as the third metal (Fig. 3.7 b), there was an increase in the catalytic activity as the composition of the nanoparticle reached $Rh_{0.2}Pt_{0.2}Mn_{0.6}$, but as the amount of Mn was further increased, the catalytic activity of the catalysts decreased.

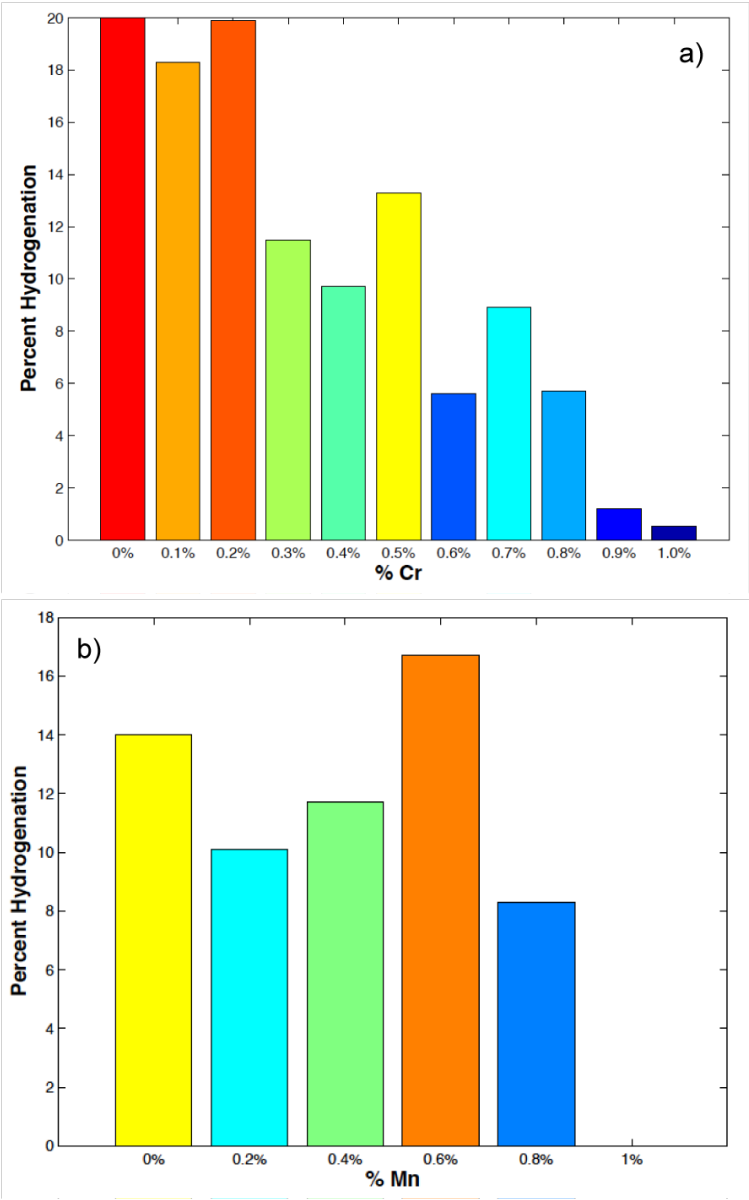

Figure 3.7. a) RhPtCr/Al_2O_3 and b) RhPtMn/Al_2O_3 hydrogenation results. The percent hydrogenation was measured after 4 hours and was determined by gas chromatography.

For RuPt, the addition of Mn and Mo was examined to determine the effect on the catalytic activity. As Mn was added to RuPt to give a catalyst containing 0.1% Mn, there was a dramatic increase in the catalytic activity. As the amount of Mn was further

increased, the catalytic activity held steady until the quantity of Mn reached 0.3%, and after that as the amount of Mn was further increased, the catalytic activity steadily decreased until the catalyst was completely deactivated. When Mo was used as the third metal, there was a slight increase in activity as the amount of Mo was increased to 0.1%, but from this point as the amount of Mo was further increased, the catalytic activity of the trimetallic catalyst dramatically decreased until the catalyst was completely deactivated.

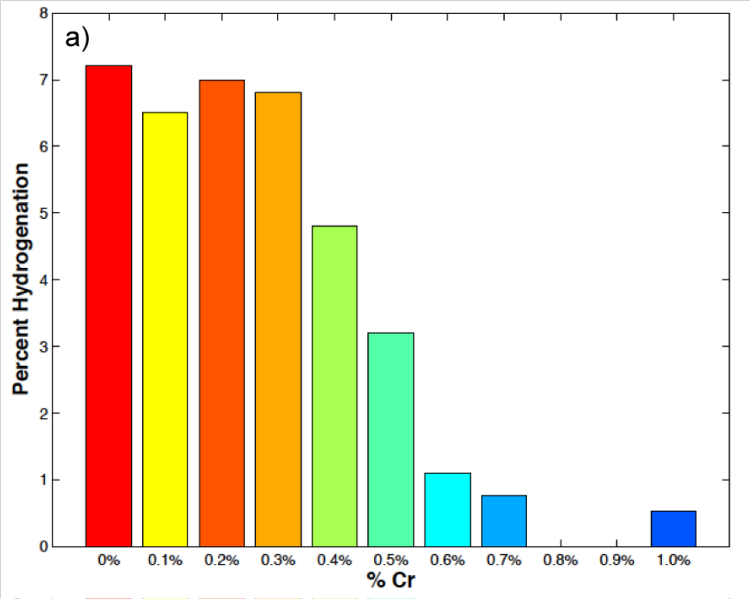

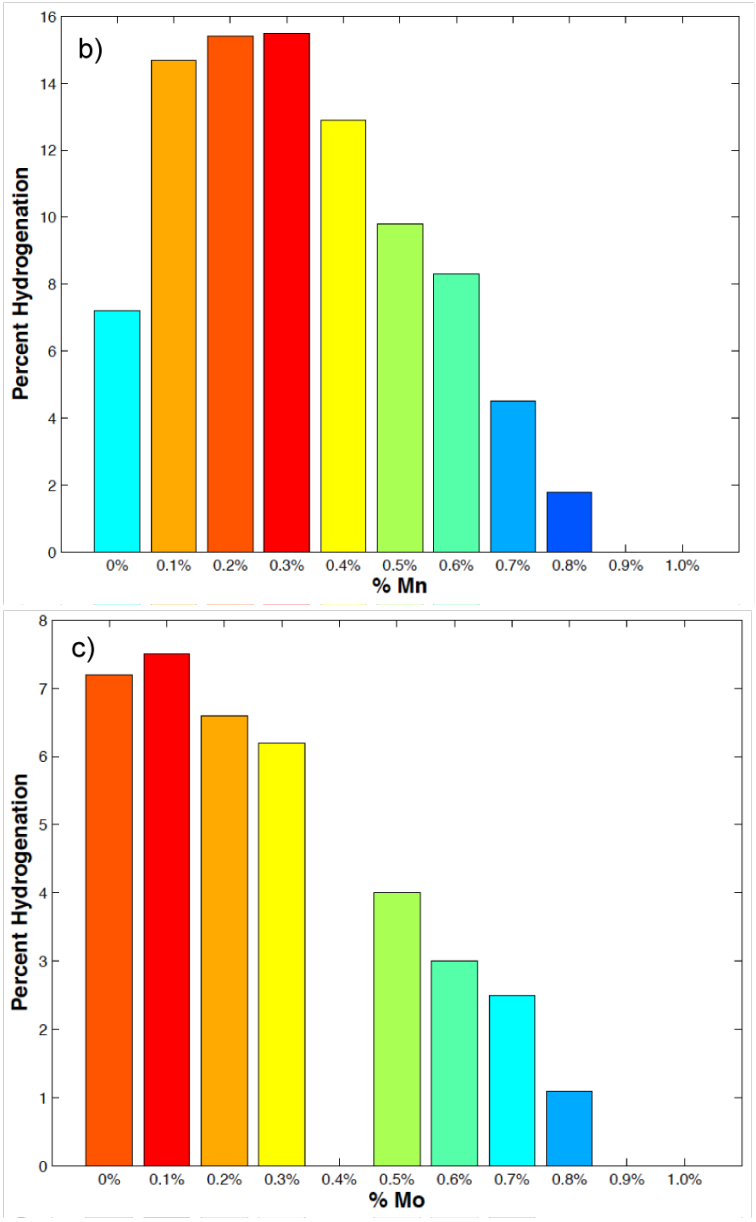

Figure 3.8. RuPtCr/Al_2O_3, b) RuPtMn/Al_2O_3 and c) RuPtMo/Al_2O_3 hydrogenation results. The percent hydrogenation was measured after 4 hours and was determined by gas chromatography.

The last set of trimetallic catalysts that were screened for catalytic activity were those that were combinations of the metals that composed the parent bimetallic catalysts

(Rh, Pt, Ir and Ru), and the results are shown in Fig. 3.9. The activities of these trimetallic catalysts were compared to the catalytic activity for the RhPt bimetallic catalyst (the left most entry), which was the highest obtained for all of the bimetallic catalysts previously examined for the hydrogenation of toluene under ambient conditions. From Fig. 3.9, it can be seen that the RhPtIr and RhPtRu catalysts exhibited a catalytic activity higher than that of the RhPt catalyst, and the RuPtIr and IrRhRu catalysts have an activity lower than that determined for the RhPt catalyst. A combination of the four metals, or a tetrametallic catalyst was also synthesized and screened, and from Fig. 3.9 it can be seen that it has an activity comparable to that of the RhPt catalyst.

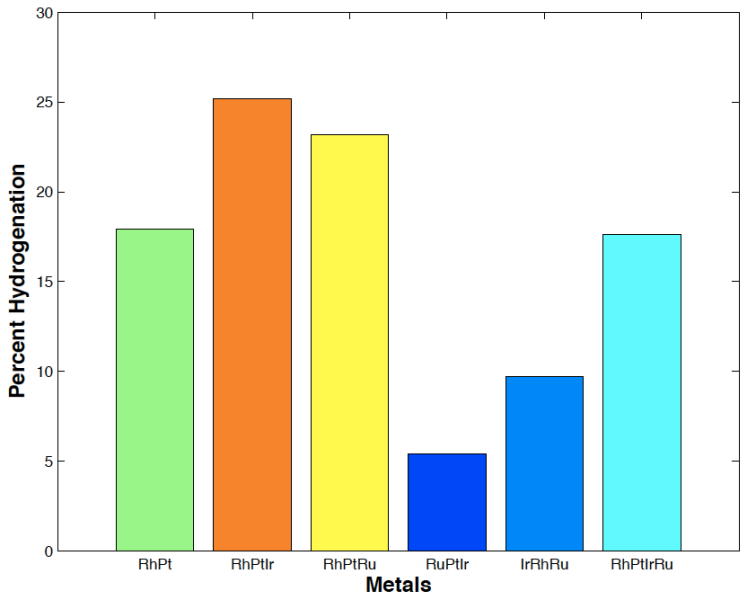

Figure 3.9. Miscellaneous tri- and tetrametallic hydrogenation results. The percent hydrogenation was measured after 4 hours and was determined by gas chromatography.

Screening of Catalysts Supported on Mixed Metal Oxides for Mono-, Poly-, and Heteroaromatic Hydrogenation Activity

Using toluene as a model substrate, the effect on the catalytic activity due to varying the identity of the metals in the catalyst was previously described. The next step in this study was to a) vary the composition of the catalyst support and b) to study the hydrogenation of poly- and heteroaromatic substrates. The motivation behind varying the composition of the catalyst support was the more acidic the catalytic support, the more able the catalyst would be to hydrogenate polyaromatic and heteroaromatic substrates. To make the catalyst support more acidic, a more acidic metal oxide or a mixed metal oxide could be used. By using a mixed metal oxide, the structure of the metal oxide becomes more amorphous which causes it to possess a higher quantity of acidic sitesdue to an increase in the number of exposed cations. Based on this, we chose 6 catalysts (Rh, RhPt, RuPt, IrRh, IrPt and RhPtIr) and three different metal oxides (Al_2O_3, SiO_2 and TiO_2) to prepare 72 catalysts. Using binary combinations of the three metal oxides in different ratios, 12 different catalyst supports were used.

The methodology used to synthesize the heterogeneous mono-, bi- and trimetallic nanoparticle catalysts involved a one-pot approach in which the metal chloride salts, the water sensitive metal alkoxides, and hydrochloric acid were mixed together. To modify the composition of the catalyst support, the ratios of the different metal alkoxides (and subsequently the amount of solvent, water and hydrochloric acid) were varied according to the desired final composition. An acid catalyzed sol-gel synthesis route was chosen and used throughout because it allowed for flexibility of using different metal alkoxides without requiring modification of the synthesis procedure.

Initially, all 72 catalysts (6 different nanoparticle compositions and 12 different support compositions) were screened for the hydrogenation of toluene, naphthalene, pyridine, indole, quinoline, thiophene and benzothiophene at a pressure of 75 psi H_2 for a reaction time of 4 hours using the High-Throughput Facility at the Centre for Catalysis Research and Innovation at the University of Ottawa. Upon subsequent analysis of the reaction mixtures by GC-MS, it was observed that while some degree of catalytic activity was observed for the hydrogenation of toluene, naphthalene, indole, quinoline and benzo[b]thiophene, no hydrogenation was observed for pyridine or thiophene using any of the 72 different catalysts (Fig. 3.10). While the unsuccessful hydrogenation of thiophene has been reported, there has been success with pyridine.[8] In addition, 16 of the 72 catalysts were inactive for all of the substrates examined. While the initial catalyst screening results yielded some interesting results and trends, in most cases, the amount of product formed was very small compared to results previously obtained in bulk under similar conditions. As a result, the five active substrates were screened again using 56 of the 72 catalysts at a pressure of 150 psi H_2 for 24 hours, and the reaction mixtures were once again analyzed by GC-MS. A visualization approach of the data was chosen to allow for easier identification of active catalysts and trends, with the results shown in Figs. 3.11, 3.14-3.17.

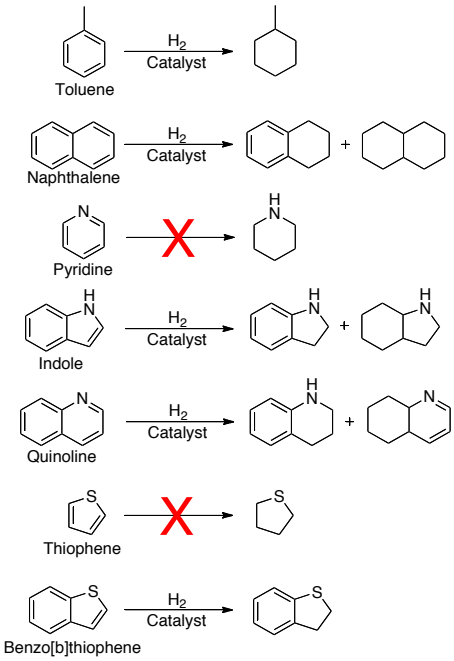

Figure 3.10. Aromatic substrates and the observed hydrogenation products as determined by GC-MS analysis.

In Fig. 3.11, shown along the x axis are the various support compositions, on the z axis are the different metal nanoparticle compositions, and on the y axis are the percent hydrogenation values as determined by GC-MS after 24 hours. Even though the hydrogenation of toluene was previously thoroughly studied,[37] it was examined again because we knew that our synthesized catalysts were active for the hydrogenation of toluene under ambient conditions, so it acted as a "double check" to ensure the synthesized catalysts were still active, and that there were no design flaws in the experimental set up. For the hydrogenation of toluene, only the fully hydrogenated product, methylcyclohexane was detected via GC-MS. It appeared that the most active catalyst support was Al_2O_3, though mixed metal oxide supports that were rich in Al_2O_3 (with the exception of Al_2O_3(25%)-SiO_2(75%)) also demonstrated a higher activity than

those poor in Al_2O_3. If there was no Al_2O_3 present in the catalyst support, supports that were rich in TiO_2 also demonstrated some activity for the hydrogenation of toluene though the observed percent hydrogenation values were lower than those obtained when Al_2O_3 was present. These results suggest that some quantity of Al_2O_3 is desirable in the catalyst support in order for an appreciable catalytic activity to be observed under the chosen reaction conditions. A similar trend was observed for the hydrogenation of ethene using Rh on SiO_2, SiO_2(75%)-Al_2O_3(25%) and SiO_2(50%)-Al_2O_3(50%) where higher hydrogenation activities were observed for the catalyst supports which contained a higher percentage of Al_2O_3.[38] The metal nanoparticle compositions that demonstrated the highest activity for the hydrogenation of toluene appeared to be the Rh_1, $Rh_{0.5}Pt_{0.5}$ and the $Rh_{0.33}Pt_{0.33}Ir_{0.33}$ combinations, though all of the other bimetallic catalysts did demonstrate some degree of activity, suggesting that if an active catalyst support was used then the reaction did not depend on the composition of the metal nanoparticles.

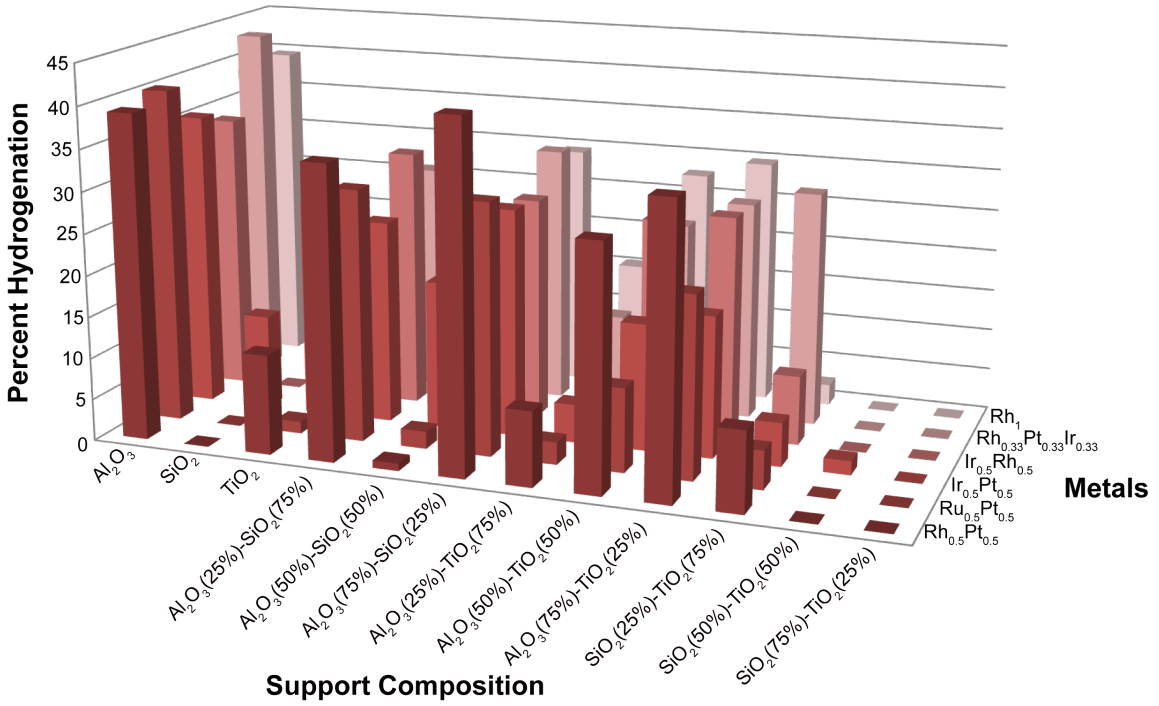

Figure 3.11. Toluene hydrogenation results. The percent hydrogenation was measured after 24 hours of stirring at 150 psi hydrogen pressure, and the only observed product was methylcyclohexane.

To more clearly show the trends in catalytic activity as a function of support, the percent hydrogenation results as a function of support composition using the $Rh_{0.5}Pt_{0.5}$ nanoparticles for the hydrogenation of toluene is shown in Fig. 3.12. The average percent hydrogenation value was determined to be 17.5%, and is indicated by the blue line in Fig. 3.12. By considering which catalysts exhibited a catalytic activity above the average value, it can be seen that all of the more active catalysts contained some percentage of Al_2O_3. Furthermore, with the exception of the Al_2O_3(25%)-SiO_2(75%) support composition, all of the more active catalyst supports contain at least 50% Al_2O_3.

The exception to this trend is the Al_2O_3(50%)-SiO_2(50%) support composition which did not give active catalysts.

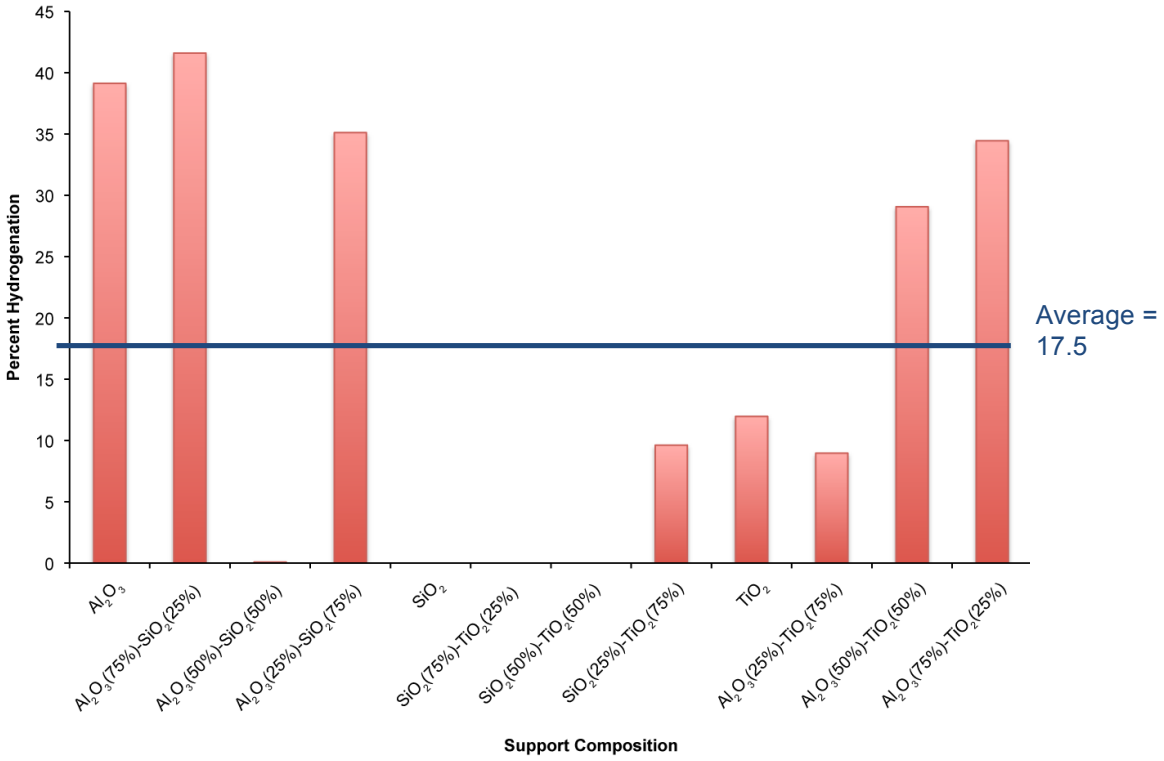

Figure 3.12. Graph showing the trend in catalytic activity as a function of support composition using the $Rh_{0.5}Pt_{0.5}$ nanoparticles for toluene hydrogenation.

From Fig. 3.12 it can also be seen that any catalysts supported on SiO_2, SiO_2(50%)-TiO_2(50%) and SiO_2(75%)-TiO_2(25%) were inactive for the hydrogenation of toluene. To determine whether or not this lack in catalytic activity could be attributed to the size of the nanoparticles since catalytic activity does depend on the nanoparticle size, TEM images were obtained for the same nanoparticle composition ($Rh_{0.5}Pt_{0.5}$) on three different metal oxides (Fig. 3.13). It was observed that $Rh_{0.5}Pt_{0.5}$ nanoparticles supported

on Al_2O_3 had a diameter of 3.06 nm, a diameter of 5.18 nm when supported on SiO_2 and 2.22 nm when supported on TiO_2. The nanoparticles supported on SiO_2 are much larger than those supported on the other two metal oxides, and the lack of catalytic activity demonstrated by these nanoparticles could be attributed to their larger size. This suggests that that the size of the nanoparticles may be controlled by the composition of the catalyst support.

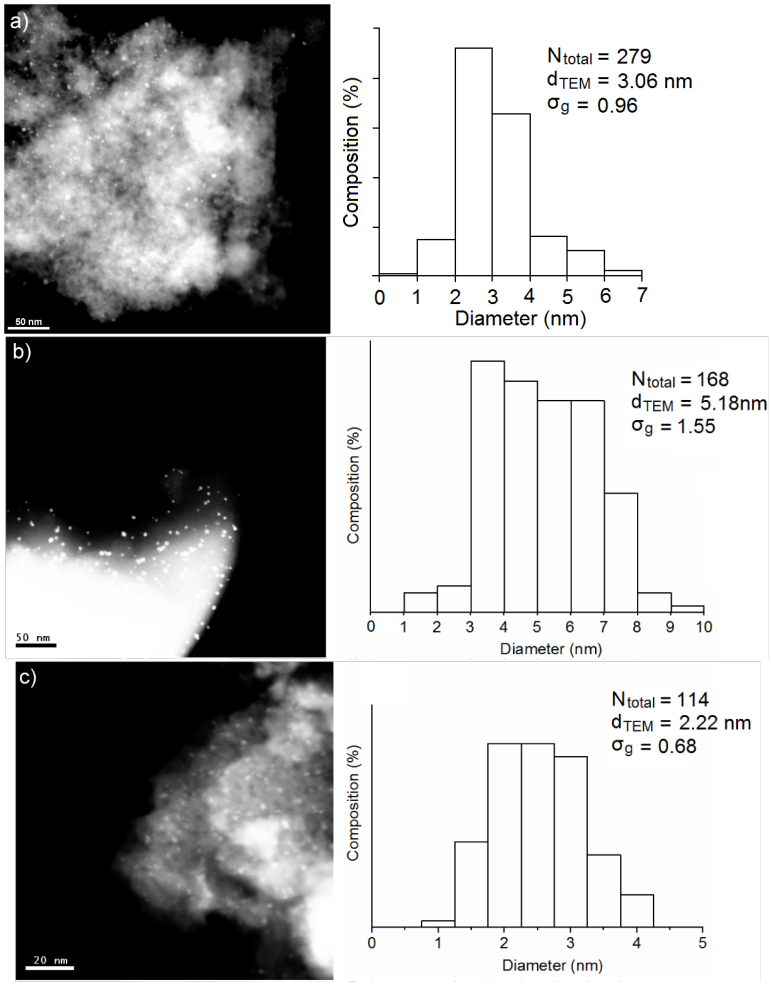

Figure 3.13. Dark field TEM images and particle size histograms for a) $Rh_{0.5}Pt_{0.5}/Al_2O_3$, b) $Rh_{0.5}Pt_{0.5}/SiO_2$, and c) $Rh_{0.5}Pt_{0.5}/TiO_2$.

For the hydrogenation of naphthalene (Fig. 3.14), in most cases only the partially hydrogenated product, 1,2,3,4-tetrahydronaphthalene was observed, though for a few select catalysts the fully hydrogenated decahydronaphthalene product was also observed. When considering the trends in activity as a function of the nanoparticle composition, the Rh_1 and $Rh_{0.5}Pt_{0.5}$ nanoparticle compositions demonstrated the highest catalytic activity while the $Ir_{0.5}Pt_{0.5}$ and $Ru_{0.5}Pt_{0.5}$ nanoparticle compositions tended to be the least active. As compared to the toluene hydrogenation results, there also appeared to be fewer catalysts that were active for the hydrogenation of naphthalene than for toluene. Catalysts supported on Al_2O_3(25%)-SiO_2(75%) appeared to exhibit the most consistent activity, while some of the other catalyst supports, such as Al_2O_3 and Al_2O_3(75%)-TiO_2(25%) were only active when certain metal combinations were used. Furthermore, the percent hydrogenation scale shown on the y-axis for the hydrogenation of naphthalene was much smaller than the scale for the hydrogenation of toluene, demonstrating the challenge that the hydrogenation of polyaromatic hydrocarbons presents. Overall, it can be observed that the choice of metal nanoparticle composition and metal oxide support is much more crucial than it was for the hydrogenation of toluene.

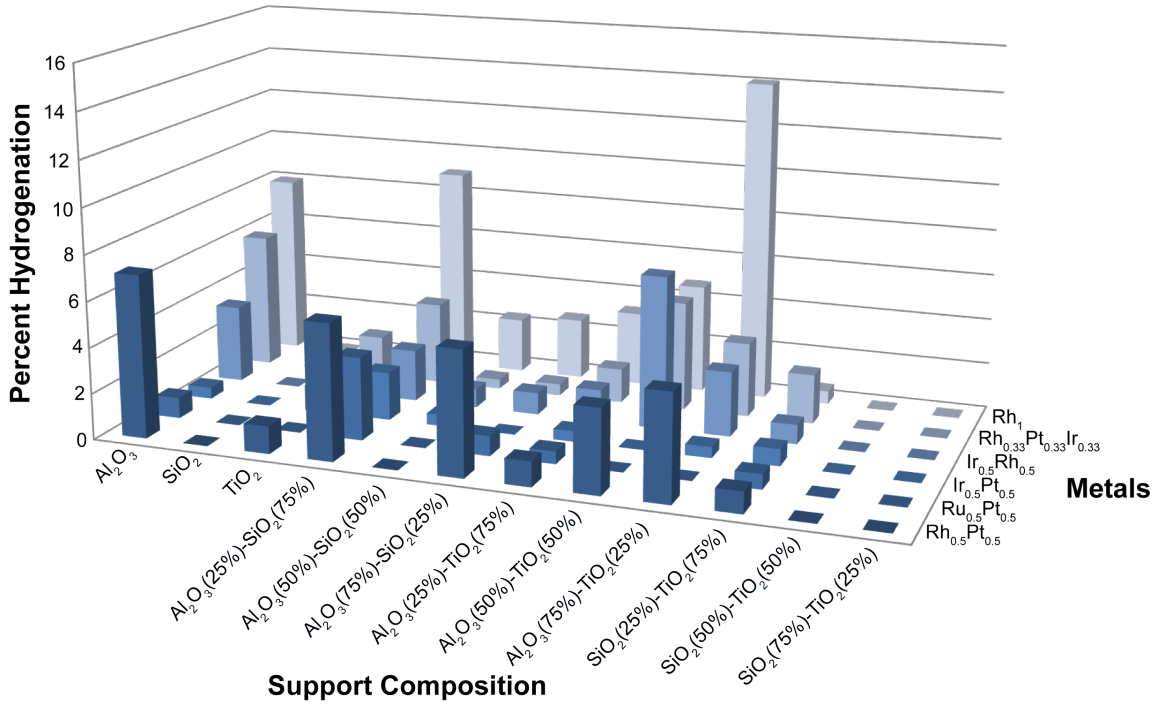

Figure 3.14. Naphthalene hydrogenation results. The percent hydrogenation was measured after 24 hours of stirring at 150 psi hydrogen pressure, and the observed products were 1,2,3,4-tetrahydronaphthalene and decahydronaphthalene.

Substantially different results were observed when considering the screening results for the hydrogenation of indole (Fig. 3.15). Both the partially hydrogenated (2,3-dihydroindole) and fully hydrogenationed products (octahydroindole) were observed. Again, the same five catalyst supports demonstrated active nanoparticle catalysts, but it was much more obvious which metal nanoparticle compositions were catalytically active. Specifically, $Rh_{0.5}Pt_{0.5}$, $Ir_{0.5}Rh_{0.5}$ and Rh_1 were the most active nanoparticle compositions, and essentially the other metallic nanoparticle compositions were inactive for the hydrogenation of indole. Unlike the screening results for the hydrogenation of toluene

and naphthalene, there were even fewer catalysts that were active for the hydrogenation of indole. However, these results were very promising because they indicate that not only are our catalysts are robust enough to resist poisoning by this N-heteroaromatic compound, they can begin to hydrogenate it under these mild reaction conditions.

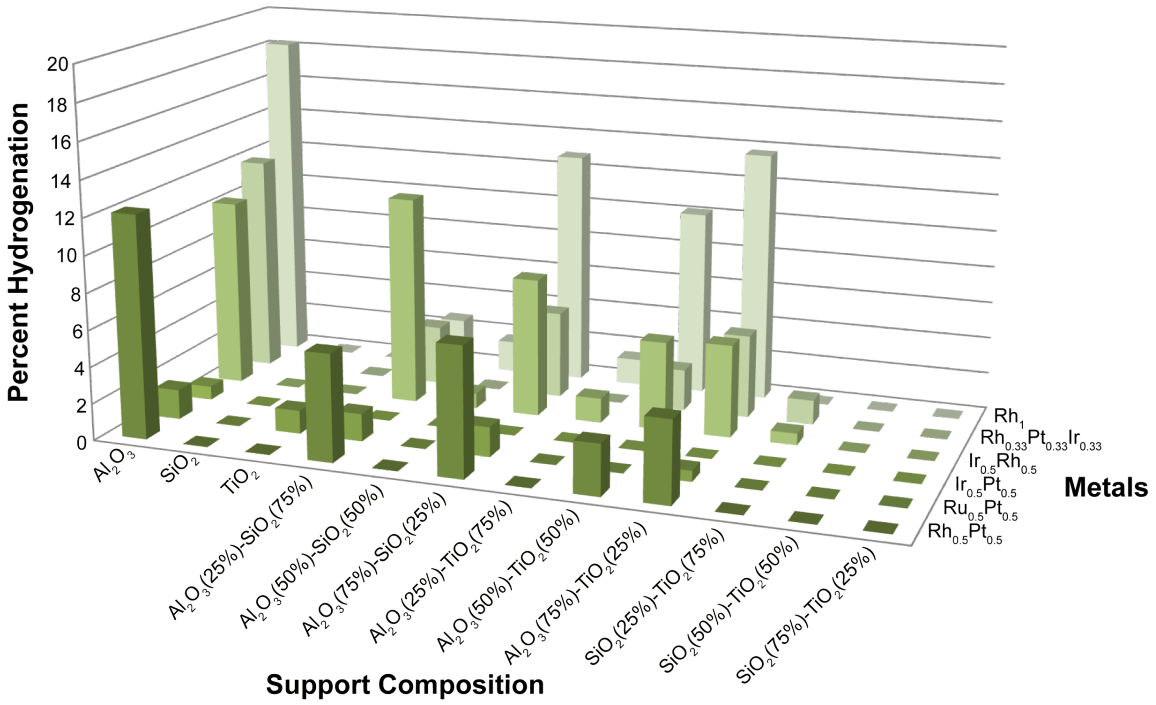

Figure 3.15. Indole hydrogenation results. The percent hydrogenation was measured after 24 hours of stirring at 150 psi hydrogen pressure, and the observed products were 2,3-dihydroindole and octahydroindole.

For the quinoline hydrogenation results (Fig. 3.16) what was most intriguing was the observed percent hydrogenation values, which exceeded those observed for the hydrogenation of any of the other substrates examined. This was unusual since the hydrocarbon analogue of quinoline, naphthalene, does not exhibit percent hydrogenation

values nearly this high, which demonstrated the effect that the nitrogen atom in the aromatic ring had on the catalytic activity. This could be attributed to the support being acidic and the substrate is basic leading to a stronger attraction for quinoline to the catalyst support than for naphthalene, facilitating the hydrogenation reaction. The same support trends as for the other substrates were also observed, though it was much more pronounced with these results since only those five catalyst supports gave an appreciable percent hydrogenation value, and catalysts supported on other supports had very low activities. However, if one of those five active supports was used, then any of the six metal nanoparticle compositions were active, though $Rh_{0.5}Pt_{0.5}$ and Rh_1 appear to be consistently the most active. The observed products for the hydrogenation of quinoline were the partially hydrogenated 1,2,3,4-tetrahydroquinoline and 5,6,7,8-tetrahydroquinoline. The fully hydrogenated decahydroquinoline was not observed under these reaction conditions, because typically much more harsh conditions (temperatures in the rate of 175-280ºC, hydrogen pressure between 1595 and 3046 psi H_2 and an acidic solvent) are required for complete hydrogenation.[1]

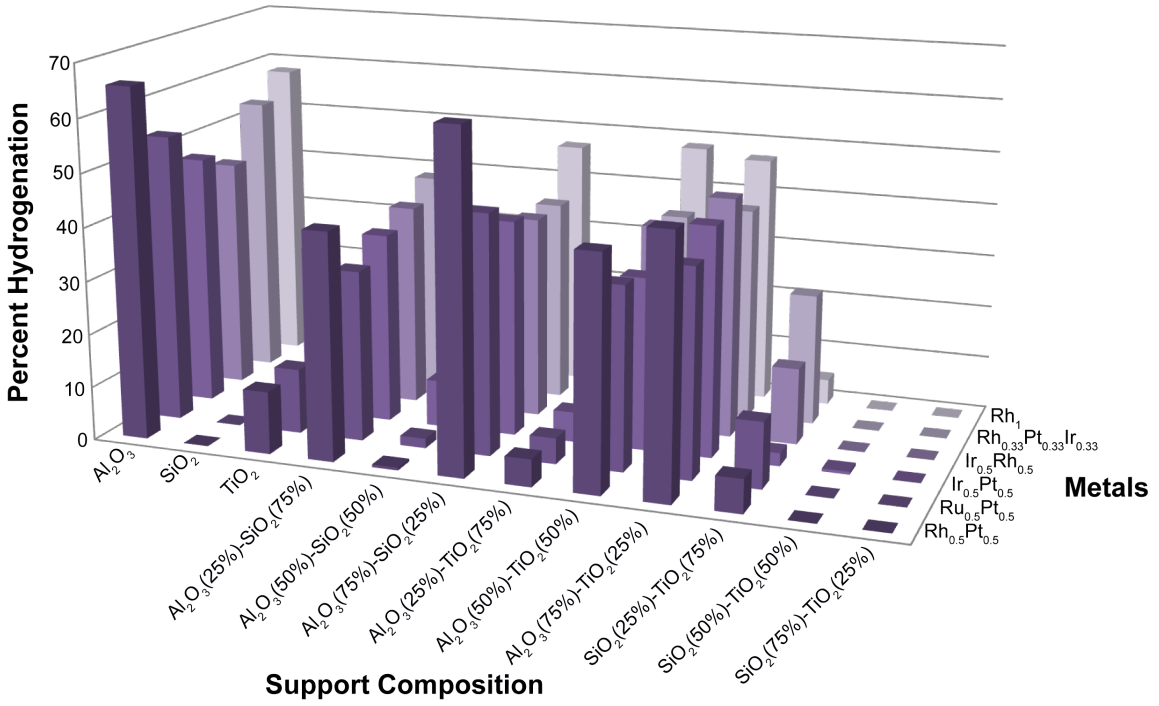

Figure 3.16. Quinoline hydrogenation results. The percent hydrogenation was measured after 24 hours of stirring at 150 psi hydrogen pressure, and the observed products were 1,2,3,4-tetrahydroquinoline and 5,6,7,8-tetrahydroquinoline.

Lastly, the 72 catalysts were screened for the hydrogenation of benzothiophene, a model S-heteroaromatic compound. While some of the catalysts demonstrated some catalytic activity for the hydrogenation of benzothiophene, the values for the percent hydrogenation were significantly lower (< 4%) than any of those previously observed for any of the other substrates (Fig. 3.17). This indicated that while some degree of hydrogenation was occurring, the catalyst was becoming deactivated fairly quickly, and was likely being poisoned by this sulfur containing substrate. The most active metal combinations for the hydrogenation of benzothiophene were $Rh_{0.5}Pt_{0.5}$, $Ir_{0.5}Rh_{0.5}$, $Rh_{0.33}Pt_{0.33}Ir_{0.33}$ and Rh_1. The most active catalyst supports appear to be Al_2O_3,

Al_2O_3(25%)-SiO_2(75%), Al_2O_3(75%)-SiO_2(25%), Al_2O_3(50%)-TiO_2(50%) and Al_2O_3(75%)-TiO_2(25%). Even though the percent hydrogenation values were low, it is promising that these catalysts demonstrated some degree of hydrogenation before being poisoned.

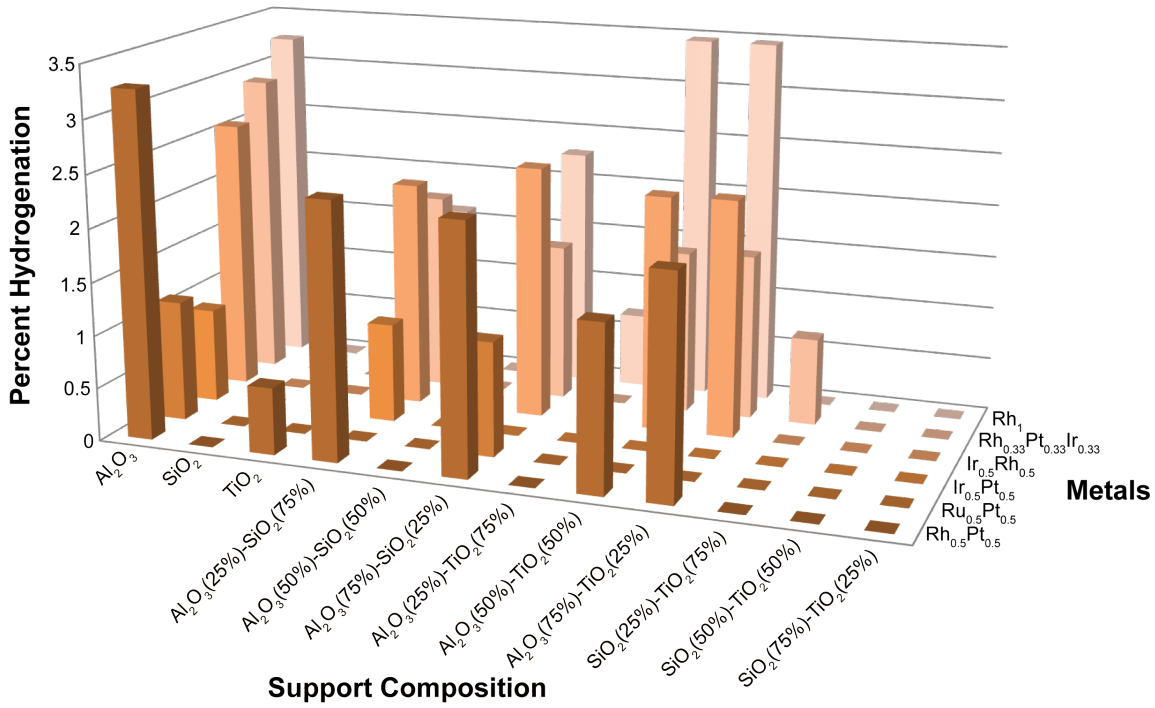

Figure 3.17. Benzothiophene hydrogenation results. The percent hydrogenation was measured after 24 hours of stirring at 150 psi hydrogen pressure, and the only observed product was 2,3-dihydrobenzothiophene.

Once the 72 different nanoparticle catalysts had been screened for activity for the hydrogenation of toluene, naphthalene, pyridine, indole, quinoline, thiophene and benzothiophene, several catalysts were chosen for further studies in bulk. $Rh_{0.5}Pt_{0.5}/Al_2O_3$ was chosen because it was one of most active bimetallic catalysts overall. Rh_1/Al_2O_3 and

$Rh_1/Al_2O_3(25\%)$-$SiO_2(75\%)$ were selected for several reasons. These two catalysts were quite active for the hydrogenation of naphthalene, and it would also allow us to determine the effect of using a mixed metal oxide support would have on the catalytic activity of the nanoparticle catalysts. $Rh_{0.33}Pt_{0.33}Ir_{0.33}/Al_2O_3$ was chosen because it was the only trimetallic nanoparticle catalyst that exhibited some potential for enhanced catalytic activity, and the commercial 0.5% Rh/Al_2O_3 catalysts was selected because it is a readily available commercial catalyst. As well, only two substrates were chosen for further studies: naphthalene and quinoline. Naphthalene was chosen because it is a simple polyaromatic hydrocarbon, both the partially hydrogenated and fully hydrogenated products were observed, and a variety of catalysts demonstrated activity for this substrate. Quinoline was selected because it has the same structure as naphthalene except that a nitrogen atom replaced one of the carbon atoms, allowing the effect on the catalytic activity by incorporating in a heteroatom to be studied. Furthermore, during the initial screening process, the highest observed percent hydrogenation values were obtained when quinoline was used as the substrate. Even though the majority of the catalysts that were screened for the hydrogenation of toluene were quite active, toluene was not chosen for further studies because it had already been studied in depth using $Rh_{0.5}Pt_{0.5}/Al_2O_3$.[37]

Bulk Temperature, Pressure and Loading Studies

To measure the naphthalene hydrogenation rates in bulk, a pressure reactor was used, and the decrease in hydrogen pressure was monitored as a function of time. The observed rates were measured using the first two hours of the hydrogenation data,

thought the reaction was monitored for at least 7 hours. The rates were measured at initial pressures of 74, 147, 294, and 441 psig at ambient temperatures using 7 different catalysts with the results shown in Figure 3.18. Both tetrahydronaphthalene and decahydronaphthalene were observed for many of the catalysts during the course of the reactions. Usually, tetrahydronaphthalene is the first product observed during the hydrogenation of naphthalene, and if a reaction is allowed to run for a long enough period of time, decahydronaphthalene may be detected.[8]

Immediately noticeable was the commercial 0.5% Rh/Al_2O_3 catalyst demonstrated a much higher catalytic activity than any of the other synthesized catalysts. Also, as the pressure increased while the temperature was held constant, there was a corresponding increase in the observed rate. The increase in rate appeared to be fairly linear as the pressure was increased to 294 psig, but as the pressure was further increased to 441 psig, the increase in observed rate deviated from linearity and appeared to plateau. For the most active catalyst (the commercial 0.5% Rh/Al_2O_3 catalyst at a pressure of 441 psig) a total pressure drop of 14 psi was observed during the first two hours of the catalytic reaction. With the synthesized catalysts, most demonstrated a drop in catalytic activity when the pressure was increased from 74 psig to 147 psig, but the catalytic activity increased as the pressure was further increased to 294 psig and 441 psig. The only catalyst that did not demonstrate this trend in activity was the Rh_1/Al_2O_3 catalyst, which was not active until the pressure reached 294 psig, and the $Rh_{0.5}Pt_{0.5}/Al_2O_3$ catalyst, which exhibited an increase in catalytic activity at 147 psig, but then the catalytic activity decreased as the pressure was further increased. The majority of the catalysts also

exhibited their highest catalytic activity at a pressure of 441 psig, with the exception of $Rh_1/Al_2O_3(75\%)$-$SiO_2(25\%)$ and $Rh_{0.5}Pt_{0.5}/Al_2O_3$.

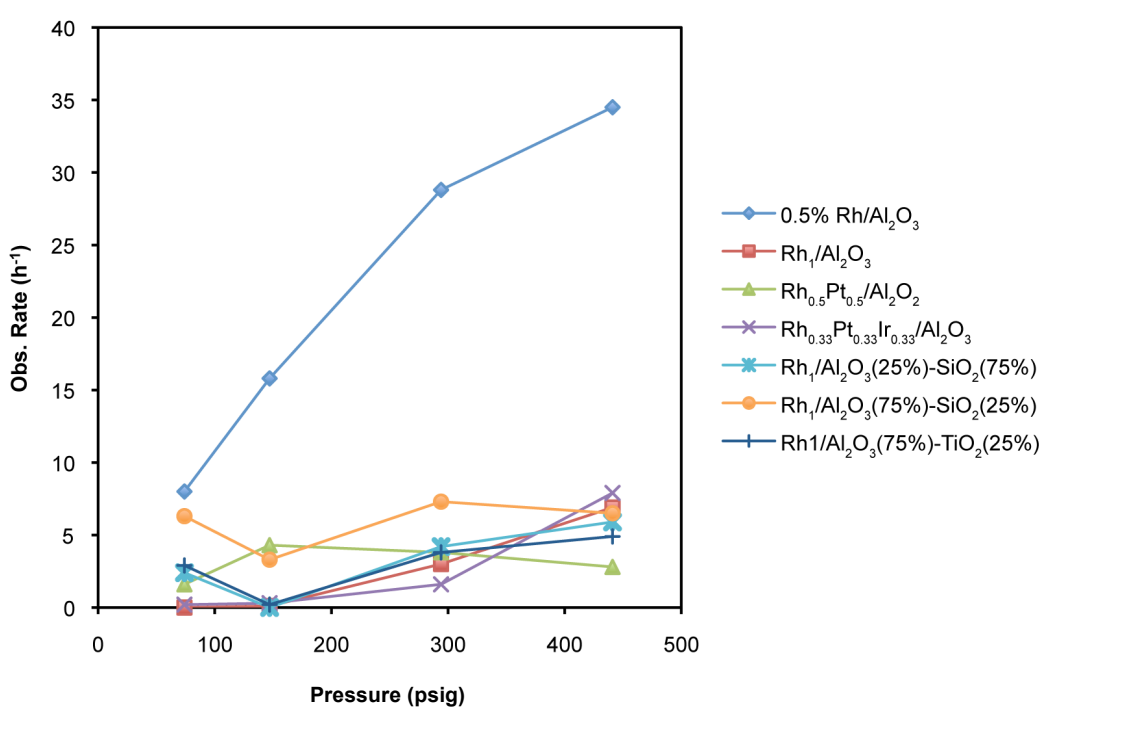

Figure 3.18. Observed rates for the hydrogenation of naphthalene at room temperature and various pressures using select catalysts.

A similar pressure study was performed using quinoline as the substrate. The same hydrogenation setup and procedure was used as with the naphthalene hydrogenation experiments, and the results are shown in Fig. 3.19. Both the partially hydrogenated (1,2,3,4-tetrahydroquinoline) and fully hydrogenated (decahydroquinoline) products were formed. At lower pressures (74 and 147 psig), the $Rh_{0.5}Pt_{0.5}/Al_2O_3$ catalyst was the most active catalyst, followed by the commercial 0.5% Rh/Al_2O_3 catalyst and then the $Rh_{0.33}Pt_{0.33}Ir_{0.33}/Al_2O_3$ catalyst. However, at higher pressures (294 and 441 psig), the

commercial 0.5% Rh/Al_2O_3 catalyst was the most active, followed by the bimetallic $Rh_{0.5}Pt_{0.5}/Al_2O_3$ catalyst and then the trimetallic $Rh_{0.33}Pt_{0.33}Ir_{0.33}/Al_2O_3$ catalyst. For the most active catalyst (the commercial 0.5% Rh/Al_2O_3 catalyst at a pressure of 441 psig) a total pressure drop of 15 psi was observed during the first two hours of the catalytic reaction. It also appeared that overall, the catalyst supported on the mixed metal oxide support ($Rh_1/Al_2O_3(25\%)$-$SiO_2(75\%)$) was the least active catalyst regardless of the reaction pressure. When the activity of the Rh_1 catalyst supported on the mixed metal oxide was compared to the activity of the Rh_1 catalyst on the Al_2O_3 support, it seemed that incorporation of SiO_2 into the support caused a decrease in the catalytic activity. However, both Rh_1/Al_2O_3 and $Rh_1/Al_2O_3(25\%)$-$SiO_2(75\%)$ exhibited similar trends in activity as the pressure was increased: a decrease in activity as the pressure increased to 147 psig, and then increases in activity as the pressure was further increased. None of the other catalysts exhibited these trends in activity.

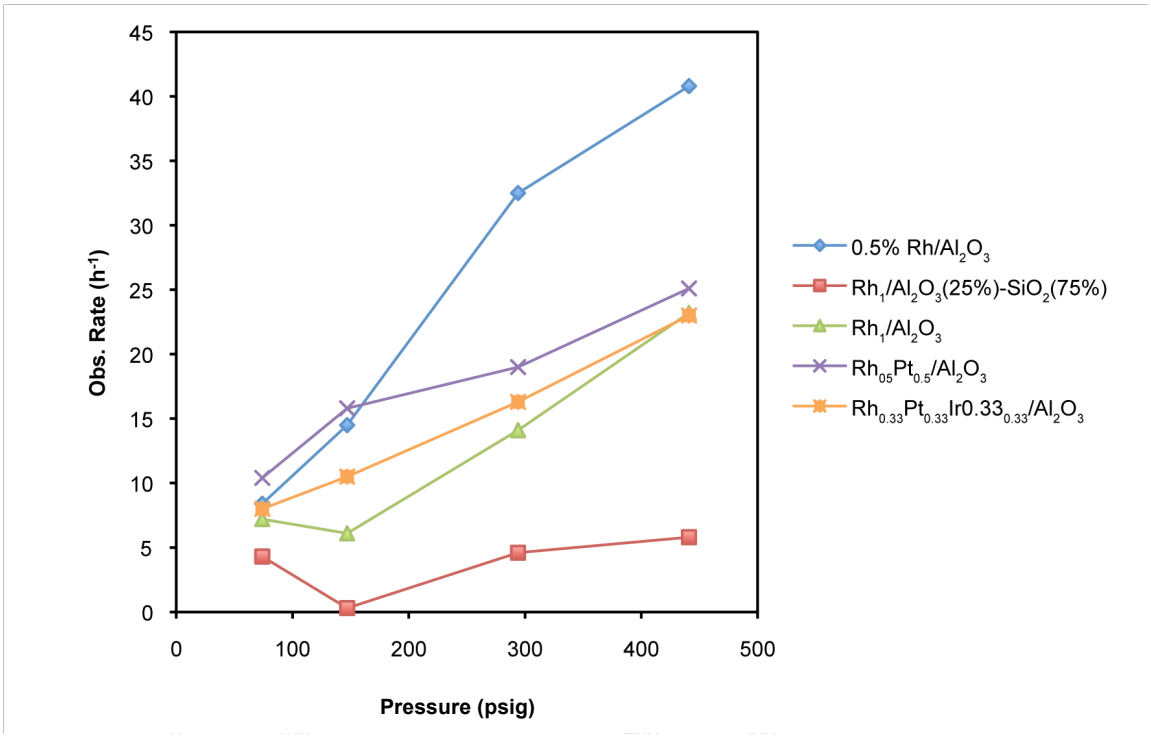

Figure 3.19. Observed rates for the hydrogenation of quinoline at room temperature and various pressures using select catalysts.

The temperature of the naphthalene hydrogenation reactions was also varied while the pressure was held constant at 294 psig H_2. The observed rates were measured at 22, 40, 60 and 80ºC using 7 different heterogeneous nanoparticle catalysts. Both the partially hydrogenated 1,2,3,4-tetrahydronaphthalene and fully hydrogenated decahydronaphthalene products were formed. From the graph in Fig. 3.20 of the temperature of the hydrogenation reaction versus the observed rates, it can be seen that the commercial 0.5% Rh/Al_2O_3 catalyst substantially outperforms any of the synthesized nanoparticle catalysts. For the most active catalyst (the commercial 0.5% Rh/Al_2O_3 catalyst at a temperature of 40ºC) a total pressure drop of 26 psi was observed during the

first two hours of the catalytic reaction. The activity of the commercial catalyst also does not appear increase linearly as the temperature of the hydrogenation reaction was increased. There was a significant decrease in activity observed as the temperature of the reaction was increased from 40 to 60ºC, and then the activity held constant as the temperature reached 80ºC. Similarly, the Rh_1/Al_2O_3 catalyst displayed an increase in activity as the temperature was increased from 22ºC to 40ºC, then a decrease as the temperature was increased to 60ºC, and finally an increase as the temperature was increased to 80ºC. All of the other synthesized catalysts showed an increase in activity as the temperature was increased to 40ºC, and then the activity decreased as the temperature was further increased.

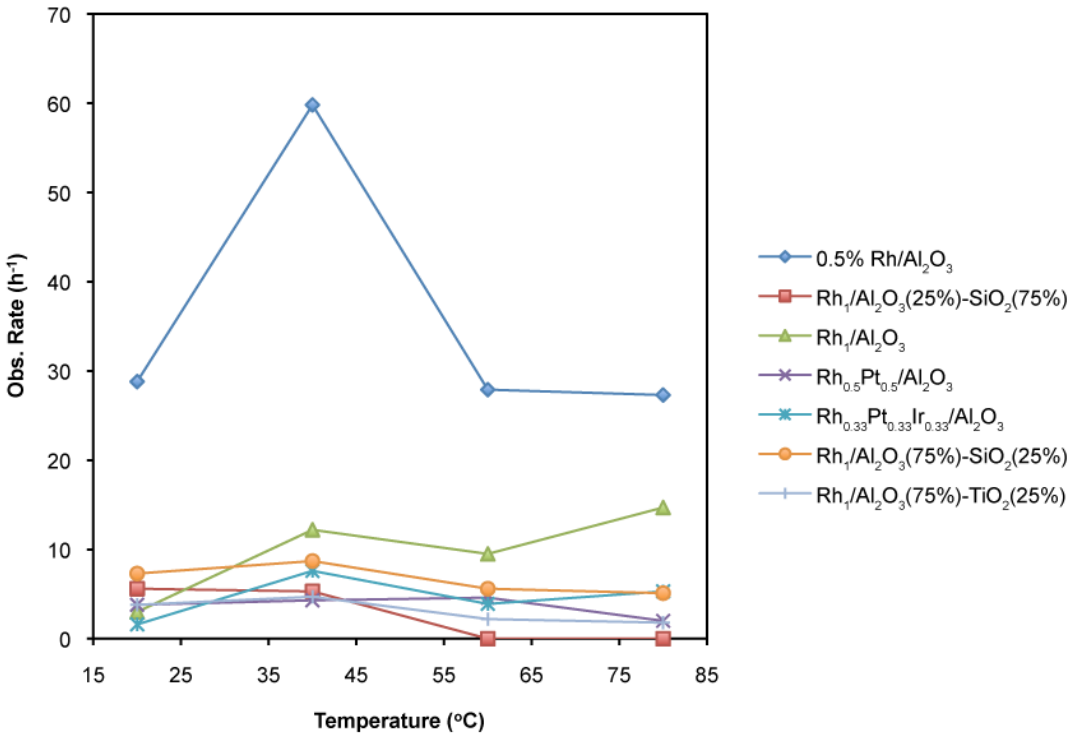

Figure 3.20. Observed rates for the hydrogenation of naphthalene at 294 psig H_2 and various temperatures using select catalysts.

The hydrogenation of quinoline at constant pressure (15 psi H_2) and various temperatures was also studied using several catalysts (Fig. 3.21). Unlike the previous temperature and pressures studies, this study was performed on a Schlenk line at atmospheric hydrogen pressure. The progress of the reactions was monitored by GC, in which a sample of the reaction mixture was analyzed ever 15 minutes for the first two hours of the reaction, followed by every hour for an additional five hours. Furthermore, because the reactions were being monitored by GC, decahydronaphthalene was added as an internal standard. The first two hours of data was used to calculate the observed rates, and only the partially hydrogenated product, 1,2,3,4-tetrahydroquinline, was detected via GC. The commercial 0.5% Rh/Al_2O_3 and $Rh_{0.5}Pt_{0.5}/Al_2O_3$ catalysts demonstrated very similar catalytic activities at all of the temperatures studied. The commercial catalyst demonstrated a slightly higher catalytic activity at 22ºC, but the $Rh_{0.5}Pt_{0.5}/Al_2O_3$ catalyst exhibited a comparable or higher activities at 40, 60 and 80ºC. The next most active catalyst was the monometallic Rh_1/Al_2O_3 catalyst, which showed a decrease in activity at 40ºC, but then a large increase in activity as the temperature was further increased to 60ºC. The activity stayed constant as the temperature approached 80ºC. The trimetallic $Rh_{0.33}Pt_{0.33}Ir_{0.33/}Al_2O_3$ catalyst exhibited an increase in activity as the temperature was increased to 40ºC, a decrease at 60ºC and an increase at 80ºC. Finally, the $Rh_1/Al_2O_3(25\%)$-$SiO_2(75\%)$ catalyst was inactive at 15 psi H_2 and at all temperatures studied.

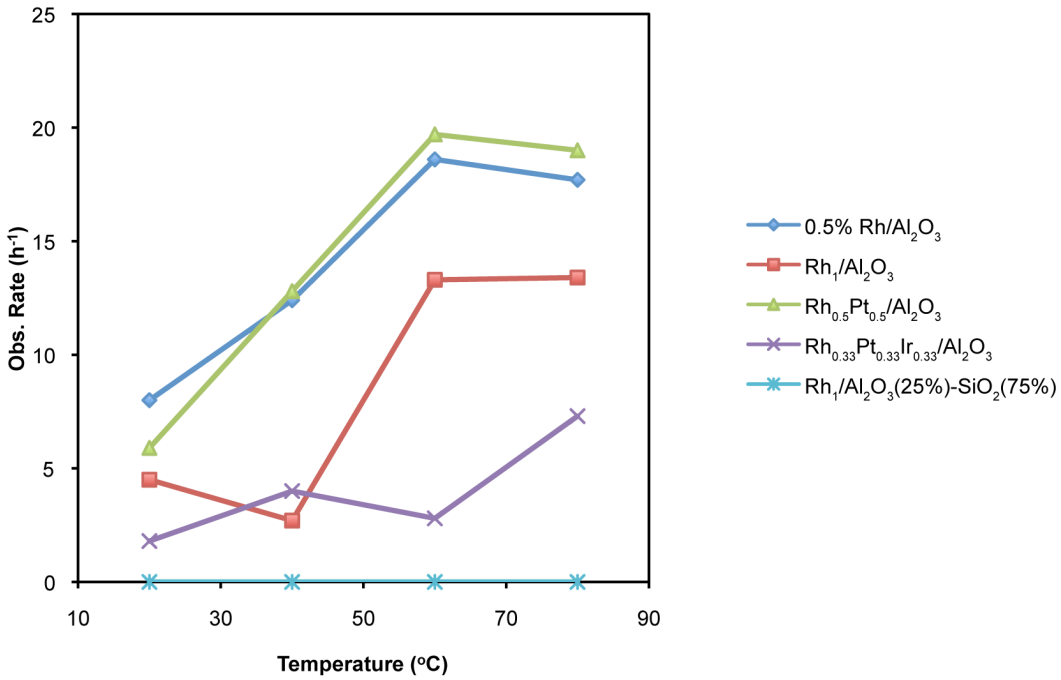

Figure 3.21. Observed rates for the hydrogenation of quinoline at 15 psi H_2 and various temperatures using select catalysts. The observed rate was measured using the amount of 1,2,3,4-tetrahydroquinoline formed per mol of metal in the catalyst per hour.

Once the temperature and pressure studies were completed for the hydrogenation of naphthalene and quinoline, the activity for each catalyst was then measured using the combination of the most active pressure and the most active temperature in an attempt to achieve the maximum catalytic activity for each catalyst. Shown in Fig. 3.22 are the results using naphthalene as the substrate. It can be seen that the only situation in which a combination of the most active pressure and temperature lead to a higher activity was using the $Rh_1/Al_2O_3(75\%)$-$TiO_2(25\%)$ catalyst and the Rh_1/Al_2O_3 catalyst. With the other catalysts, there was either no significant increase in the catalytic activity, such as with the

$Rh_{0.5}Pt_{0.5}/Al_2O_3$ and $Rh_1/Al_2O_3(75\%)$-$SiO_2(25\%)$ catalysts, or there was a decrease in the catalytic activity, like with 0.5% Rh/Al_2O_3 and $Rh_{0.33}Pt_{0.33}Ir_{0.33}/Al_2O_3$.

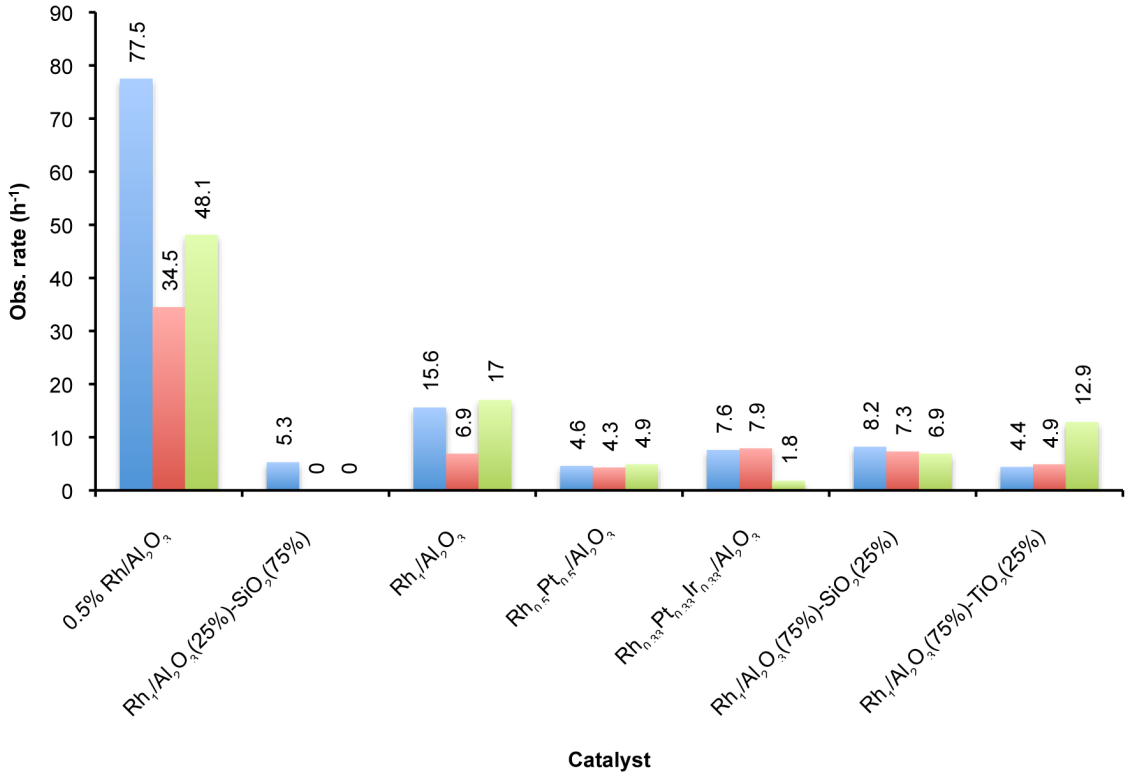

Figure 3.22. Comparison of the observed rates for the hydrogenation of naphthalene at constant pressure and various temperatures, constant temperature and various pressures and combination of the most active temperature and pressure. Blue: highest obs. rate in temperature studies at 294 psig H_2. Red: highest obs. in pressure studies at 295 K. Green: obs. rate at best pressure and best temperature.

A combination of the most active temperature and pressure were also used for the hydrogenation of quinoline in an attempt to determine the most active conditions for the studied catalysts. From Fig. 3.23, for all catalysts except $Rh_1/Al_2O_3(25\%)$-$SiO_2(75\%)$, the

combination of the most active temperature and pressure yielded a higher catalytic activity than either the most active pressure at 295 K or the most active temperature at 294 psig H_2. The Rh_1/Al_2O_3, $Rh_{0.5}Pt_{0.5}/Al_2O_3$ and $Rh_{0.33}Pt_{0.33}Ir_{0.33}/Al_2O_3$ catalysts all gave similar activities when then most active temperature and pressure combinations were used. The other synthesized catalyst, $Rh_1/Al_2O_3(25\%)$-$SiO_2(75\%)$, exhibited a very low activity for the hydrogenation of quinoline, and was only active at elevated pressures. However, the commercial catalyst demonstrated a much higher catalytic activity than any of the synthesized catalysts with an observed rate of 74 h^{-1}.

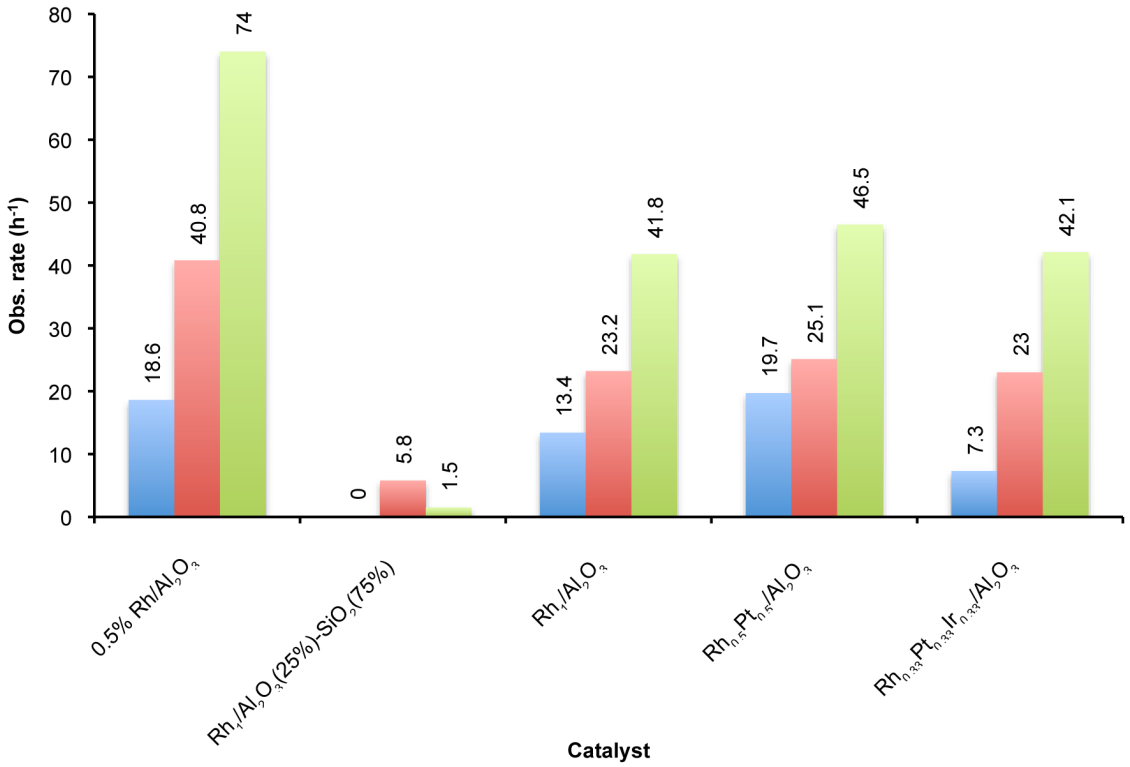

Figure 3.23. Comparison of the observed rates for the hydrogenation of quinoline at constant pressure and various temperatures, constant temperature and various pressures and combination of the most active temperature and pressure. Blue: highest obs. rate in temperature studies at 294 psig H_2. Red: highest obs. in pressure studies at 295 K. Green: obs. rate at best pressure and best temperature.

Finally, the quantity of quinoline was varied to determine the amount substrate loading that each catalyst could tolerate. Previously all studies had been performed using a one hundred fold molar excess of substrate when compared to the molar amount of metal in the catalysts. By examining a higher substrate loading, higher catalytic rates may be obtained and the longevity of a catalyst can be examined. A loading study was performed using the 0.5% Rh/Al_2O_3, Rh_1/Al_2O_3, $Rh_{0.5}Pt_{0.5}/Al_2O_3$ and $Rh_{0.33}Pt_{0.33}Ir_{0.33}/Al_2O_3$

catalysts and substrate ratios of 200, 500 and 1000 in addition to the previously studied ratio of 100 (Fig. 3.24). Both the partially hydrogenated (1,2,3,4-tetrahydroquinoline) and fully hydrogenated (decahydroquinoline) products were formed.

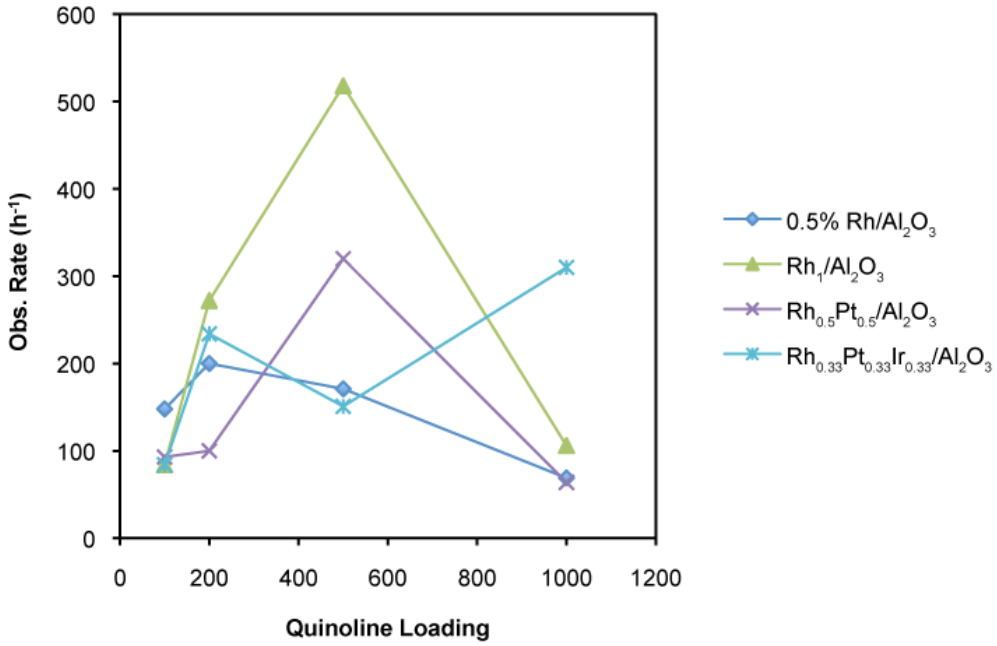

Figure 3.24. Quinoline loading study in which the observed rate was measured as a function of the molar ratio of quinoline. The observed rate is given as mole of H_2 consumed per mole of metal in catalyst per hour. The reactions were run at 441 psig H_2, and either 60 or 80ºC depending on which temperature would yield the highest catalytic activity for a given catalyst.

At the lowest loading ratio of 100, the commercial 0.5% Rh/Al_2O_3 catalyst was the most active, with the other three synthesized catalysts giving similar catalytic activities. The Rh_1/Al_2O_3 catalyst demonstrated the highest catalytic activity at loading ratios of 200, followed by the $Rh_{0.33}Pt_{0.33}Ir_{0.33}/Al_2O_3$ catalyst and the commercial 0.5%

Rh/Al_2O_3 catalyst. The Rh_1/Al_2O_3 catalyst also exhibited the highest catalytic activity at a loading ratio of 500, followed by the bimetallic $Rh_{0.5}Pt_{0.5}/Al_2O_3$ catalyst and the commercial 0.5% Rh/Al_2O_3 catalyst. For the most active catalyst overall (the Rh_1/Al_2O_3 catalyst at a temperature of 80ºC and an initial pressure of 441 psig) a total pressure drop of 110 psi was observed during the first two hours of the catalytic reaction. At the highest loading ratio examined, the trimetallic $Rh_{0.33}Pt_{0.33}Ir_{0.33}/Al_2O_3$ catalyst demonstrated a significantly higher catalytic activity than any of the other examined catalysts. The next most active catalyst was the Rh_1/Al_2O_3 catalyst, followed by the commercial 0.5% Rh/Al_2O_3 catalyst and the bimetallic $Rh_{0.5}Pt_{0.5}/Al_2O_3$ catalyst. For the commercial catalyst, the highest catalytic activity was obtained when the quinoline ratio was 200. At higher ratios of 500 and 1000, the catalytic activity decreases, suggesting that at higher ratios substrate inhibition was occurring. The Rh_1/Al_2O_3 catalyst demonstrated the highest catalytic activity at a ratio of 500, and upon further increasing the quinoline loading ratio, there was a dramatic drop in the catalytic activity suggesting that substrate inhibition was occurring at a loading ratio of 1000. For the bimetallic $Rh_{0.5}Pt_{0.5}/Al_2O_3$ catalyst, it appears to be exhibiting similar trends in activity as those observed for the Rh_1/Al_2O_3 catalyst. Lastly, the trimetallic $Rh_{0.33}Pt_{0.33}Ir_{0.33}/Al_2O_3$ catalyst exhibited an increase in activity as the ratio was increased to 200, a decrease at 500, and then a further increase at 1000.

The last set of experiments that were performed was the neat or solventless hydrogenation of quinoline using the same catalysts that were used for the quinoline loading study. No solvent was used, and 9.0 ml of quinoline was added giving a substrate to metal ratio of 2000:1, which was higher than the loading ratios used during

the quinoline loading study. The results from the neat quinoline hydrogenation study are shown in Table 3.1. From these results, it can be clearly seen that all of the studied catalysts were active for this reaction despite the lack of solvent. The observed rate was measured using the first two hours of the hydrogen consumption data, and the rate was given as the mol of H_2 consumed per mol of metal in the catalyst. The reaction was allowed to continue until the decrease in hydrogen pressure was < 1 psi/hour, and at the end of each reaction a portion of the reaction mixture was analyzed by GC. For each catalyst, only tetrahydroquinoline was detected as the hydrogenation product. Considering the activities demonstrated by the different catalysts, the commercial 0.5% Rh/Al_2O_3 catalyst demonstrated the highest observed rate with a value of 214 h^{-1}, though the Rh_1/Al_2O_3 catalyst exhibited a similar activity with an observed rate of 205 h^{-1}. For the most active catalyst (the commercial 0.5% Rh/Al_2O_3 catalyst at a temperature of 60ºC and an initial pressure of 441 psig) a total pressure drop of 49 psi was observed during the first two hours of the catalytic reaction. The bimetallic $Rh_{0.5}Pt_{0.5}/Al_2O_3$ catalyst demonstrated an observed rate of 141 h^{-1} and the trimetallic $Rh_{0.33}Pt_{0.33}Ir_{0.33}/Al_2O_3$ catalyst was the least active with an observed rate of 69 h^{-1} despite the trend previously seen in Fig. 3.24 for the quinoline loading study. However, despite the different rates observed for the catalysts, they all yielded similar product distributions once the reaction was stopped. For each catalyst, it appears that only 70% of the quinoline was hydrogenated to tetrahydroquinoline before the reaction had essentially stopped. This suggests that despite the fact that some of the catalysts are faster than others, they all yield the same product distribution. Another interesting point to note are the lengths of time observed before the reaction appeared to stop. Despite the fact that the Rh_1/Al_2O_3 catalyst was not

quite as active as the commercial 0.5% Rh/Al_2O_3 catalyst, it obtained the same product distribution in only 93 hours while it took 115 hours for the commercial catalyst. This suggests the activity of the commercial 0.5% Rh/Al_2O_3 catalyst was decreasing during the course of the reaction when compared to the Rh_1/Al_2O_3 catalyst.

Table 3.1. Neat Quinoline Hydrogenation Results using Select Catalysts.[a]

Catalyst	Obs. rate (h^{-1})[b]	Time (h)	% Quinoline	% Tetrahydroquinoline
Comm. 0.5% Rh/Al_2O_3	214	115	27.1	72.9
Rh_1/Al_2O_3	205	93	28.7	71.3
$Rh_{0.5}Pt_{0.5}/Al_2O_3$	141	145	29.5	70.5
$Rh_{0.33}Pt_{0.33}Ir_{0.33}/Al_2O_3$	69	156	28.2	71.8

[a] **Reaction conditions**: 441 psig H_2, 60 or 80°C, no solvent, 3.8 x 10^{-5} mol metal, substrate/cat. = 2000:1 = 0.076 mol quinoline.

[b] Observed rate given as mol of hydrogen consumed per hour, and was measured using the first two hours of hydrogen consumption data.

Materials Characterization

Both XPS and TEM were used to characterize the synthesized catalysts to obtain information about the oxidation state of the metals and the size of the metal nanoparticles. Both the $Rh_{0.5}Pt_{0.5}/Al_2O_3$ and 0.5% Rh/Al_2O_3 catalysts were previously characterized, and the results are shown in Chapter 2. Shown in Figs 3.25-3.27 are the XPS results for the $Rh_{0.33}Pt_{0.33}Ir_{0.33}/Al_2O_3$ catalyst. Charge neutralization was done using an electron gun to prevent charging of the same during analysis, and all binding energies

were compared to those in the NIST XPS database to determine the oxidation states of the relevant metal peaks. From Fig 3.25, the binding energy of the Rh 3d peak was measured to be 306.9 eV, indicating the metal is in the zero oxidation state. Because the Pt 4f and Al 2p peaks overlap in an XPS spectra, a curve-fitting program was used to obtain information about the Pt 4f peak. The binding energy of the Pt 4f peak was determined to be 71.4 eV, indicating the metal is in the zero oxidation state (Fig. 3.26). The binding energy of the Ir $4f_{7/2}$ peak was measured to be 60.7 eV, indicating the metal was in the zero oxidation state (Fig. 3.27). XPS spectra were also obtained for Rh_1/Al_2O_3 (Fig 3.28) and $Rh_1/Al_2O_3(25\%)$-$SiO_2(75\%)$ (Fig. 3.29). For Rh_1/Al_2O_3 the binding energy of the Rh 3d peak was determined to be 308.3 eV, suggesting that the Rh was oxidized to Rh(III). For $Rh_1/Al_2O_3(25\%)$-$SiO_2(75\%)$, the binding energy of the Rh 3d peak was measured to be 308.7 eV, also indicating that the Rh was oxidized to Rh(III). While the XPS characterizations were performed *ex situ* it is unlikely that the oxidized Rh nanoparticles are being reduced under the catalytic conditions because elevated temperatures (> 450 K) are usually required to observe appreciable reduction.[39]

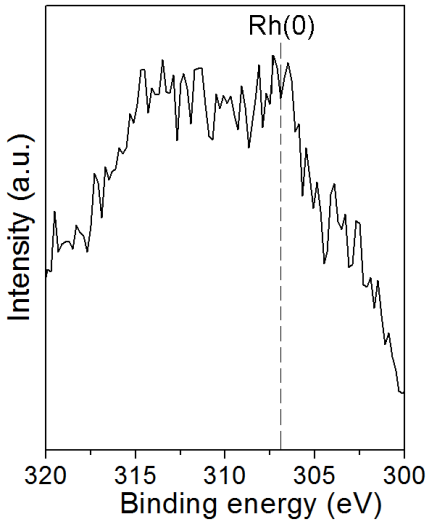

Figure 3.25. High resolution XPS spectrum of Rh in $Rh_{0.33}Pt_{0.33}Ir_{0.33}/Al_2O_3$. The Rh 3d peak has a binding energy of 306.9 eV indicating it is in the zero oxidation state.

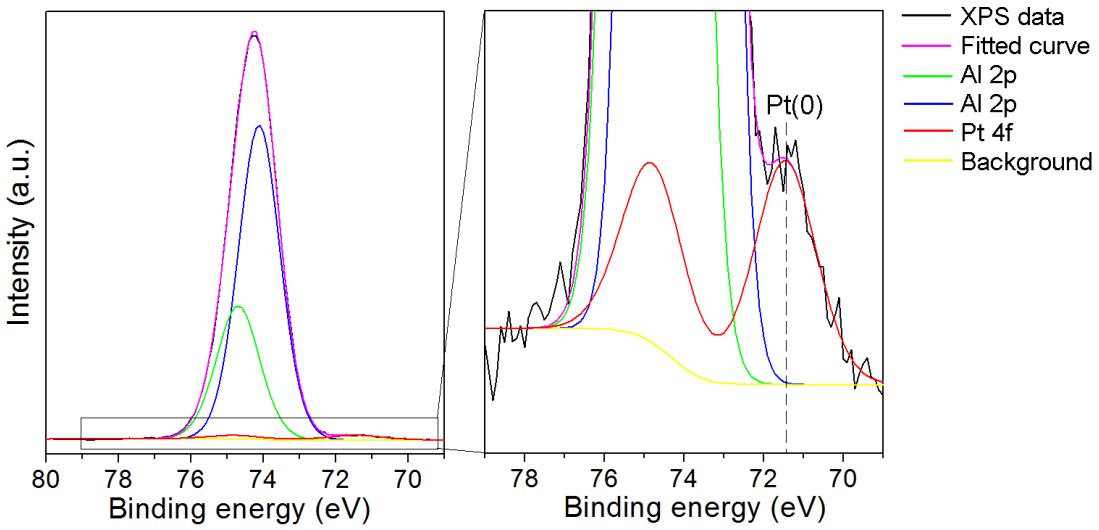

Figure 3.26. High resolution XPS spectra of Pt in $Rh_{0.33}Pt_{0.33}Ir_{0.33}/Al_2O_3$. The Pt 4f peak at 71.4 eV indicates that it is Pt(0).

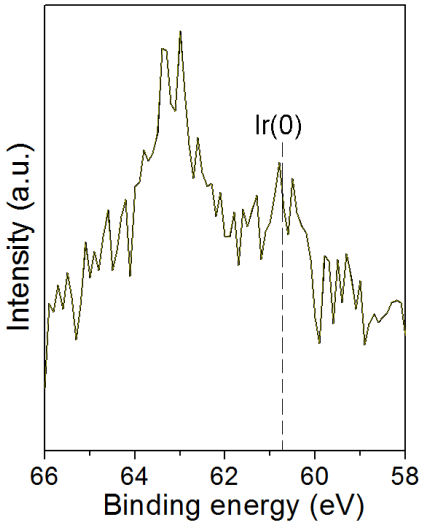

Figure 3.27. High resolution XPS spectrum of Ir in $Rh_{0.33}Pt_{0.33}Ir_{0.33}/Al_2O_3$. The apparent Ir $4f_{7/2}$ peak is at 60.7 eV, which corresponds to Ir(0).

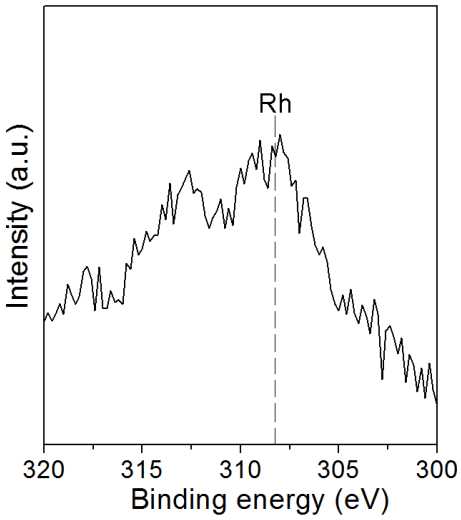

Figure 3.28. High resolution XPS spectrum of Rh in Rh_1/Al_2O_3. The Rh 3d peak has a binding energy of 308.3 eV, suggesting that the Rh was oxidized to Rh(III).

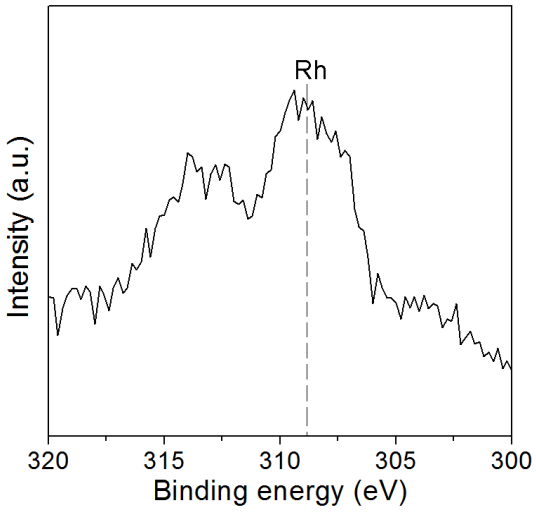

Figure 3.29. High resolution XPS spectrum of Rh in $Rh_1/Al_2O_3(25\%)$-$SiO_2(75\%)$. The Rh 3d peak binding energy is 308.7 eV, which suggests that the Rh was oxidized to Rh(III).

While XPS provided information on the oxidation states of the metals present in the nanoparticle catalysts, it does not provide any insight into the size of the nanoparticles. To obtain this information, TEM images and nanoparticle histograms were obtained for the Rh_1/Al_2O_3 (Fig. 3.30), $Rh_1/Al_2O_3(25\%)$-$SiO_2(75\%)$ (Fig. 3.31) and $Rh_{0.33}Pt_{0.33}Ir_{0.33}/Al_2O_3$ (Fig. 3.32) catalysts. From the TEM image for the Rh_1/Al_2O_3 catalyst, small nanoparticles can be seen. The nanoparticle size was measured to be 2.6 $\pm$ 0.5 nm, highlighting the very small size of these nanoparticles. From the TEM image and nanoparticle histogram for the $Rh_1/Al_2O_3(25\%)$-$SiO_2(75\%)$ catalyst, the nanoparticle size was measured to be 2.7 $\pm$ 0.7 nm. The average nanoparticles size for the $Rh_{0.33}Pt_{0.33}Ir_{0.33}/Al_2O_3$ catalyst was determined to be 2.7 $\pm$ 0.6 nm from the TEM image.

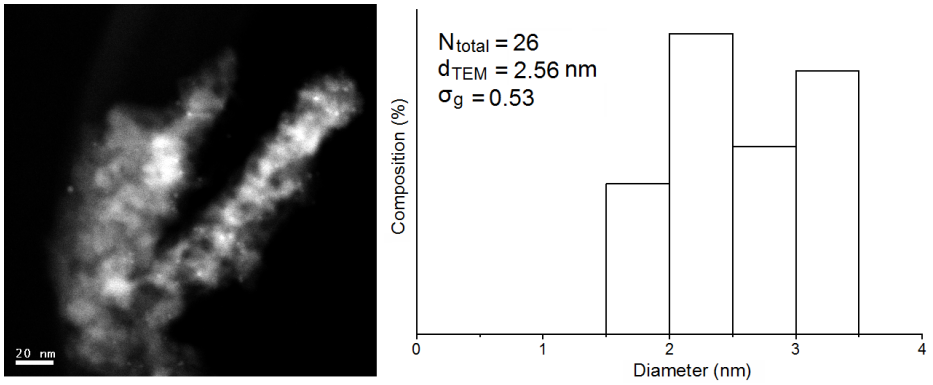

Figure 3.30. Dark field TEM image and particle size histogram for Rh_1/Al_2O_3.

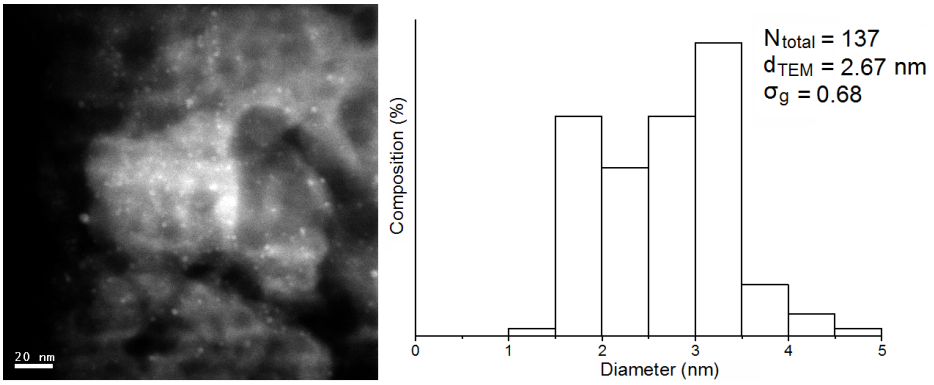

Figure 3.31. Dark field TEM image and particle size histogram for Rh_1/Al_2O_3(25%)-SiO_2(75%).

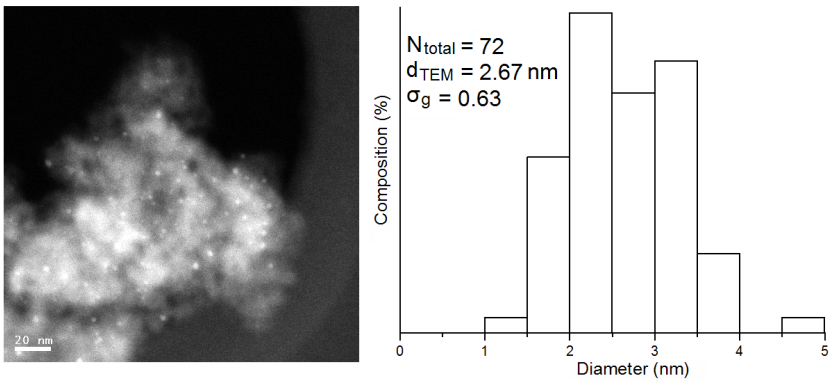

Figure 3.32. Dark field TEM image and particle size histogram for $Rh_{0.33}Pt_{0.33}Ir_{0.33}/Al_2O_3$.

From the nanoparticle sizes obtained from the TEM images, the surface areas of each catalyst and the TOF may be determined using the same methodology as described in Chapter 2. For the $Rh_{0.5}Pt_{0.5}/Al_2O_3$ catalyst, a total surface area of 0.433 m^2 was calculated, 0.240 m^2 for the commercial 0.5% Rh/Al_2O_3 catalyst, 0.488 m^2 for the Rh_1/Al_2O_3 catalyst and 0.486 m^2 for the $Rh_{0.33}Pt_{0.33}Ir_{0.33}/Al_2O_3$ catalyst. While these values are within an order of magnitude of each other, they do give different corrected TOF values. Using the observed rate values for the neat hydrogenation of quinoline given in Table 3.1, the TOF (corrected for total surface area) was determined to be 7.31 x 10^{-3} mol of H_2 consumed per hour per m^2 for the $Rh_{0.5}Pt_{0.5}/Al_2O_3$ catalyst, 3.39 x 10^{-2} for the commercial 0.5% Rh/Al_2O_3 catalyst, 1.60 x 10^{-2} for the Rh_1/Al_2O_3 catalyst and 5.40 x 10^{-3} for the trimetallic $Rh_{0.33}Pt_{0.33}Ir_{0.33}/Al_2O_3$ catalyst. These values give relative TOFs of 1 for the $Rh_{0.5}Pt_{0.5}/Al_2O_3$ catalyst, 4.6 for the commercial 0.5% Rh/Al_2O_3 catalyst, 2.19 for the Rh_1/Al_2O_3 catalyst and 0.74 for the trimetallic $Rh_{0.33}Pt_{0.33}Ir_{0.33}/Al_2O_3$ catalyst. Based on the corrected TOF values, the commercial 0.5% Rh/Al_2O_3 catalyst appears to be twice as active based on surface area when compared to the Rh_1/Al_2O_3 catalyst whereas when simply based on the molar amount of metal they give very similar observed rates.

3.3 Conclusions

In this chapter, the synthesis and screening of a large number of trimetallic catalysts for the hydrogenation of toluene under ambient conditions was described. Through this screening approach, one trimetallic catalyst was selected for further studies. A series of mono-, bi- and trimetallic nanoparticle catalysts supported on mixed metal oxides were synthesized and screened for the hydrogenation of several mono-, poly-, and heteroaromatic substrates utilizing the facilities at the Centre for Catalysis Research and Innovation at the University of Ottawa. Overall, six nanoparticle compositions supported on 12 different mixed metal oxides were synthesized and were screened for hydrogenation activity for seven different substrates. Five of the seven substrates were successfully hydrogenated under the chosen reaction conditions, and 56 of the 72 examined catalysts were catalytically active.

Several catalysts were then chosen for further studies for the hydrogenation of naphthalene and quinoline. For both substrates, temperature and pressure studies were performed to determine the conditions under which the highest catalytic activity could be obtained. A loading study was also conducted using quinoline as a substrate to obtain information about the longevity of the catalysts.

Finally, TEM and XPS were used to characterize the active catalysts that were used for the bulk hydrogenation studies. The $Rh_{0.5}Pt_{0.5}/Al_2O_3$ and $Rh_{0.33}Pt_{0.33}Ir_{0.33}/Al_2O_3$ catalysts were determined to consist of small, zero oxidation state nanoparticles. The

commercial 0.5% Rh/Al_2O_3, Rh_1/Al_2O_3 and $Rh_1/Al_2O_3(25\%)$-$SiO_2(75\%)$ catalysts were found to be comprised of small, oxidized nanoparticles.

3.4 Experimental

Materials.

$RuCl_3 \bullet XH_2O$ (99.9%-Ru), $IrCl_3 \bullet XH_2O$ (99.9%-Ir), $Na_2PtCl_4 \bullet XH_2O$, $RhCl_3 \bullet XH_2O$ (38-41% Rh), and 0.5% Rh/Al_2O_3 (pellets) were purchased from Strem Chemicals. Aluminum-sec-butoxide (95%), titanium (IV) isopropoxide (95%), pyridine (HPLC Grade, 99.5+%), quinoline (98%), indole (99%), thiophene (99%) and benzothiophene (98+%), decahydronaphthalene (98%) were purchased from Alfa Aesar. Naphthalene was purchased from Caledon. Tetraethoxysilane (TEOS) was purchased from Fluka. Ethanol (100%, anhydrous) was purchased from Commercial Alcohol. Millipore water was used throughout. Hydrochloric acid (concentrated) was purchased from EMD. Isopropanol and toluene were purchased from Fischer Scientific. Isopropanol was dried over molecular sieves and stored under argon until used. Toluene was purified through a solvent purification system and was stored under argon until used. Hydrogen, argon, and 5% hydrogen / 95% argon were supplied by Praxair.

Instrumentation.

A Cavro MSP 9500 Automated Sample Processor purchased from Symyx was used to dispense the substrate solutions into the sample plates. A High Pressure Reactor

and Heated Orbital Shaker System (HOSS) purchased from Symyx were used for the reaction testing at a temperature of 22ºC and at an orbital shaking speed of 450 rpm. An Agilent 5975B GC-MS was used to analyze the components of the hydrogenation reaction during the catalyst screening. A Parr pressure vessel, model 4774-T-SS-3000 and a model 4838 controller with a pressure display module was used to monitor the progress of the bulk hydrogenation reactions. A Varian CP-3800 Gas Chromatograph with a CP-4800 autosampler with a fused silica capillary column and a FID detector was used to analyze the samples of the reaction mixture during the bulk hydrogenation reactions. For the TEM analysis, a JEOL JEM-2200FS TEM was used in STEM mode. For XPS a Kratos Analytical, Axis-Ultra instrument was used for the sample analysis. XPS were performed under UHV conditions ($<10^{-8}$ Torr).

Trimetallic Catalyst Synthesis.

The procedure for the trimetallic catalyst synthesis is similar to that used for the synthesis of the bimetallic catalysts.[37] 0.133 M solutions of the required metal salts in ethanol were prepared, as was a 1.788 M solution of aluminum-sec-butoxide in dichloromethane and a solution consisting of 1.0 ml ethanol, 13 μl concentrated hydrochloric acid and 71 μl of water. The sample holders were centered on the stir plate, and glass coated stir bars (5 mm x 6 mm) were added to each well. The desired amount of each metal salt solution was added quickly (in under one second) to each well to give the desired metal loading and ratio of the two metals (e.g. 6.67 μl of each metal salt solution would give a 1:1:1 ratio of the three metals with a total metal loading of 1 mol %). Then 300 μl of ethanol followed by 298 μl of 1.788 M aluminum-sec-butoxide were

quickly (under one second) added to each well via pipette. After stirring for approximately five minutes, 218 μl of the ethanol/hydrochloric acid/water solution was quickly (under one second) added. Each sample holder was covered with parafilm; the parafilm was punctured several times above each well and the solution was allowed to age and dry overnight in laboratory ambient conditions. After processing, each sample holder was placed in a vial, which was capped with a septum.

Bulk Catalyst Synthesis.

Catalysts were synthesized based on the previously published procedure.[37] Briefly, 0.133 M metal salt solutions in ethanol and a 1.788 M aluminum sec-butoxide solution in dichloromethane were prepared. A solution consisting of 20.0 ml ethanol, 0.260 ml concentrated hydrochloric acid and 1.42 ml Millipore water was also prepared. 0.375 ml of each of the metal salt solutions (for a 50:50 ratio of the two metals for a total metal loading of 1%) was added to a 100 ml polypropylene beaker followed by the following amounts of ethanol, 1.788 M aluminum sec-butoxide, titanium (IV) isopropoxide, tetraethoxysilane (TEOS), and after stirring for 5 minutes, EtOH/HCl/H_2O, depending on the desired composition of the support material.

Table 3.2. Amounts of Reagents and Solvents Required for Catalyst Synthesis.

Support Composition	EtOH (ml)	1.788 M $Al(OBu)_3$ (ml)	Titanium (IV) isopropoxide (ml)	TEOS (ml)	EtOH/HCl/H_2O (ml)
Al_2O_3	11.3	11.2	0	0	8.1
SiO_2	5.6	0	0	2.18	4.1
TiO_2	5.6	0	3.0	0	4.1
Al_2O_3(25%)- SiO_2(75%)	7.0	2.8	0	1.64	5.1
Al_2O_3(50%)- SiO_2(50%)	8.4	5.6	0	1.09	6.1
Al_2O_3(75%)- SiO_2(25%)	9.8	8.4	0	0.545	7.1
Al_2O_3(25%)- TiO_2(75%)	7.0	2.8	2.25	0	5.1
Al_2O_3(50%)- TiO_2(50%)	8.4	5.6	1.5	0	6.1
Al_2O_3(75%)- TiO_2(25%)	9.8	8.4	0.75	0	7.1
SiO_2(25%)- TiO_2(75%)	5.6	0	2.25	0.545	4.1
SiO_2(50%)- TiO_2(50%)	5.6	0	1.5	1.09	4.1
SiO_2(75%)- TiO_2(25%)	5.6	0	0.75	1.635	4.1

Each solution was allowed to age and dry overnight in laboratory ambient conditions. Once completely dry, all catalysts were calcined in air in a tube furnace using the following program: heat to 65ºC (rate 1ºC/min), hold at 65ºC for 30 minutes, heat to 250ºC (rate 1ºC /min), hold at 250ºC for 3 hours, cool to 25ºC (rate 1ºC /min). Then the catalyst was hydrogen annealed under a 5% H_2 / 95% Ar atmosphere as follows: heat to 300ºC (rate 5ºC/min), hold at 300ºC for 3 hours, cool down to 25ºC rapidly by opening the furnace. The catalyst was stored under Ar until used.

Trimetallic Catalyst Screening.

A solution of 7.7 ml isopropanol, 0.456 ml decahydronaphthalene (internal standard) and 0.380 ml toluene was prepared. A necessary number of lines on the Schlenk line were split with Y joints and additional tubes were attached. A syringe barrel was inserted into the end of each tube and a needle was attached to each syringe. As described earlier (Catalyst screening synthesis of 1 mol% metal loading) each sample holder containing the prepared catalyst is located in an individual vial. The septum on

each vial was pierced with a needle that was attached to the Schlenk line (Fig. 2.7). The vials underwent three of the following cycles: the vials were placed under vacuum and then back filled with Ar. This was repeated with Ar and then with H_2. 1 ml of isopropanol was added to the bottom of each vial (but not to the sample holder), to minimize evaporation losses from the sample holder. Next, 0.77 ml of the previously prepared solution was added to each sample holder. The vials were stirred for 4 hours under 15 psi H_2 and at 22ºC. After 4 hours, each sample holder was removed from the vial. As much of the reaction mixture as possible was removed from the sample holder with a Pasteur pipette. The reaction mixture was filtered through a different Pasteur pipette packed with a small amount silica gel directly into a GC vial. The substrate and products were diluted with 1.0 ml dichloromethane. The screening hydrogenation results obtained for $Rh_{0.5}Pt_{0.5}/Al_2O_3$ were performed in triplicate.

Screening Hydrogenation using Facilities and Equipment at CCRI.

Each plate that was tested contained 96 vials, and in each vial 2 x 3 mm borosilicate glass beads were added (Fig. 3.33). The appropriate amount of catalyst (9-16 mg depending on the composition of the catalyst) was manually weighed into each vial to an accuracy of $\pm$ 0.4 mg. After each vial contained the appropriate amount of catalyst, the plate was placed into Cavro MSP 9500 Automated Sample Processor. 0.38M substrate solutions in isopropanol were prepared in 20 ml vials and these vials were also loaded into the sample processor. The sample processer was then programmed to dispense 0.4 ml of the appropriate substrate solution into each vial. Once all of the substrate solutions had been dispensed, the plate was removed from the sample processer,

and was sealed with a top metal plate consisting of a Teflon sheet with a hole above each vial, a silicon sheet with a hole above each vial and a metal plate with one-way check values (Fig. 3.34). The top plate was then screwed down securely and the plate was then encased in a batch reactor (Fig. 3.35). The batch reactor was then leak tested by pressurizing with nitrogen and monitoring the pressure for several minutes. If there was no change in pressure, then the nitrogen gas was vented, and the batch reactor was purged with hydrogen three times by slowly pressurizing the batch reactor to the desired pressure, and then slowly depressurizing it. After purging, the batch reactor was pressurized a final time, and then sealed. The batch reactor was disconnected from the gas line and loaded into the HOSS (Fig. 3.36). The HOSS was then programmed to operate at 22ºC at 450 rpm for the allotted amount of time. After the allotted amount of time, the HOSS was stopped, and the batch reactor was removed, and depressurized very slowly. The batch reactor was then disassembled, the plate was removed from the batch reactor, and the vials were transferred into a different plate for analysis. The analysis plate was then sealed with a top plate consisting of a solid Teflon sheet, a solid rubber sheet, and then the top metal plate that had holes directly above each vial (Fig. 3.37). The top plate was then screwed down securely to prevent cross-contamination from the other vials. This plate was then loaded into the GC-MS for analysis.

Figure 3.33. Screening plate containing 96 vials.

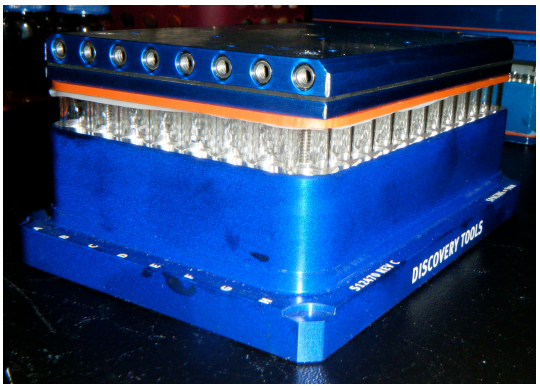

Figure 3.34. Assembled screening plate with top plate.

Figure 3.35. Batch reactor.

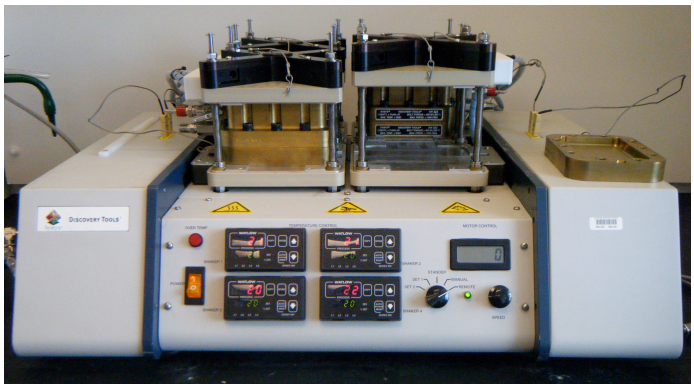

Figure 3.36. Heated orbital shaker system (HOSS).

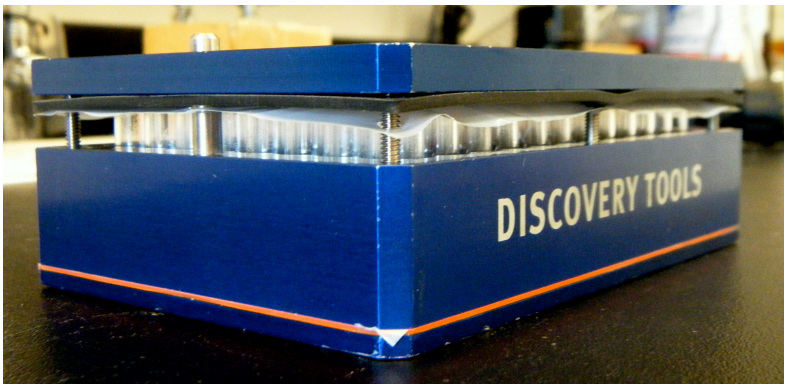

Figure 3.37. Plate used for GC-MS analysis.

Bulk Hydrogenation - Naphthalene pressure and temperatures studies, quinoline pressure study, combination studies.

The appropriate amount of catalyst to give 3.8 x 10^{-5} mol of metal was weighed into a 20 ml glass beaker and a glass coated stir bar was added. Then a 0.38 M solution of the substrate in iso-propanol was prepared, and 10.0 ml of this solution was added to the beaker. The beaker was then placed into the bottom of the Parr reactor with the gas

inlet in the reaction solution (and the temperature thermocouple for the temperature and combination studies). The Parr reactor was assembled, and the reactor was purged 3 times with H_2 by pressurizing followed by venting of the H_2 gas. The reactor was then pressurized to the desired pressure, (and allowed to come to the set temperature for the temperature and combination studies) the recorder program was started, and the speed of the stir plate was set. The pressure of the reaction was monitored for a minimum of 7 hours. At the end of each hydrogenation reaction, the reactor was disassembled and a sample of the reaction mixture was analyzed by gas chromatography to determine the hydrogenation products.

Bulk Hydrogenation – Quinoline temperature study.

An appropriate amount of catalysts to give 3.8×10^{-5} mol of metal was weighed into a 3-neck round bottom flask. A glass coated stir bar was added to the flask, and then a reflux condenser was added to the middle neck of the round bottom flask. A gas adapter was attached to the top of the reflux condenser, and the other two necks on the round bottom flask were sealed with septa. The round bottom flask was then placed into an oil bath that had been heated to the desired temperature. The flask and reflux condenser were then purged with Ar by playing the entire apparatus under vacuum, and then back filling it with Ar. This was repeated twice more, and then 10.0 ml of iso-propanol were transferred into the round bottom flask. Then the flask and reflex condenser were purged with hydrogen by briefly placing the entire apparatus under vacuum and then back filling it with H_2. This was repeated for a total of 5 times. Next 0.59 ml (3.8×10^{-3} mol) of decahydronaphthalene (internal standard) and 0.45 ml (3.8 x

10^{-3} mol) of quinoline were added via syringe. The reaction was monitored every 15 minutes for the first 2 hours, and then every hour for an additional 5 hours. To measure the progress of the hydrogenation reaction 0.2 ml portions were removed from the reaction mixture, and were filtered into a GC vial for analysis. Then 0.5 ml of dichloromethane was run through the used filter into the same GC vial, and finally an additional 1.0 ml of dichloromethane was added.

Bulk Hydrogenation – Quinoline loading study.

The appropriate amount of catalyst to give 3.8 x 10^{-5} mol of metal was weighed into a 20 ml glass beaker and a glass coated stir bar was added. Then 10.0 ml of iso-propanol was added followed by the desired amount of quinoline to give the correct quinoline to catalyst ratio (0.9 ml for a 200:1 ratio, 2.25 ml for a 500:1 ratio, 4.5 ml for a 1000:1 ratio). The beaker was then placed into the bottom of the Parr reactor with the gas inlet and the thermocouple in the reaction solution. The Parr reactor was assembled, the stir plate was set to a stir speed of 7 and the reactor was purged 3 times with H_2 by pressurizing followed by venting of the H_2 gas. The reactor was then pressurized to the desired pressure and allowed to come to the set temperature, and the recorder program was started. The pressure of the reaction was monitored until the decrease in pressure was <1 psi/hour, and the reactor was repressurized as needed. At the end of each hydrogenation reaction, the reactor was disassembled and a sample of the reaction mixture was analyzed by gas chromatography to determine the hydrogenation products and their amounts.

Bulk Hydrogenation – Neat quinoline hydrogenation study.

This study was performed following the procedure outlined for the quinoline loading study, except no iso-propanol was added, and 9.0 ml of quinoline was used for each catalyst.

Sample preparation for XPS and TEM

XPS: The dried sample was first finely grounded to reduce the particle size. The ground powders were then placed into a die and pressed into a pellet under high pressure. The pellet was then used for XPS analysis. TEM (before hydrogenation): Raw samples were carefully ground with a mortar and pestle for 20 minutes. The average particle size is less then 100 nm after ground. A small amount of the ground powder was then mounted on a carbon-coated grid for TEM analysis. TEM (after hydrogenation): After reaction, the solvent was removed/vaporized under vacuum overnight. The raw sample was then ground and sprayed on a carbon coated TEM grid.

3.5 References

(1) Campanati, M.; Vaccari, A.; Piccolo, O. *J. Mol. Catal. A: Chem.* **2002**, *179*, 287-292.

(2) Narayanan, R.; El-Sayed, M. A. *J. Phys. Chem. B* **2005**, *109*, 12663-12676.

(3) Yoo, J. W.; Hathcock, D. J.; El-Sayed, M. A. *J. Catal.* **2003**, *214*, 1-7.

(4) Yoon, B.; Wai, C. M. *J. Am. Chem. Soc.* **2005**, *127*, 17174-17175.

(5) Venezia, A. M.; La Parola, V.; Pawelec, B.; Fierro, J. L. G. *Appl. Catal., A* **2004**, *264*, 43-51.

(6) Yoon, B.; Pan, H. B.; Wai, C. M. *J. Phys. Chem. C* **2009**, *113*, 1520-1525.

(7) Owusu-Boakye, A.; Dalai, A. K.; Ferdous, D.; Adjaye, J. *Energy & Fuels* **2005**, *19*, 1763-1774.

(8) Park, I. S.; Kwon, M. S.; Kang, K. Y.; Lee, J. S.; Park, J. *Adv. Synth. Catal.* **2007**, *349*, 2039-2047.

(9) Hiyoshi, N.; Rode, C. V.; Sato, O.; Masuda, Y.; Yamaguchi, A.; Shirai, M. *Chem. Lett.* **2008**, *37*, 734-735.

(10) Hiyoshi, N.; Miura, R.; Rode, C. V.; Sato, O.; Shirai, M. *Chem. Lett.* **2005**, *34*, 424-425.

(11) Hiyoshi, N.; Inoue, T.; Rode, C.; Sato, O.; Shirai, M. *Catal. Lett.* **2006**, *106*, 133-138.

(12) Hiyoshi, N.; Osada, M.; Rode, C. V.; Sato, O.; Shirai, M. *Appl. Catal., A* **2007**, *331*, 1-7.

(13) Park, K. H.; Jang, K.; Kim, H. J.; Son, S. U. *Angew. Chem., Int. Ed.* **2007**, *46*, 1152-1155.

(14) Gao, H.; Angelici, R. J. *J. Am. Chem. Soc.* **1997**, *119*, 6937-6938.

(15) Deshmukh, R. R.; Lee, J. W.; Shin, U. S.; Lee, J. Y.; Song, C. E. *Angew. Chem., Int. Ed.* **2008**, *47*, 8615-8617.

(16) Santana, R. C.; Jongpatiwut, S.; Alvarez, W. E.; Resasco, D. E. *Ind. Eng. Chem. Res.* **2005**, *44*, 7928-7934.

(17) Pawelec, B.; Campos-Martin, J. M.; Cano-Serrano, E.; Navarro, R. M.; Thomas, S.; Fierro, J. L. G. *Environ. Sci. Technol.* **2005**, *39*, 3374-3381.

(18) Zhao, A. Q.; Zhang, X. F.; Chen, X.; Guan, J. C.; Liang, C. H. *J. Phys. Chem. C* **2010**, *114*, 3962-3967.

(19) Zhang, Z. G.; Okada, K.; Yamamoto, M.; Yoshida, T. *Catalysis Today* **1998**, *45*, 361-366.

(20) Liang, C.; Zhao, A.; Zhang, X.; Ma, Z.; Prins, R. *Chem. Commun.* **2009**, 2047-2049.

(21) Pan, H. B.; Wai, C. M. *J. Phys. Chem. C* **2009**, *113*, 19782-19788.

(22) Ma, Y. M.; Wei, X. Y.; Zhou, X.; Cai, K. Y.; Peng, Y. L.; Xie, R. L.; Zong, Y.; Wei, Y. B.; Zong, Z. M. *Energy & Fuels* **2009**, *23*, 638-645.

(23) Yuan, T.; Fournier, A. R.; Proudlock, R.; Marshall, W. D. *Environ. Sci. Technol.* **2007**, *41*, 1983-1988.

(24) Yuan, T.; Marshall, W. D. *Journal of Hazardous Materials* **2005**, *126*, 149-157.

(25) Deng, J. P.; Shih, W. C.; Mou, C. Y. *Chemphyschem* **2005**, *6*, 2021-2025.

(26) Sanchez-Delgado, R. A.; Machalaba, N.; Ng-A-Qui, N. *Catal. Commun.* **2007**, *8*, 2115-2118.

(27) Mevellec, V.; Roucoux, A. *Inorganica Chimica Acta* **2004**, *357*, 3099-3103.

(28) Grobas, J.; Bolivar, C.; Scott, C. E. *Energy & Fuels* **2007**, *21*, 19-22.

(29) Campanati, M.; Casagrande, M.; Fagiolino, I.; Lenarda, M.; Storaro, L.; Battagliarin, M.; Vaccari, A. *J. Mol. Catal. A: Chem.* **2002**, *184*, 267-272.

(30) Leger, B.; Denicourt-Nowicki, A.; Olivier-Bourbigou, H.; Roucoux, A. *Inorg. Chem.* **2008**, *47*, 9090-9096.

(31) Hu, L.; Xia, G.; Qu, L.; Li, M.; Li, C.; Xin, Q.; Li, D. *J. Catal.* **2001**, *202*, 220-228.

(32) Sidhpuria, K. B.; Parikh, P. A.; Bahadur, P.; Jasra, R. V. *Ind. Eng. Chem. Res.* **2008**, *47*, 4034-4042.

(33) Miller, J. T.; Mojet, B. L.; Ramaker, D. E.; Koningsberger, D. C. *Catalysis Today* **2000**, *62*, 101-114.

(34) Klein, J.; Lettmann, C.; Maier, W. F. *J. Non-Cryst. Solids* **2001**, *282*, 203-220.

(35) Frenzer, G.; Maier, W. F. *Ann. Rev. Mater. Res.* **2006**, *36*, 281-331.

(36) Klein, S.; Thorimbert, S.; Maier, W. F. *J. Catal.* **1996**, *163*, 476-488.

(37) Dehm, N. A.; Zhang, X.; Buriak, J. M. *Inorg. Chem.* **2010**, *49*, 2706-2714.

(38) Sermon, P. A.; Walton, T. J.; Luengo, M. A. M.; Vong, M. S. W. *Journal of the Chemical Society-Faraday Transactions* **1991**, *87*, 199-202.

(39) Newton, M. A.; Fiddy, S. G.; Guilera, G.; Jyoti, B.; Evans, J. *Chemical Communications* **2005**, 118-120.

Chapter 4

Conclusions

This thesis has discussed the development and application of a simple screening approach for the synthesis and screening of heterogeneous nanoparticle catalysts for the hydrogenation of mono-, poly- and heteroaromatic substrates under mild conditions. To conclude, this chapter highlights the results of each chapter and addresses further applications for our synthesized nanoparticle catalysts as well as potential research directions for heterogeneous nanoparticle catalysis.

4.1. Summaries of Chapters

Chapter 1

Chapter 1 discussed the background behind this thesis research. The concept of nanoparticles as highly active catalysts was introduced, followed by the advantages of utilizing nanoparticle catalysts and the criterion to prepare catalytically active nanoparticles. Then the two different types of nanoparticles (soluble and supported) and their various synthetic approaches, advantages and disadvantages were described.

Since this body of work focuses on supported nanoparticle catalysts, specifically those supported on metal oxides, the reasoning behind using metal oxides as catalytic supports was explained. The synthesis of common metal oxides and how their properties could be tailored by modifying the synthesis parameters were described.

Lastly, the concept of combinatorial materials chemistry was introduced as a method to quickly and efficiently synthesize and test new materials for a desired property. The goals behind this approach as well as the challenges and limitations were discussed. Several pertinent examples from the literature were introduced to indicate the current state of this field as it applies to heterogeneous catalyst discovery.

Chapter 2

In Chapter 2, an industrial application of nanoparticle catalysts as they pertain to oil sands upgrading and aromatic hydrogenation was briefly introduced. Several current problems with the industrial catalysts used for oil sands upgrading were identified, leading to widespread interest in developing new classes of catalysts that are active under milder conditions and are more nitrogen and sulfur tolerant. Bimetallic nanoparticle catalysts were introduced as a possible method to achieve some of the previously mentioned goals with regards to new catalysts development. Then, as a model reaction, monoaromatic hydrogenation using nanoparticle catalysts was discussed. Several examples of nanoparticle catalysts that were active under mild conditions were given, demonstrating the challenge that this reaction presents.

While a limited number of bimetallic nanoparticle catalysts had been previously explored as aromatic hydrogenation catalysts, we were interested in investigating a broader range of nanoparticle compositions. By using a combinatorial approach for the synthesis and catalysts screening, we would be able to screen a much larger range of nanoparticle compositions in a quick and time efficient manner than by synthesizing and testing each unique catalyst individually.

The procedure for the synthesis and screening of heterogeneous bimetallic nanoparticle catalysts for the hydrogenation of toluene was described. Using 13 different transition metals, a series of mono- and bimetallic nanoparticle catalysts supported on alumina were synthesized. When these nanoparticle catalysts were screened for the hydrogenation of toluene, several new active bimetallic catalysts were identified (RhPt, RhIr, RuPt, IrPt). Next, while maintaining a constant metal loading, the ratios of the two metals in the bimetallic catalysts were systematically varied to determine the ideal ratio of the two metals so that the maximum catalytic activity could be achieved.

Following any screening or combinatorial approach, potential hits must be confirmed by thorough testing in bulk. The five active mono- and bimetallic nanoparticle catalysts were synthesized in bulk and were tested for the hydrogenation of toluene under ambient conditions. Other variables including metal loading, solvent, temperature, pressure and ratio of toluene to metal were also examined. Through the temperature studies, the activation energy was calculated to be to be 30.4 kJ/mol. This activation energy is moderate when compared to those previously reported for arene hydrogenation.

A series of CS_2 poisoning experiments were performed on the $Rh_{0.5}Pt_{0.5}/Al_2O_3$ and commercial 0.5% Rh/Al_2O_3 catalysts in triplicate to determine the number of catalytically active sites present, and to allow for more accurate comparison of the activities of the two catalysts. Upon performing the poisoning study, the amount of CS_2 required to completely deactivate each catalyst was calculated to be 0.081 mol CS_2 / mol total metal for the $Rh_{0.5}Pt_{0.5}/Al_2O_3$ catalyst and 0.046 mol CS_2 / mol total metal for the 0.5% Rh/Al_2O_3 catalyst, indicating that there were more catalytically active sites present in the bimetallic catalyst that in the commercial catalyst. When the corrected TOFs were calculated,

similar values were obtained. The need for a higher quantity of catalyst poison (CS_2) for the bimetallic catalysts suggests that there are more active (but less reactive) sites than in the commercial 0.5% Rh/Al_2O_3 catalyst.

Finally, TEM, XPS and BET were used to characterize the active nanoparticle catalysts. Through the use of standard materials characterization techniques, all of the bimetallic catalysts were determined to consist of small, zero oxidation state nanoparticles that were well dispersed throughout the alumina supports.

Chapter 3

Chapter 3 described the expansion of the work begun in Chapter 2. While the concept of monoaromatic hydrogenation under mild conditions was previously discussed in detail, in Chapter 3 both poly- and heteroaromatic hydrogenation were briefly introduced. These two types of aromatic hydrogenation are also of interest to the industrial sector as means of further upgrading bitumen into synthetic crude oil. However these reactions are quite challenging due to the difficulty in obtaining deep hydrogenation of the polyaromatic hydrocarbons, and the possibility that the heteroaromatic substrates will behave as catalytic poisons. Bimetallic nanoparticle catalysts were briefly introduced once again, and a few examples from the literature were given to demonstrate the potential for increased activity and poison tolerance that these bimetallic catalysts possess. Next both poly- and heteroaromatic hydrogenation were discussed in detail with relevant examples from the literature being given. In addition to investigating poly- and heteroaromatic hydrogenation, the use of mixed metal oxides as catalyst supports was also

of interest. The chemistry behind mixed metal oxides, and how the use of metal oxides as catalyst supports can increase the catalysts sulfur and nitrogen tolerance were described.

While previously the effect on the catalytic activity by varying the nanoparticle composition was investigated, a third metal was introduced to the nanoparticle composition. Using the four active bimetallic nanoparticle compositions discovered in Chapter 2, a third metal was added to these binary combinations. It was found that for the majority of the trimetallic catalysts, the incorporation of a third metal caused a decrease in the catalytic activity for the hydrogenation of toluene under ambient conditions. However, when the four metals that made up the active bimetallic catalysts that were identified in chapter two were used to make a series of trimetallic catalysts, one new catalyst demonstrated potential.

Next, we expanded our previous screening approach to include poly- and heteroaromatic substrates and mixed metal oxides as catalyst supports. Using 6 nanoparticle compositions and 12 metal oxides supports, 72 new heterogeneous nanoparticle catalysts were synthesized and tested for the hydrogenation of toluene, naphthalene, pyridine, indole, quinoline, thiophene and benzothiophene using the facilities at the Centre for Catalysis Research and Innovation (CCRI) at the University of Ottawa. Five of the seven substrates were successfully hydrogenated, and 56 of the 72 catalysts were observed to be active under the working conditions.

Based on the results obtained at CCRI, several catalysts were chosen for further studies in bulk for the hydrogenation of naphthalene and quinoline. Both temperature and pressure studies were performed on both substrates using five different catalysts. A loading study was also performed using quinoline as the substrate where it was observed

that while the commercial 0.5% Rh/Al_2O_3 catalyst was the most active at lower quinoline loadings, the trimetallic $Rh_{0.33}Pt_{0.33}Ir_{0.33}/Al_2O_3$ catalyst was by far the most active at higher quinoline loadings. Finally, TEM and XPS were used to characterize the active nanoparticle catalysts.

4.2. Proposed Research Directions

Selective Ring Opening

Continuing with the exploration of the catalytic activity of these mono-, bi- and trimetallic heterogeneous nanoparticles for oil sands upgrading, the selective ring opening of the previously hydrogenated aromatic compounds could be explored. Selective ring opening is one of the methods proposed to improve upon the quality of distillate fuels by enhancing the cetane number and density.[1,2] Selective ring opening refers to the opening of cycloalkane rings without a loss of reactant molecular weight.[2] For example, ideally the selective ring opening product of decahydronaphthalene would be decane, the resulting linear alkane. However, it is not straightforward and a multitude of desirable and undesirable products may be obtained *via* selective ring opening (Fig. 4.1).

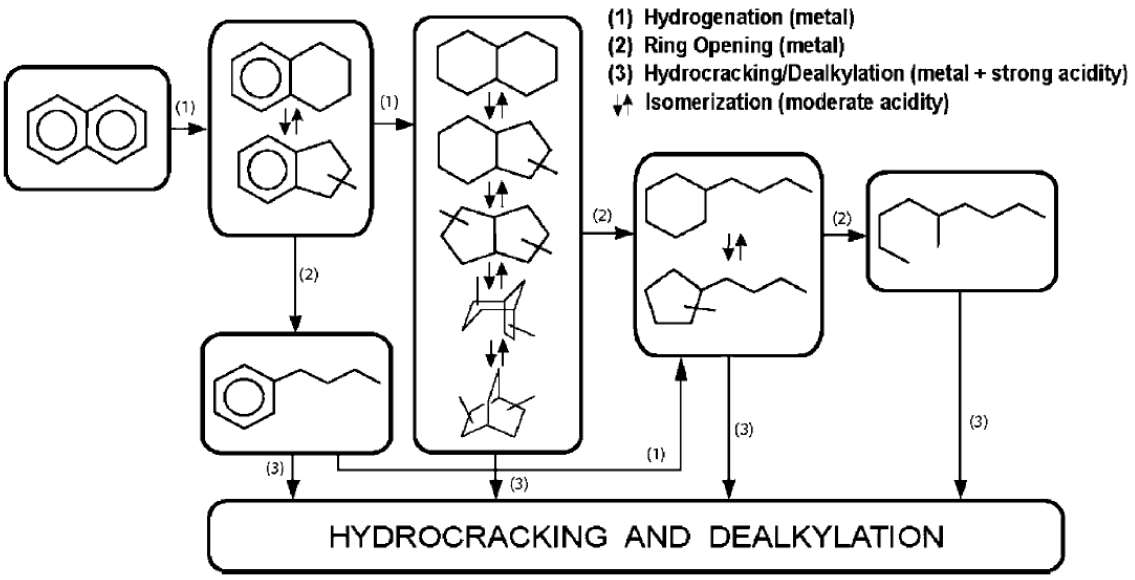

Figure 4.1. Key reactions during the conversion of polyaromatic hydrocarbons to alkanes.[2,a]

Selective ring opening activity has been previously established using a variety of nanoparticle catalysts supported on metal oxides. For example, cyclohexane ring opening has been studied using both Rh/Al_2O_3 and Ir/Al_2O_3 catalysts, and it was observed that Ir catalyst demonstrated a higher cyclohexane conversion than the Rh catalysts.[1] For the Ir catalyst, the main products were *n*-hexane and *n*-pentane whereas for the Rh catalyst there was significant formation of benzene. A nickel-alumina catalyst was used for the selective ring opening of cyclohexane and methylcyclopentane.[3] Alumina-supported Rh catalysts were also used for the ring opening of methylcyclopentane.[4] Pt/SiO_2, Pt/Al_2O_3, Ni/Al_2O_3, Ru/SiO_2, Ir/Al_2O_3, Ru/Al_2O_3, and Rh/Al_2O_3 were used for the selective ring

[a] Reprinted from J. Catal., Vol. 210, McVicker, G. B.; Daage, M.; Touvelle, M. S.; Hudson, C. W.; Klein, D. P.; Baird, W. C.; Cook, B. R.; Chen, J. G.; Hantzer, S.; Vaughan, D. E. W.; Ellis, E. S.; Feeley, O. C. "Selective ring opening of naphthenic molecules." 137-148, Copyright 2002, with permission from Elsevier.

opening of naphthenic compounds.[2] One pervasive trend throughout the selective ring opening literature is the use of alumina or silica as the catalyst support. These acidic metal oxides are a necessity in order for the selective ring opening reaction to proceed. Due to our previous choice in employing metal oxides as the catalytic supports, there appears to be no need to modify our catalysts in order to obtain selective ring opening activity.

While previously all of the catalytic hydrogenation reactions had been performed under ambient or mild conditions, the conditions required for selective ring opening are much harsher. Temperatures in range of 468 to 823 K and hydrogen pressures between 147 and 794 psi are often required.[1-4] Due to these extreme conditions, a different apparatus such as a fixed-bed down flow or continuous flow reactor is required. Furthermore, for the detection and analysis of the reaction products, both the quantity and identity of each product must be determined, making a detection system such as GC-MS critical.

Characterization of Supported Nanoparticle Catalysts

One of the challenges associated with employing supported nanoparticle catalysts is characterizing the structure and composition of these catalysts. While we were primarily concerned in this body of work with how the catalytic activity was affected by varying factors such as the composition of the metal nanoparticles, the type of metal oxide support, the type of substrate, temperatures, pressures and substrate loadings, only minimal materials characterization was performed to confirm that the supported catalysts consisted of primarily small, zero oxidation state nanoparticles. Further materials

characterization especially of the metal nanoparticles is a necessity, but is particularly challenging because of the large quantity of metal oxide support that is present when compared to the amount of metal nanoparticles.

While further characterization of the metal nanoparticles is of primary interest, more detailed characterization of the metal oxide support may also be performed. There exist a wide variety of techniques than can be used to characterize complex porous amorphous mixed oxides,[5] though only a few select examples will be discussed here. The surface area of the catalysts was measured in Chapter 2, but this was the only characterization performed that would provide information about the metal oxide support. Further characterization that could be performed would include measurements of the porosity of the metal oxide support. This information is typically obtained through N_2 absorption measurements, and would determine whether the support was microporous, mesoporous or macroporous.

In addition to obtaining information about the surface area and porosity of the metal oxide support, the crystallinity could be determined by powder XRD. The metal oxides employed in this body of work can all demonstrate different crystal structures depending on the calcination conditions used. For example, the most common crystal structure of alumina is corundum, though it also possesses five other crystal phases.[6] Due to the low calcincation temperatures (250ºC) that were employed for all of the supported nanoparticle catalysts, we had been operating under the assumption that the metal oxides would likely be amorphous. However, this was never confirmed.

Lastly, in terms of characterization of the metal oxide support, the degree of acidity could be determined. As previously discussed, the acidity of the support does

have an effect on the catalytic activity for aromatic hydrogenation. Typically, more acidic supports are expected to be more active for aromatic hydrogenation. In lieu of some of the trends observed with regards to the catalyst support, it is of interest to determine if the differences in activity could be correlated to the different acidities of the metal oxides, especially for the mixed metal oxide catalyst supports. In addition, there are different types of acidic sites that may be present on the metal oxide support: Brønsted acid and Lewis acid. The ratio of the two different types of acidic sites may also be determined by studying the adsorption of pyridine via IR spectroscopy.[7] Different adsorption peaks will be observed depending on whether the pyridine has coordinated to Lewis acid sites, or if there is formation of the pyridinium ion formed on Brønsted acid sites.

While preliminary characterization of the nanoparticles within the catalyst had been performed via TEM and XPS, there is still a lot that is unknown about these nanoparticles, and about the structure and composition of bimetallic nanoparticles in general. Whereas the characterization of the metal oxide support was fairly straightforward, characterization of the nanoparticles is much more challenging. For example, XRD could also be used to obtain information about the crystallinity of the nanoparticles. However, this is where the large percentage of the metal oxide becomes quite problematic. This information would be quite useful though, but it is unknown whether or not these nanoparticles are crystalline or amorphous. It is probable that they are amorphous because amorphous nanoparticles would likely posses more steps and edges than crystalline nanoparticles. Furthermore, the reduction or hydrogen anneal step was performed under mild enough conditions that it is unlikely that the nanoparticles became crystalline.

As previously mentioned, the surface area of the entire catalyst could be measured via BET. It would be of interest to obtain information about the exposed surface area of the nanoparticle catalysts due to the nature of their synthesis. Because the metal oxide was first synthesized, and then the metal salt was reduced to form the nanoparticles, it is not known how many of the metal nanoparticles are actually exposed. Some of the formed nanoparticles may be completely encapsulated by the metal oxides, some may be partially encapsulated and some may be encapsulated just enough to keep them attached to the metal oxide support. While the CS_2 study that was performed in Chapter 2 did provide some information about the number of catalytically active sites available, it does not really tell us about how much of the surface area of nanoparticles were exposed. This data would give us an indication if the quantity of exposed nanoparticles varied from catalyst to catalysts, and using rough calculations we would also be able to determine how many of the metal nanoparticles were buried and rendered inactive by the metal oxide support.

One of the large remaining challenges associated with the field of bimetallic nanoparticles is determination of the structure and composition of the aforementioned nanoparticles. As previously discussed, there are a variety of structures that nanoparticles can form upon the incorporation of a second metal, including core-shell or alloy structures, and it is very arduous to tell the difference between these two structures and this problem is further exasperated when these nanoparticles are on a catalytic support. There has been one thorough study where a structural and architectural evaluation of both alloy and core-shells nanoparticles was performed. Using EXAFS, XANES, XRD and FE-TEM/EDS, they were able to obtain spatially resolved structural information on very

small bimetallic nanoparticles.[8] A similar study on our catalysts would be of interest because it is not known what type of bimetallic structures our nanoparticles have formed. It is probable that the majority of the bimetallic combinations have formed alloys, though there may be a few select cases when a more core-shell like structure has resulted.

Template Assisted Synthesis of the Metal Oxide Catalyst Support

As was previously mentioned, little was done to control the structure of the metal oxide catalytic support other than using an acidic catalyst during the sol-gel synthesis to ensure a more amorphous material with a larger surface area. It would therefore be interesting to attempt to control the structure of the catalyst support to determine if there would be an effect on the catalytic activity or the selectivity. This can be achieved through a template-assisted synthesis approach in which an organic template, typically a surfactant, is added during the sol-gel synthesis procedure. By using a template, the resulting metal oxide can be highly ordered with a tailored pore size. This occurs because under certain conditions, the surfactants can form micelles which usually take on a rod-like shape.[5] The metal oxide adheres to the surface of the micelles and when the surfactant is removed, only the metal oxide is left behind giving rise to a highly porous material. This approach has been applied to a wide variety of metal oxides where the pore size can by tuned by varying the templates size and type.[9-30] Cationic, anionic and neutral surfactants have been used for the synthesis of isotropic, hexagonal, cubic or laminar mesostructures.[5] To remove the templates, mild conditions must be used to preserve the structure of the metal oxide before further hydrothermal or solvothermal treatments.[5]

Another group of templates are composed of pore structure replicas and can be divided into two classes: endotemplates and exotemplates.[5] Endotemplates represent the pores and are incorporated into the gel. The previously mentioned micelles are an example of an endotemplate, and once the endotemplate is removed, the resulting voids form the pores of metal oxide. With exotemplates, the metal oxide forms within the pores of the organic template, so when the template is removed the resulting pores are from the voids left from the organic template. Essentially, exotemplates are three-dimenstional negatives.[5] Endotemplates are typically used for the formation of zeolites or molecular sieves while exotemplates are use to form mesoporous or mixed oxides.[5]

By structuring the metal oxide catalyst support through the use of a template-assisted method, the pore size of the metal oxide can be tuned. By using a variety of organic templates to tailor the pore size of the metal oxide catalytic support, the catalytic activity and selectivity may be altered. For example, Ru nanoparticles supported on nanozeolite frameworks have demonstrated very high catalytic activites for the hydrogenation of aromatics.[31]

In situ Materials Characterization

One of the remaining challenges in the field of nanoparticle catalysis is materials characterization of the nanoparticles during the course of the catalytic reaction. Typically the nanoparticles are characterized before being used in a catalytic reaction and then again after the reaction has completed. This requires that the nanoparticles are isolated from the reaction mixture, and thus it is difficult to know the structure and chemistry of the nanoparticles while the reaction is proceeding because of the changes that may occur upon

isolating the nanoparticles for characterization. These *ex situ* characterizations are also frequently performed under high vacuum or low temperatures, further changing the conditions in which the nanoparticles are characterized.

Ambient-pressure XPS (AP-XPS) has been previously used to obtain *in situ* characterization information.[32,33] AP-XPS has been used under a series of CO pressures ranging from ultrahigh-vacuum conditions to 1 Torr of CO to monitor the changes in binding energies as the CO coverage changed on a Pt(557) surface and to determine the CO coverage as a function of pressure.[33] Ambient-pressure XPS in the Torr pressure range in combination with tunable X-ray energy from synchrotron sources has been used under oxidizing, reducing, and catalytic conditions to investigate the structure of three bimetallic nanoparticle catalysts (Rh_xPd_{1-x}, Rh_xPt_{1-x}, and Pd_xPt_{1-x}).[33] They found that both the Rh_xPd_{1-x} and Rh_xPt_{1-x} nanoparticles underwent reversible changes in surface composition and oxidation state when the reaction conditions varied from oxidizing to reducing or catalytic but there was no change observed for the Pd_xPt_{1-x} nanoparticles.[33]

Another frequently used *in situ* characterization technique is scanning tunneling microscopy (STM). STM was used to image Pt(557) under a series of CO pressures ranging from ultrahigh-vacuum conditions to 1 Torr of CO to monitor the restructuring that occurred on the Pt stepped surfaces.[32] They observed that as the CO pressure increased, the initially straight steps became wavy, and then eventually broke down into nanoclusters which had a triangular shape, demonstrating how the structure of a catalyst observed under *ex situ* conditions is drastically different from those observed under *in situ* conditions. High-pressure STM has also been used to visualize reactant molecules on the surface of Pt(111).[34] Cyclohexene hydrogenation and dehydrogenation were investigated

using STM under reaction conditions of 200 mTorr H_2, 20 mTorr of cyclohexene and 5 mTorr CO, and under these conditions a superstructure of chemisorbed CO molecules on the surface of Pt(111) was observed.[34]

In situ environmental TEM (ETEM) has been used for direct imaging of catalyst-gas molecule reactions under operating temperatures.[35] In ETEM, a gas reaction cell is used inside of an electron microscope column, and direct observations of atomic motion and chemical modification of the catalyst while it is a liquid or gas environment. For example, ETEM has been used to show nanoparticle coarsening and atomic migration of Cu particles supported on carbon at 200°C in H_2 balanced by He, while *ex situ* TEM did not show these changes.[35] ETEM of Cu/Al_2O_3 and other metal/ceramic oxide systems under varying environments have also given evidence for the diffusion of metal nanoparticles through the bulk substrate.[35,36] Lastly, ETEM has been used to examine the role of different gas environments used for methanol synthesis (H_2 and CO) on CuPd/C. They observed that the both nature and shape of the nanoparticles varied depending on the gaseous environment.[35]

By using some of these *in situ* materials characterization techniques (AP-XPS, STM and ETEM), a better understanding of the structure and oxidation state of these nanoparticle catalysts under catalytic conditions may be obtained. Furthermore, restructuring or changes in nanoparticle shape or oxidation state may also be observed using these *in situ* characterization techniques.

4.3 References

(1) Rodriguez-Gattorno, G.; Aleman-Vazquez, L. O.; Angeles-Franco, X.; Cano-Dominguez, J. L.; Villagomez-Ibarra, R. *Energy & Fuels* **2007**, *21*, 1122-1126.

(2) McVicker, G. B.; Daage, M.; Touvelle, M. S.; Hudson, C. W.; Klein, D. P.; Baird, W. C.; Cook, B. R.; Chen, J. G.; Hantzer, S.; Vaughan, D. E. W.; Ellis, E. S.; Feeley, O. C. *J. Catal.* **2002**, *210*, 137-148.

(3) Miki, Y.; Yamadaya, S.; Oba, M. *J. Catal.* **1977**, *49*, 278-284.

(4) Teschner, D.; Matusek, K.; Paal, Z. *J. Catal.* **2000**, *192*, 335-343.

(5) Frenzer, G.; Maier, W. F. *Ann. Rev. Mater. Res.* **2006**, *36*, 281-331.

(6) Levin, I.; Brandon, D. *J. Am. Ceram. Soc.* **1998**, *81*, 1995-2012.

(7) Klein, S.; Thorimbert, S.; Maier, W. F. *J. Catal.* **1996**, *163*, 476-488.

(8) Alayoglu, S.; Zavalij, P.; Eichhorn, B.; Wang, Q.; Frenkel, A. I.; Chupas, P. *ACS Nano* **2009**, *3*, 3127-3137.

(9) Yang, P. D.; Zhao, D. Y.; Margolese, D. I.; Chmelka, B. F.; Stucky, G. D. *Nature* **1998**, *396*, 152-155.

(10) Putlitz, B. Z.; Hentze, H. P.; Landfester, K.; Antonietti, M. *Langmuir* **2000**, *16*, 3214-3220.

(11) Terribile, D.; Trovarelli, A.; Llorca, J.; de Leitenburg, C.; Dolcetti, G. *Catalysis Today* **1998**, *43*, 79-88.

(12) Grosso, D.; Illia, G. J. D. A. S.; Crepaldi, E. L.; Charleux, B.; Sanchez, C. *Adv. Func. Mater.* **2003**, *13*, 37-42.

(13) de Farias, R. F.; Arnold, U.; Martinez, L.; Schuchardt, U.; Jannini, M. J. D. M.; Airoldi, C. *Journal of Physics and Chemistry of Solids* **2003**, *64*, 2385-2389.

(14) Shchukin, D. G.; Caruso, R. A. *Chem. Mater.* **2004**, *16*, 2287-2292.

(15) Tian, B. Z.; Liu, X. Y.; Tu, B.; Yu, C. Z.; Fan, J.; Wang, L. M.; Xie, S. H.; Stucky, G. D.; Zhao, D. Y. *Nature Mater.* **2003**, *2*, 159-163.

(16) Sinha, A. K.; Suzuki, K. *Angew. Chem., Int. Ed.* **2005**, *44*, 271-273.

(17) Tian, B. Z.; Liu, X. Y.; Zhang, Z. D.; Tu, B.; Zhao, D. Y. *Journal of Solid State Chemistry* **2002**, *167*, 324-329.

(18) Blin, J. L.; Leonard, A.; Yuan, Z. Y.; Gigot, L.; Vantomme, A.; Cheetham, A. K.; Su, B. L. *Angew. Chem., Int. Ed.* **2003**, *42*, 2872-2875.

(19) Nagamine, S.; Sasaoka, E. *Journal of Porous Materials* **2002**, *9*, 167-173.

(20) Lyons, D. M.; Ryan, K. M.; Morris, M. A. *Journal of Materials Chemistry* **2002**, *12*, 1207-1212.

(21) Kosuge, K.; Singh, P. S. *J. Phys. Chem. B* **1999**, *103*, 3563-3569.

(22) Zheng, J. Y.; Pang, J. B.; Qiu, K. Y.; Wei, Y. *Microporous and Mesoporous Materials* **2001**, *49*, 189-195.

(23) Schattka, J. H.; Shchukin, D. G.; Jia, J. G.; Antonietti, M.; Caruso, R. A. *Chem. Mater.* **2002**, *14*, 5103-5108.

(24) Antonelli, D. M.; Ying, J. Y. *Angew. Chem., Int. Ed.* **1995**, *34*, 2014-2017.

(25) Antonietti, M. *Current Opinion in Colloid & Interface Science* **2001**, *6*, 244-248.

(26) Lyu, Y. Y.; Yi, S. H.; Shon, J. K.; Chang, S.; Pu, L. S.; Lee, S. Y.; Yie, J. E.; Char, K.; Stucky, G. D.; Kim, J. M. *J. Am. Chem. Soc.* **2004**, *126*, 2310-2311.

(27) Hait, S. K.; Moulik, S. P. *Current Science* **2002**, *82*, 1101-1111.

(28) Carreon, M. A.; Guliants, V. V. *European Journal of Inorganic Chemistry* **2005**, 27-43.

(29) Tanev, P. T.; Pinnavaia, T. J. *Science* **1995**, *267*, 865-867.

(30) Yang, P. D.; Zhao, D. Y.; Margolese, D. I.; Chmelka, B. F.; Stucky, G. D. *Chem. Mater.* **1999**, *11*, 2813-2826.

(31) Zahmakiran, M.; Tonbul, Y.; Ozkar, S. *J. Am. Chem. Soc.* **2010**, *132*, 6541-6549.

(32) Tao, F.; Dag, S.; Wang, L. W.; Liu, Z.; Butcher, D. R.; Bluhm, H.; Salmeron, M.; Somorjai, G. A. *Science* **2010**, *327*, 850-853.

(33) Tao, F.; Grass, M. E.; Zhang, Y. W.; Butcher, D. R.; Aksoy, F.; Aloni, S.; Altoe, V.; Alayoglu, S.; Renzas, J. R.; Tsung, C. K.; Zhu, Z. W.; Liu, Z.; Salmeron, M.; Somorjai, G. A. *J. Am. Chem. Soc.* **2010**, *132*, 8697-8703.

(34) Somorjai, G. A.; Tao, F.; Park, J. Y. *Topics in Catalysis* **2008**, *47*, 1-14.

(35) Gai, P. L.; Boyes, E. D. *Electron Microscopy in Heterogeneous Catalysis*; Institute of Physics Publishing, 2003.

(36) Gai, P. L.; Smith, B. C.; Owen, G. *Nature* **1990**, *348*, 430-432.